Dynamic Modelling of a CO_2 Capture and Purification Unit for Oxy-Coal-Fired Power Plants

by

Atchariya Chansomwong

A thesis

presented to the University of Waterloo

in fulfillment of the

thesis requirement for the degree of

Doctor of Philosophy

in

Chemical Engineering

Waterloo, Ontario, Canada, 2014

Author's declaration

I hereby declare that I am the sole author of this thesis. This is a true copy of the thesis, including any required final revisions, as accepted by my examiners.

I understand that my thesis may be made electronically available to the public.

Abstract

Even though the use of renewable energy in electricity generation has significantly increased over time, coal is projected to remain as the primary fuel in electricity generation worldwide in the next decades due to its availability, stability of supply and cost. However, coal-fired power plants are the largest stationary sources of CO_2 emissions that contribute to global warming. Several technologies have been developed to mitigate CO_2 emissions from coal-fired power plants. Oxy-combustion is a promising pathway to capture CO_2 from coal fired power plants that competes favourably with other CO_2 capture technology pathways such as post-combustion and pre-combustion. Oxy-combustion has attracted attention because it provides a CO_2-enriched flue gas stream which can be further purified using a relatively simple multi-stage compression and cooling processes. Currently, there is no oxy-coal-fired power plant in commercial-scale operation. Thus, the transition towards commercial scale operation is the main challenge for this technology.

The CO_2 capture and purification unit (CO_2CPU) is an important unit in oxy-coal-fired power plants that determine the quality of the CO_2 product and energy consumption of the power plants. Several studies published on the CO_2CPU process have evaluated the performance of this system at steady state. Insight regarding the dynamic behaviour of the CO_2CPU process is very limited and a mechanistic dynamic model of the CO_2CPU is not available in open literature. Thus, research on dynamic modelling and control system development is still required to demonstrate the operability and controllability of this technology.

This study aims to develop, test and validate a dynamic model of the CO_2CPU for oxy-coal-fired power plants. Detailed mathematical models of each unit operation in the CO_2CPU are provided in this study. The main challenge was to develop a dynamic model of a multi-stream heat exchanger that involves multiple process streams and encounters both condensing and boiling two phase flows. A dynamic model that is not computationally intensive, to slow down the entire CO_2CPU plant model, and that can predict reasonable fluid

temperatures in the multi-stream heat exchanger was developed in this study. The proposed multi-stream heat exchanger model was based on a shell and tube configuration that considers only axial changes in flow, i.e., a 1D model. Likewise, the two phase region in this unit was modelled using a homogenous model, which is a simplified discretized two-phase flow model that reduces the computational effort and complexity of the multi-stream heat exchanger process model. The homogenous model takes into account the changes in the fluid properties in the two phase region to calculate the heat transfer coefficients of the multi-stream heat exchanger models. To the author's knowledge, the model presented in this study represents the first mechanistic process model that describes the transient behaviour of a CO_2CPU for oxy-fired power plant.

Two design configurations of the CO_2CPU were considered in this study, i.e. the Air Products' CO_2CPU and the CanmetENERGY's proprietary CO_2CPU (CanCO$_2$). Both plants are designed based on a two-stage flash separation process. The CanCO$_2$ is an extended design of the Air Products' CO_2CPU. The presence of an external recycle stream , recycling a portion of the CO_2 rich effluent gas stream from the first flash drum to the compressor train, in the CanCO$_2$ is a major distinction between the two CO_2CPU configurations and enhances the CO_2 capture rate for the CanCO$_2$ process. Nevertheless, the addition of this recycle stream makes the CanCO$_2$ plant model convergence more challenging than the Air Products' CO_2CPU since it adds natural feedback into the system. A systematic procedure to perform the process integration of all the unit operations considered in the CO_2CPU flowsheets was developed and presented in this study. Stand-alone unit operation models were developed, coded and then connected together one at a time. Dynamic models of the Air Products' CO_2CPU and the CanCO$_2$ were developed and validated at steady state using design data. Reasonable agreement between the developed models and the design data were obtained for both CO_2CPU configurations. Several dynamic tests were performed to gain insight into the transient behaviour of the CO_2CPU. The results obtained from the transient analyses clearly demonstrate that both CO_2CPU plants are highly nonlinear processes.

The CO_2 recovery and the CO_2 product purity obtained from the base case of both plants are similar, approximately at 89 wt% and 95 mol% respectively. The operating conditions of the first flash drum were found to play a key role on the CO_2CPU performance of both plants. In addition, both models indicate that the CO_2 recovery is more sensitive to the operating conditions than that of the CO_2 product purity. The CO_2 purity is more sensitive to the flue gas composition and responds to all changes performed in this study faster than the CO_2 recovery. Because of the recycle stream, the $CanCO_2$ response to all changes is slower than the Air Products' CO_2CPU. Nevertheless, the use of a recycle stream improves the CO_2 recovery and increases the number of manipulated variables in the $CanCO_2$, thus this system has more alternative control structures than the Air Products' CO_2CPU.

The models developed in this study can be extended to include the controllability analysis and the control structure design for the CO_2CPU; and the integration of oxy-boiler, steam cycle and also air separation unit (ASU) into a complete dynamic model of the oxy-fired power plant that will be very useful for oxyfuel combustion technology scale-up.

Acknowledgements

I would never been able to complete my dissertation without kind supports and helps from a number of people around me. It is my pleasure to convey my sincere gratitude to them in my acknowledgments.

In the first place, I would like to thank my supervisors; Prof. Peter L. Douglas, Prof. Eric Croiset, and Assist. Prof. Luis Ricardez-Sandoval, for giving me a good opportunity to pursue my educational career in Ph.D program at the University of Waterloo. I sincerely appreciate their patience, valuable guidance and kind support throughout my study.

I gratefully acknowledge Dr.Kourosh Zanganeh and Ahmed Shafeen for technical suggestions, information, and financial supports through CanmetENERGY, Ottawa, under the Canadian government's funding program "ecoENERGY Innovation Initiative (ecoEII)" and "Program for Energy Research and Development (PERD)".

Sincere appreciation is hereby extended to Prof. Thomas A. Duever, Prof. William A. Anderson, Prof. Roydon A. Fraser, and Prof. Paitoon Tontiwachwuthikul, for sharing their precious time and knowledge as committee members.

I also thank all Thai Student Association (TSA) members for warm welcome and friendly helps during my stay in Waterloo. I will always remember all the good times we spent together.

Finally, I would like to thank my family who are always by my side with unconditional love and plenty of encouragement.

Table of Contents

List of Figures

xii

List of Tables

Nomenclature

A	Area (m^2)	**Greek symbols**	
C_p	Heat capacity (J/kg K)	α	Void fraction
C_v	Flow coefficient	ρ	Density (kg/m^3)
e	Polytropic efficiency	μ	Viscosity (kg/m·s)
D	Diameter (m)	ϕ	Fugacity coefficient
g	Standard gravity (m^2/s)	η	Efficiency
G	Mass flow rate per unit area (kg/s·m^2)	ω	Acentric factor
F	Feed molar flow rate (kmol/s)	f	Fugacity
H	Enthalpy (J/kg)	**Subscripts**	
h	Liquid level (m)	1	Inlet condition
h	Heat transfer coefficient (W/m^2·K)	2	Outlet condition
k	Thermal conductivity (W/m·K)	l	Liquid phase
K	Phase equilibrium ratio	s	Shell-side
Kv	Separator design factor	t	Tube-side
L	Liquid molar flow rate (kmol/s)	v	Vapour phase
m	Polytropic temperature exponent	w	Wall condition
M_{cv}	Liquid molar hold up (kmol)	TP	Two phase
MW	Molecular weight	cv	Control volume
P	Pressure (Pa)	i	Inlet
Q	Rate of heat transfer (W)	e	Exit
R	Gas constant (m^3·Pa/K· mol)	**Subperscripts**	
SF	Split fraction	L	Liquid phase
T	Temperature (K)	V	Vapour phase
u	Velocity (ft/s)		
U	Overall heat transfer coefficient (W/m^2·K)		
v	Velocity (m/s)		
V	Vapour molar flow rate (kmol/s)		
V	Volume (m^3)		
W_P	Polytropic work (W)		
W_L	Liquid mass flow rate (lb/s)		
W_V	Vapour mass flow rate (lb/s)		
x	Vapour quality		
x_i	Mole fraction of component i in liquid mixture		
X	Schultz's generalized compressibility function		
X_{tt}	Lockhart-Martinelli parameter		
y_i	Mole fraction of component i in vapour mixture		
Y	Schultz's generalized compressibility function		
z_i	Mole fraction of component i in feed		
Z	Compressibility factor		

Chapter 1

Introduction

1.1 Introduction

The world has a constant and increasing need for energy to support its economic growth and expanding prosperity across a rising population. The global energy demand has increased dramatically since the beginning of industrialization and it is projected to continuously increase by approximately 40% in the few decades to come (IEA, 2011). Global energy is used in four main sectors, i.e. electricity generation, transportation, industry and household. Electricity generation is among the largest driver of the global energy growth, accounting for over half of the total global energy demand growth (IEA, 2011; BP, 2013a; Exxonmobil, 2013). World electricity generation has relied heavily on fossil fuels, i.e. crude oil, natural gas and coal, for more than forty years (IEA, 2011). Even though renewable energy will become more significant in the future, fossil fuels demand for electricity generation is projected to increase substantially over the coming decades (IEA, 2011; BP, 2013a; Exxonmobil, 2013). Among the fossil fuels, coal is the dominant resource for electricity generation. Proven coal reserve is enough to last for 109 years at the current rate of coal production (BP, 2013a), outlasting oil and gas reserves combined. Also, the coal price is relatively cheap and stable compared to the prices of oil and gas. These properties give coal advantages over other fuels for electricity generation and thus coal is unlikely to be phased out from the electricity supply infrastructure in the medium term.

Although the electricity supply from coal is reliable and affordable, it is the largest source of anthropogenic CO_2 emission, accounting for 41% of the total CO_2 emission in 2011. Since the coal demand has increased continuously, the accumulation of CO_2 in the atmosphere has risen accordingly. Currently, the global CO_2 concentration in the atmosphere reached 400 ppm (NASA, 2013) for the first time in recorded history. Despite the global warming controversy (an ongoing dispute about the effects of humans on global climate and about what policies should be implemented to avoid possible undesirable effects of climate

change), there is a scientific consensus that it is in favour to limit the global growth of anthropogenic greenhouse gas (GHG) emissions, especially CO_2, in the near future (Sioshansi, 2010; IEA, 2013). In 2009, the Copenhagen Accord was reached at the 15th session of the Conference of Parties (COP15) to the United Nations Framework Convention on Climate Change (UNFCCC, 2009) to limit the average rise in global temperature to no more than 2°C above pre-industrial level in order to prevent dangerous anthropogenic interference with the climate system (Randalls, 2010). Canada is one of the signatories to the UNFCCC which signed onto the Copenhagen Accord in December 2009 and committed to reduce its GHG emissions to 17% below 2005 levels by 2020 (Environment Canada, 2013). To achieve the 2°C limit, it is necessary to deploy a combination of renewable energy, energy efficiency and carbon capture and storage (CCS). While the transition to low carbon economy is in process, CCS technology is considered as an attractive option to reduce anthropogenic CO_2 emissions from power plants, in particular coal-fired units, and other carbon-intensive industries. CCS is the only technology available for capturing at least 90% of the current CO_2 emissions (IEA, 2012a; ZEP, 2013). Implementing CCS at a large scale can therefore provide time needed to fully develop sustainable energy systems for the future (ZEP, 2013). The concept of CCS is relatively straightforward: capture CO_2 from fossil fuel facilities; produce a concentrated CO_2 stream that can be transported to another facility for its permanent storage or its use in other industrial applications. Currently, there are four potential approaches for capturing CO_2 from power plants: pre-combustion, post-combustion, oxyfuel combustion and chemical looping combustion. Post-combustion captures CO_2 from the flue gas of conventional coal combustion (air-combustion) by typically using chemical absorption technique. Pre-combustion transforms coal into synthesis gas (syngas) composed of CO and H_2 via gasification process. Afterwards, the CO in syngas is converted to CO_2 by the water-gas shift reaction and can then be separated from the remaining H_2 for storage or transportation. In oxy-combustion, almost pure O_2 is used instead of air to combust coal and produce a high content CO_2 in flue gas stream which can be easily separated using a compression and cooling technique. Chemical looping uses an active metal as an oxygen carrier to transport oxygen from air to fuel. An active metal is first oxidized by air in an

oxidizer to produce a metal oxide. The metal oxide is then reacted with fuel in a reducer producing relatively high purity CO_2 and steam.

Oxy-combustion is a promising pathway to capture CO_2 from coal-based power plants that can compete favourably with other CO_2 capture technology pathways. Oxy-combustion is attractive because it provides a CO_2-enriched flue gas stream containing up to 90% CO_2 on a dry basis (GCCSI, 2012a) which is easily purified, if required, using relatively simple multi-stage compression/cooling processes. In addition, the use of pure oxygen instead of air in oxy-combustion significantly reduces the volume of the stack flue gas, thus enabling reduction in capital cost and making oxy-combustion an economically attractive CCS technology. The investment cost and the reduction in thermal efficiency of oxy-combustion plants is comparable to those of post-combustion plants (Adams and Davison, 2007; Kanniche et al., 2010; Rubin et al., 2012), while the cost of avoided CO_2 (the quantity of CO_2 emission per kWh of a power plant with CO_2 capture compared to a baseline plant without CO_2 capture) is slightly lower (Adams and Davison, 2007; Kananiche et al., 2010). The reduction in thermal efficiency of oxy-combustion plants is caused mainly by two energy-consumer sub-processes: the air separation unit (ASU) and the CO_2 compression and purification unit (CO_2CPU). Commercial ASUs are currently available based on cryogenic distillation, while both the CO_2CPU and the oxy-combustion power plants have yet to be demonstrated at full (commercial) scale. To date, oxy-combustion power plants with CO_2 capture are still under development, but a number of pilot-scale facilities and demonstration plants are already well underway providing crucial information for technology scale-up.

Numerous studies and research on oxy-combustion technology have been performed. Most studies have focused on combustion and emission characteristics, and the potential to retrofit existing air-fired power plants (Buhre et al., 2005; Jordal et al., 2004; Toftegaard et al., 2010). Likewise, several studies have been published on the CO_2CPU. The CO_2CPU is an important unit in the oxy-coal-fired power plants as it determines the quality of the CO_2 product and represents a large part of the energy consumption of the plant. A number of steady-state models of CO_2CPU were developed for various research aspects, e.g. process

3

optimization, heat integration analysis and techno-economic analysis. However, a mechanistic dynamic model of the CO_2CPU is not currently available in the literature and the research on transient analysis of the CO_2CPU is still limited. A dynamic model can provide insights regarding the operation of the process in the presence of external perturbations and uncertainty in the parameters. It is a practical tool to verify the variability of the process and to develop a controllability analysis on the system. Moreover, modern plant design methods recommend considering process dynamics and control simultaneously with steady-state plant design to obtain an efficient and profitable process operation. The integration of process design and control will make the designed process flexible and easy to control once it is in operation or expanded to commercial scale.

1.2 Research objectives

The ultimate goal of this research is to develop and validate a dynamic model of the CO_2CPU that can be used to design suitable control schemes for this process. This thesis aims to characterize the dynamic behaviour of the CO_2CPU in response to the various feed conditions, operating conditions and expected disturbances. The following tasks have been considered to achieve the research goal:

- Develop a detailed mathematical model of each unit operation in the CO_2CPU, i.e., compressor, expander, flash drum, heater, cooler and multi-stream heat exchanger.

- Integrate all unit operations to perform a dynamic model of the CO_2CPU.

- Validate the developed model at steady state using data reported in the open literature.

- Analyze the dynamic behaviour of the CO_2CPU in response to changes in flue gas conditions, operating conditions and disturbances.

1.3 Scope of Work

The dynamic model of the CO_2CPU was implemented in gPROMS (general PROcess Modelling System), an equation-oriented simulation software system that is powerful for

4

dynamic modelling; optimization; and control software system. Physical and thermodynamic properties were obtained from Multiflash™, an add-on property package available in gPROMS. The CO_2CPU can be divided into three main sections: a multi-stage compression and cooling (compressor train), CO_2 liquefaction for inerts removal (auto-refrigeration), and further compression to the end user's specifications. Two designs of the CO_2CPU were considered in this work, i.e. the Air Products' CO_2CPU and the CanmetENERGY's proprietary CO_2CPU (CanCO$_2$). The Air Products' CO_2CPU, as the name implied, was designed and proposed by Air Products plc., and presented in an IEA Greenhouse Gas R&D programme report (Dillon et al., 2005). A dynamic model was developed in this work and validated, at steady-state only, using simulation data obtained from the IEAGHG R&D programme report (Dillon et al., 2005). The CanCO$_2$ is an extension of the the Air Products' CO_2CPU design. The model was developed and validated also at steady state based on the design data of the CanCO$_2$ provided by CanmetENERGY.

1.4 Research contribution

To the best of the author's knowledge, only two dynamic simulation studies of the CO_2CPU for oxyfuel combustion are currently available in the open literature (Kuczynski et al., 2011; Pottman et al., 2010). Both studies developed a dynamic model of the CO_2CPU using commercial sequential-modular software packages, i.e. Aspen HYSYS and Honeywell's Unisim$^®$. In the sequential-modular software package, the heat transfer coefficients are required as an input for the simulation. The heat transfers coefficients do not change in accordance with the variation of fluid properties flowing through the heat exchanger. In addition, no mathematical models are provided in either of the two studies above and knowledge of the dynamic behaviour of the CO_2CPU is very limited.

This study focuses on the mechanistic dynamic model of the CO_2CPU based on an equation-oriented approach in which the heat transfer coefficients used in the multi-stream heat exchangers are considered as process variable solved simultaneously with temperatures and other process variables. A detailed mathematical model is provided. In addition, the variations of fluid properties in the two phase regions were taken into account to calculate the

heat transfer coefficients for multi-stream heat exchanger models. These qualifications give the dynamic model of the CO_2CPU great distinct advantages over the two models that were recently presented in open literature. The developed model can be considered as a first attempt at developing a rigorous mathematical dynamic modelling of a CO_2CPU for oxy-fired power plant. Moreover, the developed model can provide insight into the transient behaviour that can be further used to design a control system for the CO_2CPU. The developed model can also be extended to include the controllability analysis that will be useful for oxyfuel combustion technology scale-up.

1.5 Thesis outline

This proposal is organized as follows:

Chapter 1 provides motivations behind this research including objectives, scope of work and research contribution.

Chapter 2 provides the background to the role of coal in the global electricity generation and CCS technologies; and literature reviews on the oxyfuel combustion technology and the CO_2CPU.

Chapter 3 presents mathematical models for each unit operation in the CO_2CPU. Detailed process descriptions of the Air Products' CO_2CPU and the CanCO2 are also provided. Procedures to integrate all unit operations to perform a complete dynamic model of both CO_2CPU configurations are also explained in this chapter.

Chapter 4 presents results obtained from the Air Products' CO_2CPU model consisting of two main sections, i.e. steady state validation and transient analysis.

Chapter 5 presents results obtained from the CanCO$_2$ model. Likewise, results are divided into two main sections, i.e. steady state validation and transient analysis.

Chapter 6 concludes the results obtained from this study and provides recommendations for further studies.

Chapter 2

Research background and literature reviews

This chapter provides the background to the role of coal in the global electricity generation and oxyfuel combustion CO_2 capture technology. The first section describes how important the coal-based power plants are in the global energy mix and why the CO_2 capture and storage (CCS) technologies should be integrated into the power plants. Overviews of the CCS technologies and details of the oxyfuel combustion technology are subsequently provided. Literature reviews on the CO_2 capture and purification unit (CO_2CPU) for oxyfuel combustion plants, a focus of this research, are provided in section 2.4 and the Canada action on climate change was summarized in the last section.

2.1 Coal in the world electricity generation

2.1.1 Coal's share in the fuel mix for electricity generation

The global energy demand has increased since the beginning of industrialization and it is projected to continuously increase in the next few decades due to growth in world population and economic development. The total global energy demand will increase by approximately 40% by 2035 (IEA, 2011; BP, 2013a; Exxonmobil, 2013). The power sector is by far the largest driver behind the growing global energy demand accounting for over half of the net growth. It is estimated that the global demand for electricity will increase by 80% and could double between 2009 and 2035 as more people get access to electricity and economies expand in developing countries (IEA, 2011; BP, 2013a; Exxonmobil, 2013; World Coal Association, 2013). Today, 41% of the global electricity is generated from coal. With growing electricity demand, coal demand in the power sector is projected to increase by 48% through 2035 (IEA, 2011). The growth comes overwhelmingly from developing countries where the coal-fired power plants are forecasted to double in the coming decade. China alone contributes over half of the total increase in the global coal demand due to rapid population and economic growth. Chinese coal consumption increased by 50%, between 2005 and 2010

which was equivalent to more than the total coal demand in the United States in 2010 (IEA, 2011). Nonetheless, the share of coal in the fuel mix for power generation is estimated to fall over time, as shown in Figure 2.1.
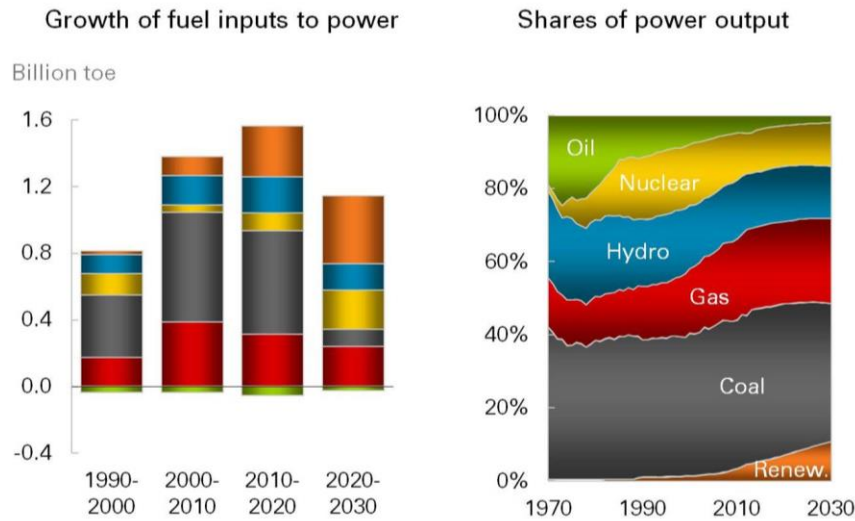
Figure 2.1 The fuel mix for power generation (BP, 2013a)

It is projected that climate change policies to control the energy-related CO_2 emissions will come in place by 2020 and then the power generation mix will move toward low-carbon technologies, such as renewable and nuclear. The shifts in fuel mix are driven by relative cost, technology developments and energy policy. Coal-base generation grows continuously between 1990 and 2020, but the growth decreases after 2020 due to the slowdown in total power growth and the leading role of both renewables and nuclear. The growth in renewable power generation is driven mainly by adopting the carbon pricing and energy subsidies. Carbon-pricing encourages investment in low-carbon power generation technologies, such as renewable and nuclear, by putting a price on CO_2 emitted (IEA, 2011). Carbon pricing, therefore, increases the total cost of electricity generation from fossil fuel power plants which are emissions-intensive, and makes the total cost of other technologies (that are relatively high) competitive. Carbon pricing along with government subsidies raise the share of renewables in the power sector fuel mix by 10% between 2010 and 2030 as shown in Figure 2.1. Although the exact share of coal in the electricity supply could decline according to

8

climate change policies in place, coal continues to play an important role in the global electricity generation in the next few decades.

2.1.2 Coal reserve and price

Coal reserves are widely distributed and available in almost every region of the world. The amount of proven recoverable coal reserves exceeds 860 billion tonnes found in almost 80 countries around the world. By contrast, 53.2% of the world's gas reserves are found in Russia, Iran and Qatar and over 50% of the world's oil reserves are located in the Middle East (World Coal Association, 2013). This global distribution provides stable and secure supply of electricity across broad political arenas.
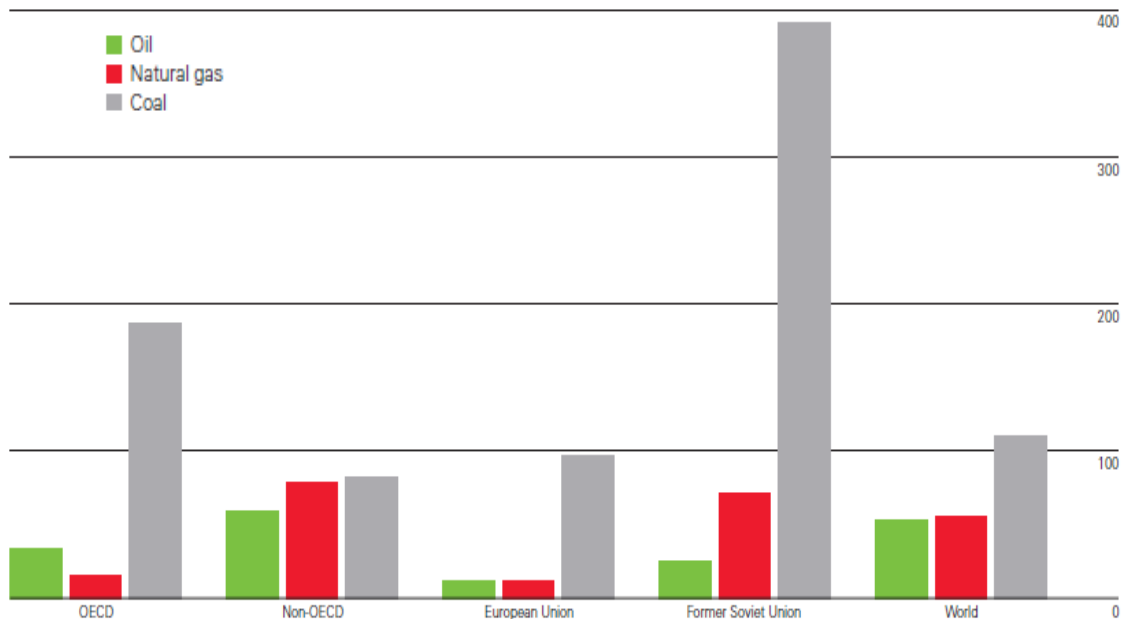
Figure 2.2 Fossil fuel reserves-to-production (R/P) ratios at end 2012, expressed in years (BP, 2013b)

The reserves-to-production (R/P) ratios of fossil fuels which are the amount of economically recoverable reserves remaining at the end of 2012 divided by the production rate in 2012 (expressed in years) are presented in Figure 2.2. The R/P ratios indicate that the world proven coal reserves in 2012 were sufficient to meet 109 years of global production while the proven

oil and gas reserves are enough to last us around 53 and 56 years, respectively. Coal outlasts oil and gas combined. The US holds the largest individual coal reserves, followed by Russia and China (BP, 2013b; World Coal Association, 2013). It should be noted that the R/P ratio is based only on the recoverable coal reserves, not the entire coal resources. The German Federal Institute for Geosciences and Natural Resources estimated that the entire coal resources are around 17 times larger than the recoverable coal reserves and account for over two thirds of all non-renewable energy sources (World Coal Association, 2013). These data illustrated that coal is the world's most abundant energy fuel. In addition, coal prices have historically been lower and more stable than oil and gas prices. Figure 2.3 shows the weighted average cost of fossil fuel prices in US power sector.
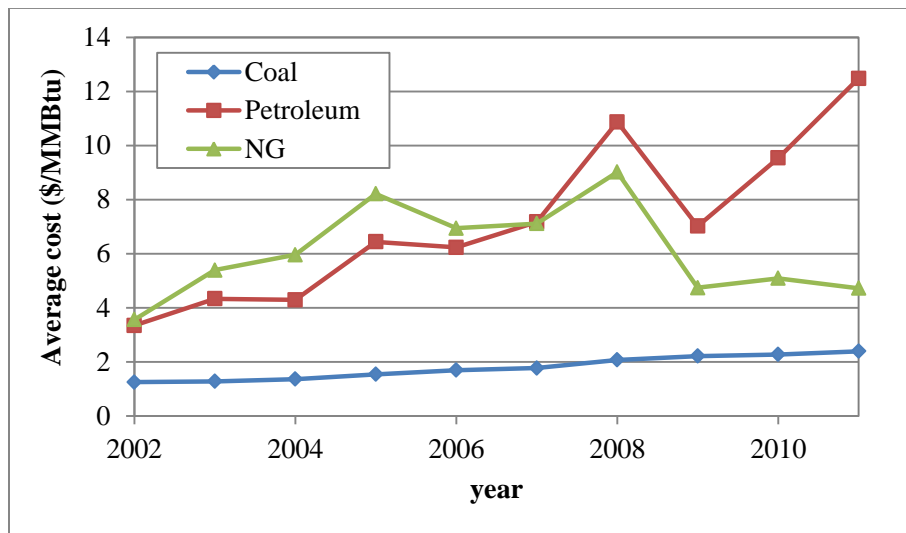
Figure 2.3 The weighted average cost of fossil fuels for the Electric Power Industry in the US (Source: EIA, 2012)

The relative low and stable cost makes coal a very attractive energy fuel and gives coal-fired power plant a cost advantage over other power technologies. Coal is likely to remain the most affordable fuel for power generation in many developing and industrialised countries for decades. Due to its abundance and affordability, coal is implausible to be phased out from the energy infrastructure in the medium term.

2.1.3 Energy-related CO_2 emission

While coal is the most abundant and affordable fuel for power generation, it is also the leading source of CO_2 emissions. Coal is the most carbon-intensive fuel and accounts for 44% of the total energy-related CO_2 emissions increase in 2012 (IEA, 2013). The current record of global CO_2 emissions from fossil-fuel combustion is 31.6 Gt, growing by 1.4% from 2011. If this growth rate is continued, a long-term global temperature will increase by at least 3.6°C (IEA, 2013). The largest contribution to the global energy-related CO_2 emissions increase is from China. The CO_2 emissions from China increased by 3.8% in 2013, which is less than half of the emission increase in 2011 and its smallest increase in the last decade (IEA, 2013). This reflects China's efforts to reduce the energy intensity and the corresponding CO_2 emission. Nevertheless, the global energy-related CO_2 emission is projected to substantially increase until 2030 due to the energy demand growth and uncertain political policies on CO_2 emission. Exxonmobil forecasted that political policy to control the CO_2 emission will have a significant impact on the power generation by 2030 (Exxonmobil, 2013). They assumed that carbon-pricing will be fully implemented by 2030 and thus shift the power generation away from coal. Power generation technology is also projected to be improved as the new technologies developed. Thus, global CO_2 emissions will drop between 2030 and 2040 due to the efficient use of energy and a shift away from coal to low-carbon technologies, as shown in Figure 2.4.
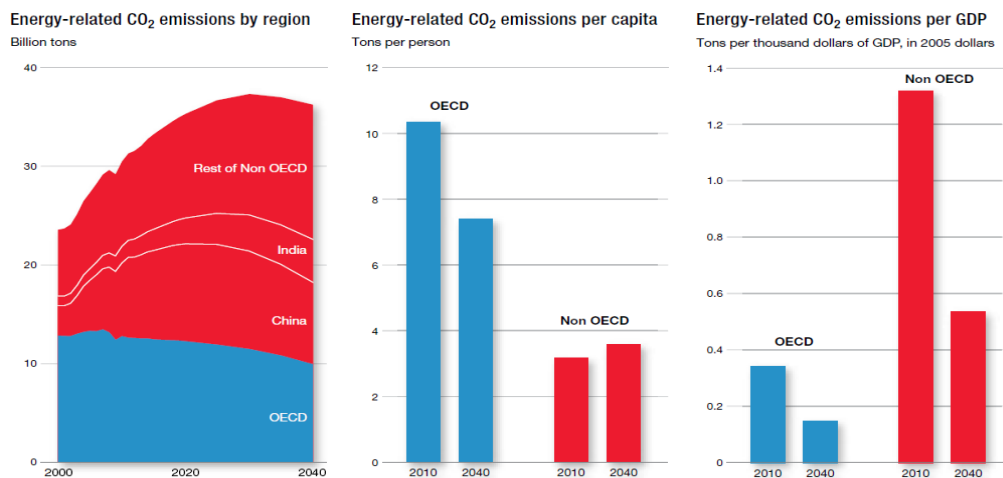
Figure 2.4 Energy-related CO_2 emission (Exxonmobil, 2013)

11

As the energy-related CO_2 emissions continues to increase political will is still lacking, the climate goal of limiting average global temperature increase to 2°C, as called for by the UN Framework Convention on Climate Change, is becoming more difficult and likely unrealistic. The International Energy Association (IEA) summarized their projection in the world energy outlook 2012 (scenario 45) that if action to reduce CO_2 emissions is not taken before 2017, all the allowable CO_2 emissions to keep a limit of 2°C increase would be locked-in by energy infrastructure existing at that time (IEA, 2012b). Their examinations indicate that no more than one-third of proven reserves of fossil fuels can be consumed prior to 2050 if the world is to achieve the 2°C goal, unless carbon capture and storage (CCS) technology is widely deployed (IEA, 2012b). To achieve the 2°C goal, it will be necessary to halve (from current levels) CO_2 emissions by 2050. CCS is the only technology capable of achieving the necessary deep cuts in CO_2 emission from coal-fired power plants (IEA, 2013). In 2010, IEA estimated that the deployment of CCS technologies will contribute to the largest CO_2 emission reduction, i.e. 31% of the entire mitigation effort needed in the power sector, as shown in Figure 2.5. While the use of nuclear and wind energies provide 19% and 11% reduction, respectively (IEA, 2010).

2%	Biomass and waste
19%	Nuclear
2%	Hydro
11%	Wind
7%	Solar PV
9%	Solar CSP
3%	Geothermal
31%	CCS
4%	IGCC coal
3%	SC/USC coal
2%	Gas efficiency
7%	Fuel switching coal to gas
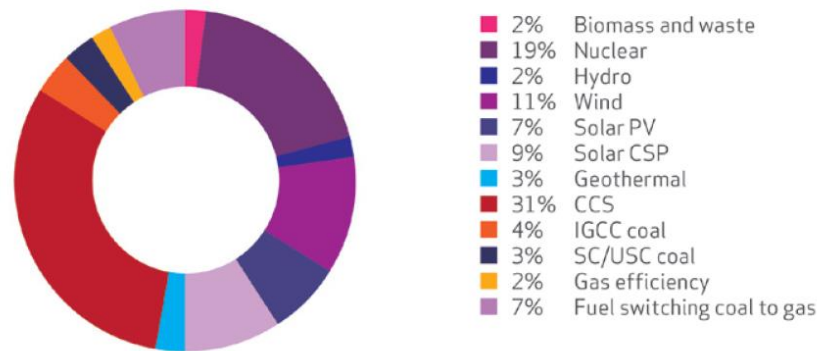
Figure 2.5 Contribution of different power sector technologies to reductions in CO_2 emissions (IEA, 2010)

Recently, the IEA proposed that retrofitting existing coal-fired power plants (that have an average efficiency less than 35% LHV) with CCS becomes an unattractive option for CO_2

emission reduction. However, deployment of CCS in high-efficiency coal-fired power plants, supercritical (SC) or ultra-supercritical (USC) plants, with efficiencies greater than 40% LHV, is more favourable (IEA, 2012a). The high efficiency coal-fired power plants integrated with CCS can reduce CO_2 emissions by 80% to 90%, bringing CO_2 intensity of coal-fired units down to less than 100 g/kWh as illustrated in Figure 2.6.
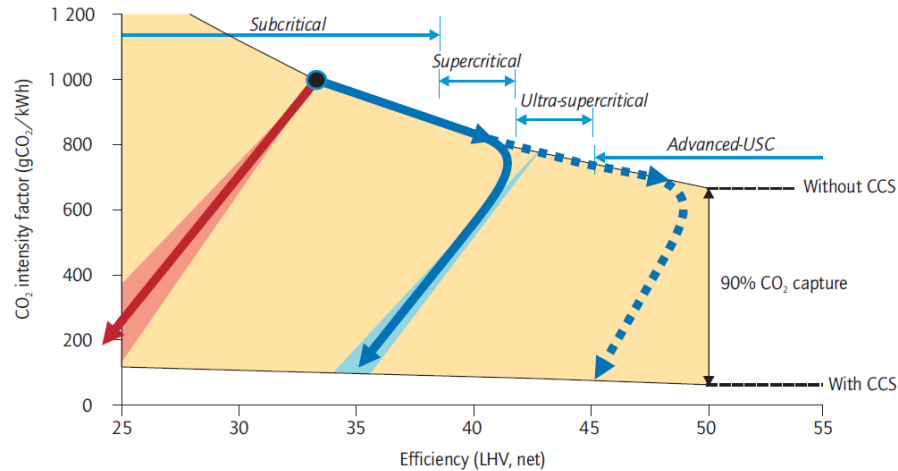
Figure 2.6 Reducing CO_2 emissions from pulverised coal-fired power generation (IEA, 2012)

These findings underline the importance of CCS as a key option to mitigate CO_2 emissions and enable coal-fired power plants to continue supplying reliable and affordable electricity in a carbon-constrained world. Details of CCS technologies are provided in the following section.

2.2 Carbon Capture and Storage (CCS)

2.2.1 Background

Carbon Capture and Storage (CCS) also referred to as Carbon Sequestration is a promising pathway to mitigate anthropogenic CO_2 emission from stationary sources such as coal-fired power plant. The CCS is comprised of three main aspects:

1) Capture: Defined as the separation or removal of CO_2 arising from fossil fuel combustion and/or other combustion processes. The main objective of CO_2 capture is to produce a concentrated CO_2 stream ready for transport and storage. Currently, there are four main pathways to capture CO_2:

- *Post-combustion* capture CO_2 from the flue gas produced by the combustion of carbonaceous fuel with air. Chemical absorption using amine solvents is typically deployed to separate the small fraction of CO_2 from a flue gas.

- *Pre-combustion* decarbonise the fuel prior to combustion by gasification to produce syngas consisting mainly of CO and H_2. The syngas is then *shifted* into CO_2 and more H_2 via a water-gas shift reaction. The high concentration of CO_2 from pre-combustion makes the separation process easier than the post-combustion.

- *Oxyfuel combustion* uses nearly pure oxygen instead of air for combustion resulting in a flue gas that is mainly CO_2 and water. The water is then easily removed by condensation, thus the CO_2 capture process in this approach is relatively simple compared to post- and pre-combustion.

- *Chemical looping combustion* converts fuel to energy using two reactors (oxidizer and reducer). A metal oxide (oxygen carrier) is circulated between two reactors to drive the chemical reactions. Air reacts with an active metal to form a metal oxide while fuel utilises the oxygen from metal oxide to produce energy. There is no direct contact between fuel and air, thus the CO_2 produced from combustion is not diluted by nitrogen and easily purified.

2) Transport: Defined as the medium to move the CO_2 to storage sites. CO_2 transportation is usually carried out via pipelines. Transportation by trucks, rail and ships are also available. The means of transportation rely on the quantity of CO_2 to be transported, the terrain and the distance between the capture plant and storage site. Pipelines are likely the most common method for large scale CO_2 transportation and already used in the US to transport CO_2 for use in Enhance Oil Recovery (EOR). Transport of CO_2 by ships is also occurring in Europe but on a small scale. Transportation both pipelines and ships do not pose

14

any higher risk than already safely managed for transporting hydrocarbons such as natural gas and oil. International standards are being developed for safe and efficient operation of CO_2 infrastructure (GCCSI, 2013)

3) Storage: Defined as a permanent sequestration of CO_2 to prevent captured emissions from entering the atmosphere. Geologic formations suitable for CO_2 storage include depleted oil and gas fields, deep coal seams, and saline formations. Injecting CO_2 into the oilfield reduces the oil viscosity and increases the reservoir pressure, helping to sweep the oil towards the production well. This method is known as CO_2 Enhance Oil Recovery (EOR). The EOR is considered a means for widespread deployment of large-scale CO_2 storage projects due to a positive commercial value of captured CO_2 obtained from EOR.

2.2.2 CCS global status

CCS has gained increasing worldwide interests over the last decade due to growing evidence of climate change, e.g. more frequent and intense storms and floods; decreasing snowpack; longer period of drought in some regions etc. CCS technologies are now well understood and the necessary components are available, but the number of large-scale integrated CCS projects is still limited. Only 12 Large-Scale Integrated CCS Projects (LSIPs) are in operation worldwide providing 25 million tonnes per year CO_2 captured as shown in Table 2.1. It is noted that the LSIPs are defined as those which involve the capture, transport and storage of CO_2 at a scale of at least 0.8 $MtCO_2$ per annum for coal-based power plants or 0.4 $MtCO_2$ per annum for industrial facilities.

Table 2.1 LSIPs in operation stage (Source: GCCSI 2013)

Project name	Country	CO_2 (MtPA)	Operation date	Capture type	Storage type
Val Verde Natural Gas Plants	US	1.3	1972	Pre-combustion (NG processing)	EOR
Enid Fertilizer CO_2-EOR Project	US	0.68	1982	Industrial separation	EOR
Shute Creek Gas Processing Facility	US	7	1986	Pre-combustion (NG processing)	EOR
Sleipner CO_2 Injection	Norway	0.85	1996	Pre-combustion (NG processing)	Deep saline formations
Great Plains Synfuel Plant and Weyburn-Midale Project	Canada	3	2000	Pre-combustion (gasification)	EOR
In Salah CO_2 storage	Algeria	Injection suspended	2004	Pre-combustion (NG processing)	Deep saline formations
Snohvit CO_2 Injection	Norway	0.6-0.8	2008	Pre-combustion (NG processing)	Deep saline formations
Century Plant	US	8.4	2010	Pre-combustion (NG processing)	EOR
Air Products Steam Methane Reformer EOR Project	US	1	2013	Pre-combustion (gasification)	EOR
Petrobras Lula Oile Field CCS Project	Brazil	0.7	2013	Pre-combustion (NG processing)	EOR
Coffeyville Gasification Plant	US	1	2013	Industrial separation	EOR
Lost Cabin Gas Plant	US	1	2013	Pre-combustion (NG processing)	EOR

None of 12 projects in operation is in the power sector. All 12 projects separate CO_2 as a part of their normal operation; therefore the incurred fewer additional costs than would a CCS project in the power sector. In addition, most of them utilise the capture CO_2 for EOR. This

highlights the role of EOR in the deployment of CCS. Deep saline storage is implemented by two projects in Norway, but it should be noted that the carbon tax in Norway is a key driver for these projects. In addition these 12 projects capture and store only 25 million tonnes per year which is equivalent to 6.25% of CO_2 emission increase in 2012 and not enough to achieve the 2ºC goal (GCCSI, 2013).

2.3 Oxyfuel combustion

2.3.1 Process overview

Because this research focuses on the oxy-coal-fired power plants, a more detailed overview of oxyfuel combustion technology for CO_2 capture is provided in this section. The oxyfuel combustion technology was initially introduced for the purpose of enhanced oil recovery in 1982 (Abraham et al., 1982; Horn and Steinber, 1982). This technology was of great interest in the mid-90s when global warming effects started to gain public attention. The process flow diagram of an oxy-coal combustion process is illustrated in Figure 2.6 with indications of the necessary flue gas treatment units: Selective Catalytic Reduction (SCR) for NO_x removal, Electrostatic Precipitator (ESP) for particulate removal and Flue Gas Desulfurization (FGD). Nearly pure oxygen, supplied from an Air Separation Unit (ASU), is used for burning coal to produce a high CO_2 content flue gas. The current methods of oxygen production are cryogenic distillation, adsorption using multi-bed pressure swing units and polymeric membranes. However, to date cryogenic distillation is the most commercially efficient technique for large scale application of ASU (Toftegaard et al., 2010). The flue gas from oxy-combustion consists mainly of CO_2 and H_2O while some impurities, e.g. SO_x, NO_x, HCl, Ar and excess oxygen may be presented depending on the fuel and the particular oxy-combustion operation. A high CO2 content flue gas stream obtained from oxy-combustion can be easily purify using a compression and cooling technique. Ash resulting from combustion is normally removed by the ESP before a portion of flue gas is recycled back to the boiler.
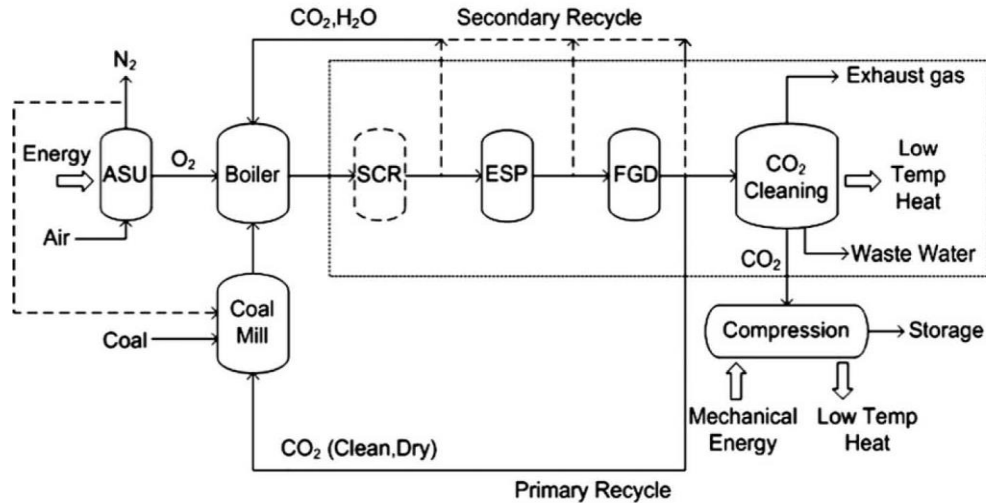
Figure 2.7 Process flow diagram of oxy-coal combustion system (Hadhipaschalis et al., 2009)

The recycle streams are necessary because the combustion of coal in pure oxygen results in a high flame temperature of about 3773 K (3500°C) which can damage the furnace materials. The acceptable combustion temperature in an oxy-coal-fired boiler is therefore limited to about 2173 K (IPCC, 2005). The recycled flue gas is used not only to control the combustion temperature but also to make up the volume of the missing N_2 to ensure there is enough gas to carry the heat through the boiler (Wall, 2007; Toftegaard et al., 2010). The ash-free flue gas is further cleaned in the flue gas desulphurization unit (FGD) and then fed to the CO_2 cleaning and compression. The combined CO_2 cleaning and compression units in Figure 2.7 are referred to as the CO_2 Capture and Purification Unit or CO_2CPU. In the CO_2CPU, the CO_2 is captured and purified from the treated flue gas containing inert impurities (e.g. N_2, O_2, Ar) and water, and then compressed to meet the transportation and storage site requirements. This technique offers the possibility of a zero-emission power plant using the oxyfuel combustion technology since almost all the CO_2 can be captured with this method (Jordal et al., 2004). Also, the fact that N_2 is eliminated from air prior to burn coal in the furnace reduces the overall gas flow rate and NO_x emissions from an oxy-coal-fired power plant. Moreover, the size of the boiler and flue gas treatment units in an oxy-coal-fired power plant

are smaller, less complex and less expensive than similar equipment used in conventional PC plants. Therefore, the capital and operating costs of an oxy-coal-fired power plant should be lower than that of a conventional PC plant. However, the cost of the ASU and additional CO_2CPU significantly reduce this potential economic benefit in oxy-combustion. As a result, the development of more efficient, less expensive ASU technology is a key continuing research challenge.

2.3.2 Current status of oxy-fired power plants

This section reviews the current status of the oxyfuel technology for power generation. Oxyfuel combustion is still under development and is not yet been demonstrated at full (commercial) scale in the power sector. However, individual component technologies are rather mature and ready for integration and demonstration at full-scale. ASUs are currently available at commercial scale. A single cryogenic ASU train can supply 5000 tonnes/day oxygen, and three trains of this capacity would be required to run a 2000 MWth oxy-fired power plant (GCCSI, 2012a). A number of vendors already deliver this ASU technology including Air Products, Air Liquide, Linde and Praxair. New ASU technologies are also under development using either membranes or oxygen-capturing adsorbents (Wall et al., 2011). Unlike ASUs, the CO_2CPU and oxy-fired boiler are not yet commercial, but the technologies are well developed and ready for integrating with other components. The current design of CO_2CPUs that is well suited for the oxy-fired power plant is based on an auto-refrigeration process (using the liquid CO_2 produced as the process refrigerant) since no external refrigerant is required, the process is more cost effective than other refrigeration processes. A number of test facilities using the auto-refrigeration CO_2CPU design have been built and research is currently underway to provide necessary information for full-scale oxy-fired power plants operation (Zanganeh et al., 2009; Wall et al., 2011; White et al., 2013). Air Products and Air Liquide are also leading vendors of the CO_2CPU technology. On the other hand, various aspects of the oxy-fired boiler have been studied, including flame characteristics, heat transfer, emissions, CFD modelling, slagging, fouling and corrosion. These studies were performed in both laboratory scale and pilot scale. Results of the research

confirm the technology's readiness for integrating into a full-scale demonstration (Buhre et al., 2005; Toftegaard et al., 2010; Davidson and Santos, 2010; Wall et al., 2011; Rubin et al., 2012).

Currently, there are five Large-Scale Integrated CCS Projects (LSIPs) based on oxyfuel combustion capture technology, but they are all still under planning (GCCSI, 2013). These LSIPs are developed for power generation but the construction period and expected start-up are still uncertain. Even though LSIPs of the oxyfuel capture technology is still under planning, numerous pilot-scale facilities and demonstration plants of oxy-fired power plants has been developed as shown in Figure 2.8.
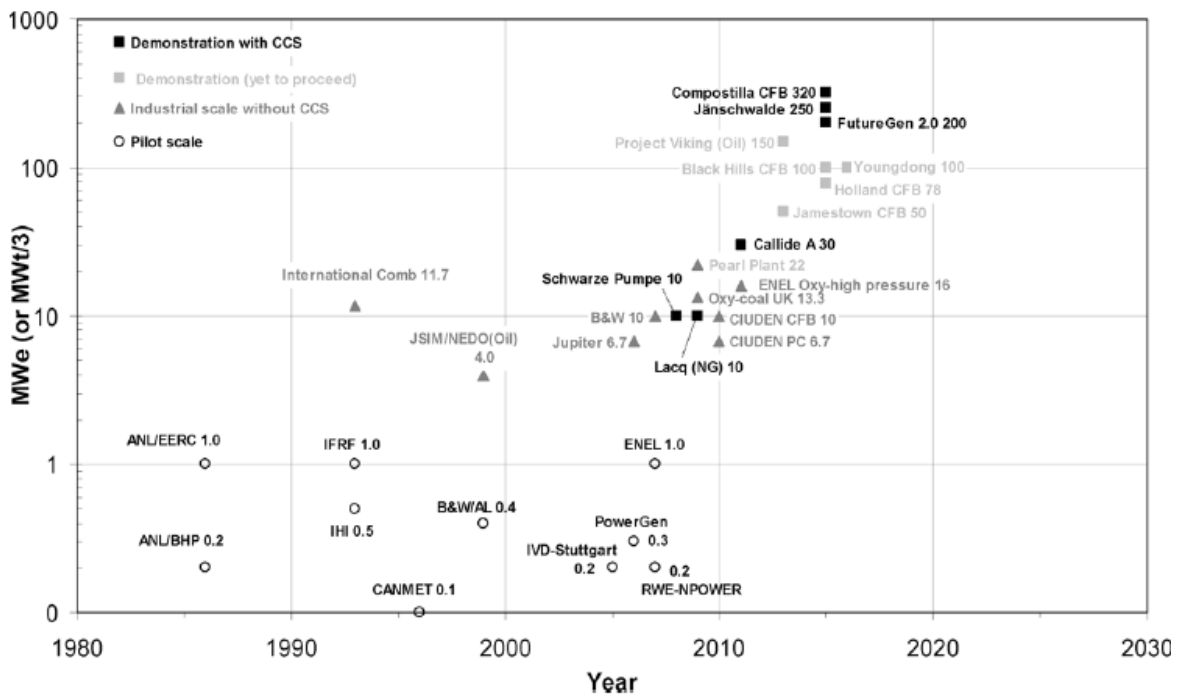
Figure 2.8 Progress towards large-scale demonstration and commercialisation plants of oxyfuel combustion technology (Wall et al., 2011)

In 2008, the world's first first full chain oxy-fuel pilot demonstration, Vattenfall's Schwarze Pumpe Pilot plant, came into operation in Germany. This pilot plant was designed for lignite with a capacity of 30 MWth. The test results are promising so far (Davidson and Santos,

20

2010; Wall et al., 2011; GCCSI, 2012a). TOTAL's Lacq project, the world's first integrated and industrial natural gas fired oxy-fuel plant was next in service in 2009 with a capacity of 30 MWth. This project included the CO_2 storage in the depleted gas reservoir. It is also the world's first pipeline injected oxy-fuel flue gas (Wall et al., 2011; GCCSI, 2012a). Two additional milestones in oxyfuel demonstration projects were recently achieved. In December 2011, CIUDEN's 30 MWth oxy-CFB (circulating fluidised bed) boiler was successfully tested in Spain (Wall et al., 2011; GCCSI, 2012a and 2012b). This plant is by far the largest pilot oxy-CFB plant in the world. In March 2012, CS Energy successfully converted a retired 100 MWth pulverized coal-fired to oxy-fired power plant at the Callide station in Queensland, Australia. The Callide project is the world's first full scale retrofit demonstration. These facilities are already well underway providing crucial information for technology scale-up. Insights into operation training and plant safety are also provided. The next milestone is to achieve the full-scale demonstration plant by 2018 ((Jäenschwalde in Gemany; Compostilla in Spain; FutureGen 2 in the US). The oxyfuel combustion technology is expected to be commercialised by 2020 (Davidson and Santos, 2010; Wall et al., 2011).

2.3.3 Oxyfuel combustion research challenges

According to pilot-plant testing, technical reports and academic studies, oxyfuel combustion is technically viable and economically competitive with other power generation technologies. Results obtained from test facilities are encouraging and promising. The technology is therefore one step toward commercialization. However, a number of barriers were also observed and further research is still required. Continuing research in oxyfuel combustion includes: (Wall et al., 2011; GCCSI, 2012):

- Non-cryogenic O_2 supply
- Higher efficiency steam circuit
- Boiler design optimised for higher O_2 concentration
- Biomass co-firing
- Thermally integrated waste heat streams
- Optimised CO_2 compression circuit

- Ultra-low emissions during wet compression
- Further vent gas treatment for higher capture efficiency
- Re-saleable use of CO_2 and acidic waste streams
- Transport of CO_2 via shared pipelines
- Start-up and shut-down procedure
- Control system

Oxy-fired power plants still require solutions reduce the energy consumption and enhance CO_2 capture and power plant efficiencies. Non-cryogenic technologies that can result in higher production rates at lower energy consumption are a research focus. To date, an ion transport membrane (ITM) is a promising O_2 supply technology. It is currently operated at pilot-scale and expected to expand to commercial scale by 2020 with a capacity up to 2000 t/day (Wall et al., 2011). Another option is the use of so-called chemical looping combustion. In a chemical looping system, the fuel is reacted with O_2 rather than air, similar to oxyfuel combustion, but the O_2 in this case is supplied by the metal oxide instead of ASU. Thus, the use of chemical looping can reduce the energy consumption and improve the power plant efficiency. To further improve the oxy-fired power plant efficiency, the use of biomass co-firing, high efficiency pressurized (supercritical or ultra-supercritical) steam cycle, and waste heat integration may also be considered. In addition, continued research on CO_2CPU is also required. The flexibility of CO_2CPU is needed to be analysed since the CO_2 capture efficiency (CO_2 product purity and CO_2 recovery) may be subject to change with fluctuating energy demand, operation of the boiler and price of carbon. Optimization of CO_2CPU capture efficiency and energy consumption is also required. In addition, process dynamics are required to develop proper start-up and shut-down procedures and design control systems for the oxy-fired power plant.

2.4 CO_2 compression (capture) and purification unit (CO_2CPU)

The CO_2 capture and purification unit (CO_2CPU) is a new concept for power plant operation. The flue gas from conventional combustion processes is normally released to the atmosphere

after treatment by several flue gas cleaning processes, such as ash removal and flue gas desulfurization. In the case of oxy-fuel combustion, the flue gas, consisting mainly of CO_2 and H_2O, is fed to the CO_2CPU in order to recover and purify the CO_2, and make it ready for transportation and sequestration. In 1999, a patent was issued to Reddy Satish (Satish, 1999) for an invention focused on a process in which CO_2 is separated from other gases using auto-refrigeration. This process compresses the flue gas and then cools the flue gas down to between -35°C and -55°C. A simple flash separation technique is then used to separate CO_2 from other gases. The tail gas and the liquidfied CO_2 produced from the flash separator remain at a very low temperature and are recirculated through the heat exchanger to assist in cooling the compressed flue gas. Hence, additional refrigerant is not required in this process. The auto-refrigeration process was extended to the new design including two-stage flash separation and presented in a report published by IEA Greenhouse Gas R&D Programme (Dillon et al., 2005). An analysis of the two-stage flash auto-refrigeration performance was also presented in this report. In 2006, Zanganeh et al., presented a pilot-scale CO_2 capture and compression unit (CO_2CCU) for integration with the CanmetENERGY's 0.3 MWth oxy-fuel combustion facility in Ottawa. This process was also designed based on two-stage flash auto-refrigeration, but a gas stream obtained from the first flash stage was partially recycled to the compressor train rather than entirely fed to the second-stage separation. The use of gas recycle stream differentiated the two-stage flash auto-refrigeration proposed by Dillon et al. (2005) from the CO_2CCU proposed by Zanganeh et al. (2006). A steady state model of CO_2CCU was developed in Aspen HYSYS using two refinery flue gas compositions (Zanganeh et al, 2006). The simulation results obtained from this study showed that the oxy-combustion CO_2 capture is a viable approach for the refinery flue gases. Another steady state process simulation of the CO_2CCU was published in 2009 (Zanganeh et al, 2009). Two case studies were performed using two different flue gas compositions to evaluate the effect of flue gas impurities on the CO_2CCU. The simulation results showed that the purity of captured CO_2 remains above 95% for both cases while the CO_2 recovery (the ratio of the amount of captured CO_2 in the product stream to the amount of CO_2 in the flue gas feed stream) decreases with increasing impurities in the flue gas stream. In 2010, a patent was

23

issued to Zanganeh and Shafeen (Zanganeh and Shafeen, 2010) for an invention of a CO_2CCU for capturing CO_2 from a mixed gas stream. Zanganeh and Shafeen (2010) claimed that the invented CO_2CCU is capable of handling a feed gas stream with CO_2 concentrations from 30% up to and exceeding 90%; and the CO_2 product purity remains at least 94%.

Pipitone and Bolland (2009) studied two purification techniques, i.e. flash separation and distillation, for capturing CO_2 in the flue gas stream obtained from two oxy-combustion power plants: natural gas fired plant and pulverized fuel fired plant. Steady state models were developed in SIMSCI PRO/II and used to determine the work and heat requirements for the purification process. The reduction in power plant output, CO_2 purity and CO_2 recovery of each separation techniques was also examined. They concluded that the flash separation technique is suitable for the low-impurity flue gas stream while distillation is suitable for the high-impurity flue gas stream.

Posch and Haider (2011) also evaluated the two-stage flash separation and distillation purification techniques for oxy-combustion plant. They simulated these two techniques in Aspen Plus using the Peng-Robinson equation of state and determined the specific compression power, specific cooling duty, CO_2 purity and CO_2 recovery. The effect of the Peng-Robinson mixing parameter (k_{ij}) was also analysed. Posch and Haider showed that the two-stage flash separation has the lower power and cooling requirements compared to the distillation technique while the k_{ij} mixing parameters of Peng-Robinson equation of state have a low influence on the purification process.

Fu and Gundersen (2011) evaluated three CO_2CPU configurations based on flash separation techniques for oxy-combustion plants, i.e., one-stage flash, two-stage flash and three-stage flash. They performed an exergy analyses and compared the performances of three CO_2CPU configurations using the exergy losses. Pinch analyses were also applied to determine the heat integration potential for reducing the power penalty (a reduction in power plant output) caused by CO_2CPU. Results showed that the plant performance can be improved by adding one additional stage of flash separation. However, a three-stage flash may not be attractive when an investment cost is considered since its performance is marginally more than the two-

stage flash configuration. A techno-economic analyse of these three CO_2CPU configurations was also performed by Fu and Gundersen (2012) who showed that the two-stage flash separation process is the most cost effective configuration. The design of the two-stage flash separation investigated by Fu and Gundersen is essentially similar to the design of the CO_2CCU proposed by Zanganeh et al, (2006).

The test results obtained from a pilot-scale CO_2 compression and purification plant was recently presented (White et al., 2013). This pilot plant was developed under a join collaboration agreement between Air Products and Vanttenfall, thus it was named as the Air Products-Vattenfall Oxyfuel CO_2 compression and Purification or ACPP. The ACPP is comprised of three main sub-units: sour compression, auto-refrigeration and membrane vent gas recovery. It is an advanced design of the one-stage flash auto-refrigeration process in which the SO_x and NO_x were removed by reacting with water and O_2 during compression (sour compression process) and the CO_2 in vent gas was recovered by membrane. The flue gas to the ACPP was taken from the Vanttenfall's 30 MWth oxyfuel pilot plant (OxPP). Experimental tests were carried out to investigate individual unit and evaluate the plant performance. Results obtained from tests are promising and support Air Products' proposed sour compression theory.

Recently, Besong et al. (2013) developed a steady state model of the CO_2CPU using Aspen HYSYS. Two configurations were considered (i.e. single flash and triple flash auto-refrigeration process). Both configurations were obtained from a patent invented by COSTAIN (a British construction and civil engineering company). Two sets of flue gas compositions were simulated to examine the effect of air ingress into the combustion process. The sensitivity analysis on the pressure in compressor train and a pinch analysis were also performed. It was observed that the triple flash separation process achieved a good performance (CO_2 purity > 98%, CO_2 recovery > 90%) over a wide range of feed conditions. The pinch analysis also indicated that the cold duty of the process streams was effectively utilized to supply the required refrigeration.

The operating conditions of the CO_2CPU determine the CO_2 product quality, energy consumption and the capital cost on the oxy-combustion plant. It is necessary, therefore, to ensure that this process can be operated at or near optimal conditions while meeting the product quality requirements. However, research on the dynamic behaviour of CO_2CPU is limited; only two simulation studies are available in the open literature. The first study is a collaborative project undertaken by Doosan Power Systems, Air Products, RWE npower, and the University of Edinburgh (Kuczenski, 2011); a dynamic model of an oxy-combustion process including air separation unit (ASU), boiler, turbine system and CO_2CPU, and the associated control systems was developed using a proprietary in-house simulation package and Aspen HYSYS®, a commercial simulation package. For the CO_2CPU, a dynamic model and control system were developed by Air Products using Aspen HYSYS®, however dynamic test results were not provided. In the second study, Pottman et al (2011) developed a dynamic model of the CO_2CPU using a proprietary in-house simulation package together with Honeywell's Unisim® simulator. Dynamic tests were applied to the model by changing the feed conditions, i.e. flow rate and CO_2 concentration, and dynamic responses were illustrated. However, mathematical models and details of basic control strategy development were not provided in either of the two studies above. Thus, research on dynamic modelling and control system development is still required for demonstrating the operability and controllability of oxy-combustion power plants.

2.5 Canadian Carbon Capture and Storage

2.5.1 Canada action on climate change

In 2011, Canada emitted approximately 530 $MtCO_2$ accounting for about 1.7% of the global CO_2 emissions in that year. CO_2 emissions increased by 1.3% year-over-year from 2010 (IEA, 2013). Even though Canada contributes a small share of the global CO_2 emissions, the Government of Canada is aware that climate change is a global challenge requiring a global solution. Thus, the Government of Canada supports efforts to protect the environment by developing policies and programs, conducting scientific research, and working with both national and international partners in the fight against climate change. Canada signed onto

the Copenhagen Accord in December 2009 and committed to reduce its greenhouse gas (GHG) emissions to 17% below 2005 levels (607 $MtCO_2e$) by 2020 (Environment Canada, 2012). This target was released nationally in January 2010 and the first investment in action on climate change was made in April 2010 by $500 million to support research in greenhouse gas emissions from building construction. Another action, in August 2010, required 5% renewable fuel content in gasoline. In 2011, $240 million was provided to support the Boundary Dam carbon capture and storage project, in Saskatchewan. In September 2012 the final regulation to reduce the greenhouse gas emissions from coal-fired electricity generation was released. Under this regulation new coal-fired electricity generation units and end-of-life units (operated more than 45 years) must achieve the standard performance of 375 grams carbon dioxide equivalent (CO_2e) per kilowatt-hour (420 t/GWh). This performance is equivalent to a high-efficiency type of natural gas generation plants. Thus, it is expected that this regulation will decrease 33% of GHG emission from electricity generation and thus step toward meeting the Canada's Copenhagen target by 2020. In addition, it is expected that the use of high standard performance will increase an annual capital expenditures of coal-fired power plants; thereby the coal is likely displaced by natural gas and other clean power technologies. The international institute for sustainable development (IISD) estimated that by 2020 18% of baseline coal-fired power plants will be integrated with CCS while 77% will be replaced by natural gas plants, and the rest will be based on renewables (Sawyer and Stiebert, 2012). With the current measures from federal, provincial and territorial governments, it is projected that the Canada's GHG emissions will be reduced to 720 $MtCO_2e$, half of its national effort to meet its Copenhagen target (Environment Canada, 2012), by 2020 as illustrated in Figure 2.9. However, there is still a gap to between the current projection and the target. This means that Canada will fail to achieve its 2020 Copenhagen target if comprehensive policies and regulations are not come in place to widespread deployments of low-carbon energy or CCS technologies.
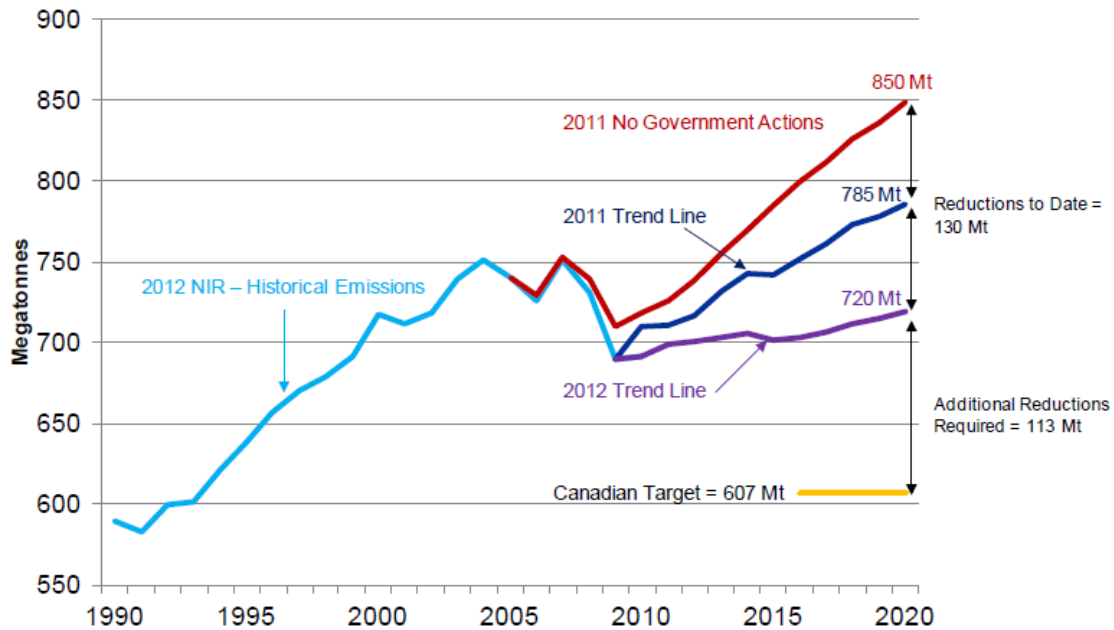
Figure 2.9 Scenarios of Canadian Emissions to 2020 (MtCO2e) (Environment Canada, 2012)

2.5.2 CCS projects in Canada

With strong regulations and continued federal support, Canada is at the leading edge of clean energy technologies to reduce the GHG emissions. Canada is one of the leaders in the development and deployment of CCS that has one large-scale fully-integrated CCS project (LSIPs) in commercial operation and another four projects under development. In 2014, Canada will make remarkable progress on large-scale CCS deployment when the Boundary Dam Integrated CCS demonstration project comes into operation, since this project will be among the first projects globally to integrate capture and storage associated with power generation (GCCSI, 2013).

28

Table 2.2 Active LSIPs in Canada

Project name	Stage	CO$_2$ (MtPA)	Start up	Capture type	Storage type	Industry
Great Plains Synfuel Plant and Weyburn-Midale Project	Operate	3	2000	Pre-combustion (gasification)	EOR	Synthetic natural gas
Alberta Carbon Trunk Line (ACTL) with Agrium CO$_2$ Stream	Execute	0.6	2015	Industrial separation	EOR	Fertiliser production
Alberta Carbon Trunk Line (ACTL) with North West Sturgeon Refinery CO$_2$ stream	Execute	1.2	2016	Pre-combustion (gasification)	EOR	Oil refining
Boundary Dam Integrated CCS Demonstration Project	Execute	1	2014	Post-combustion	EOR	Power generation
Quest	Execute	1.1	2015	Pre-combustion (gasification)	Onshore deep saline formation	Hydrogen

Recently, Canada's federal and provincial governments have committed a total of $3 billion in funding for CCS, which could lead to about six additional large-scale demonstration projects in Canada (Canada action on climate change, 2013). In addition to LSIPs, a number of research centres and test facilities were built to supports the pursuit of CCS development and deployment in Canada. Research focuses are on near-zero emissions oxyfuel technologies for pulverized coal-fired power plants, oxyfuel circulating fluidized bed combustion, high-pressure oxyfuel combustion, feasibility studies of oxyfuel combustion, gasification for CCS, computational fluid dynamics (CFD) modelling of oxyfuel combustion, CO$_2$ capture and compression technologies, post-combustion CO$_2$ capture, and advanced power cycle. The ultimate goal is to identify technologies strategies, processes and integration system pathways needed to allow CO$_2$ to be captured and stored in Canada (CanmetENERGY, 2013).

Chapter 3
Dynamic Modelling

This chapter describes a dynamic modelling of the CO_2 capture and purification unit (CO_2CPU). Because two configurations of the CO_2CPU were considered in this study, i.e. the Air Products' CO_2CPU and the CanmetENERGY's CO_2CPU (CanCO$_2$), the first section provides the process flow diagram and the process description of each plant. Fundamental laws related to chemical process modeling are also reviewed in this chapter. The conservation laws of mass and energy, which are basic equations in all unit operation models, were first presented in a general form for control volume analysis, and the Peng-Robinson equation of state used for physical and thermodynamic properties calculations are subsequently described. Mathematical models and sizing equations of each unit operation in the CO_2CPU, i.e., compressor, expander, flash drum, heater, cooler and multi-stream heat exchanger are provided afterwards. Procedures to develop the dynamic model of the Air Products' CO_2CPU and the CanCO$_2$ are explained in the last section of this chapter.

3.1 CO_2 capture and purification unit (CO_2CPU)

Two configurations of the CO_2CPU were considered in this study. Both configurations are based on a two-stage flash separation. The process description and the process flow diagram of each plant are provided below.

3.1.1 The Air Products' CO_2CPU

The IEA Greenhouse Gas R&D programme commissioned Mitsui Babcock to perform a study on feasibility and costs for CO_2 capture using oxy-combustion technology in 2005 (Dillon et al, 2005). Air Products plc., as a project partner, designed the CO_2CPU for a 500 MWe pulverized bituminous oxy-fired power plant using an in-house proprietary simulation package. This design was based on two-stage flash separation, as shown in Figure 3.1 (Dillon et al, 2005).
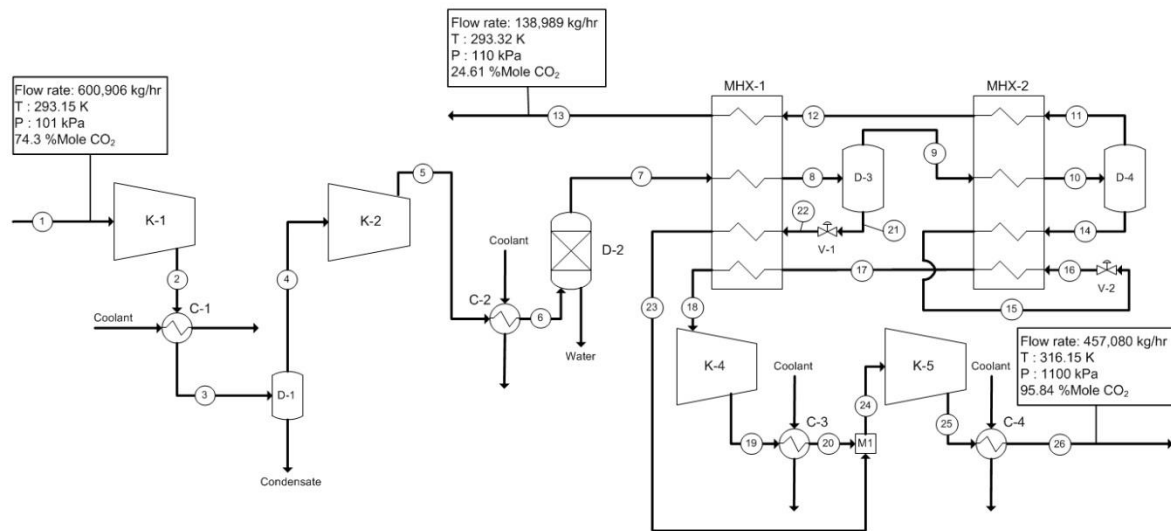
Figure 3.1 The Air Products' CO_2CPU (Dillon et al, 2005)

The flue gas from the oxy-fuel combustion process with high CO_2 content (stream 1) is sent to a compressor (K-1). The compressed flue gas is passed through a cooler, C-1, to recover high grade heat and reduce the flue gas temperature (the first step in the condensation process). The condensates contained in the flue gas stream are removed in an inter-stage separator, D-1, before the flue gas stream flows to a second compressor, K-2. The resulting compressed gas stream from K-2 is passed through another cooler (C-2) that decreases the flue gas temperature to 293.15 K. Residual water is removed from the flue gas stream in a bed dryer, D-2. The compressed flue gas free of condensates (stream 7) flows through a multi-stream heat exchanger (MHX-1). After cooling in MHX-1, stream 7 separates into two phases (stream 8) which are separated in flash drum, D-3. The liquid stream, rich in CO_2 (stream 21) leaving D-3, passes through a throttle valve (V-1) and is fed back as a coolant to MHX-1 (stream 22) while the vapour stream (stream 9), which contains impurities (Ar, N_2, O_2, SO_2, NO) and the remaining CO_2, is sent to a second multi-stream heat exchanger, MHX-2, for further CO_2 condensation. The CO_2 separation occurs in flash drum, D-4, similar to D-3. The gas stream, poor in CO_2, (stream 11), coming from D-4 is used as a coolant in both

heat exchangers, i.e., MHX-1 and MHX-2, and then vented to the atmosphere. The purified liquid CO_2 stream from D-4 (stream 15) is throttled (V-2) again and used as a coolant in heat exchangers MHX-1 and MHX-2 resulting in a vapour phase stream (stream 18). Since streams 18 and 23 are vapour, they are compressed in K-4 and K-5 to produce the purified high pressure CO_2 stream, (stream 26). The cooler, C-3, located after K-4, is used to reduce the temperature of the gas sent to K-5 while a cooler, C04, is used to decrease the temperature of the CO_2 product stream down to about 313.15 K making it suitable for transport and sequestration. The flue gas specifications considered in Dillon's study is presented in Table 3.1. It should be noted that the Air Products' CO_2CPU was considered to be located after the flue gas cleaning unit in the oxy-fired power plant. Therefore, the flue gas is free of particulates and the contents of NO_x and SO_x are small as presented in Table 3.1. According to this flue gas composition, the Air Products' CO_2CPU produces a CO_2 product with 95% purity that satisfies the basic requirements for sequestration (ANLECR&D, 2009). The CO_2 recovery, which is the ratio of the amount of captured CO_2 in the product stream to the amount of CO_2 in the flue gas feed, is approximately 91%.

Table 3.1 Flue gas specification for the Air Products' CO_2CPU model (Dillon et al, 2005)

Temperature (K)	293.15
Pressure (bar)	1
Mass flow rate (kg/hr)	600906
Composition (%mol)	
CO_2	74.3
O_2	6.1
Ar	2.4
N_2	15.0
H_2O	1.8
SO_2	0.3
NO	0.0

3.1.2 The CanmetENERGY's CO_2CPU (CanCO$_2$)

The first advanced oxy-combustion pilot-scale research facility in Canada was built in 1995 by CanmetENERGY in Ottawa. This facility supports experimental investigation of oxy-fuel combustion of various fuels, e.g., natural gas, coal, heavy oil, bitumen, bitumen emulsion, petcoke, for conventional and advanced processes and integration with flue gas cleaning technologies. In parallel, CanmetENERGY has been pursuing research and development in CO_2 capture and compression technology to recover CO_2 from oxyfuel-derived flue gas streams and to its further processing so that it meets the required specifications for transportation and storage. CanmentENERGY has developed a proprietary CO_2 capture process and built a novel trailer-mounted configuration of pilot-scale CO_2 capture and compression unit (Figure 3.2), which facilitates the transportation and relocation of the unit for field demonstration using slip-stream feed gases from large-scale commercial plants (Zanganeh et al., 2009).

Figure 3.2 Trailer-mounted configuration of pilot-scale CanCO$_2$ (Zanganeh et al., 2009)

This pilot-scale capture facility, also referred to as CanCO$_2$, is being used for CO_2 capture and multi-pollutant control experiments since 2008. The advanced pilot-scale CanCO$_2$ integrated with the oxy-fuel combustion facility at CanmetENERGY provides an excellent

platform for testing and demonstration of integrated oxy-fuel carbon capture system. The process flow diagram of CanCO$_2$ is shown in Figure 3.3.
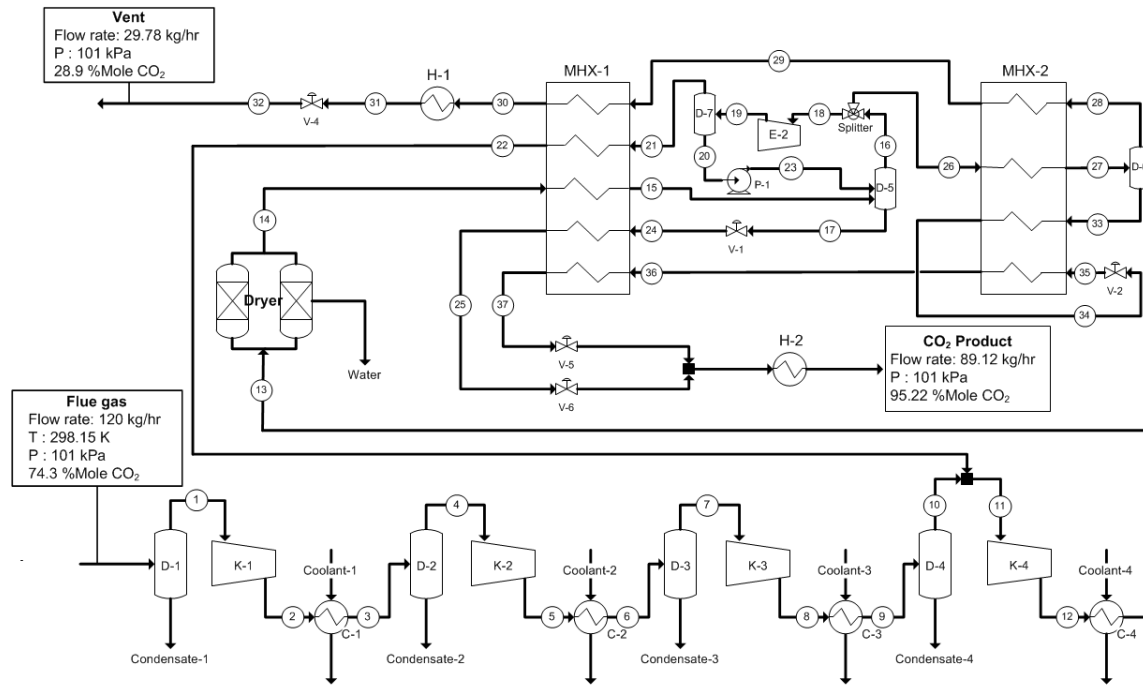
Figure 3.3 CanCO$_2$ process flow diagrams

Basically, the operation of CanCO$_2$ is similar to the Air Liquids's CO$_2$CPU. The flue gas is compressed to about 30 bars and then cooled down to about 248.15 K through the first multi-stream heat exchanger (MHX-1), and further reduced to about 218.15 K through the second multi-stream heat exchanger (MHX-2). Consequently, the liquid CO$_2$ can be captured in D-5 and D-6. But in the CanCO2, only 70% of the vapour leaving from D-5 (stream 16) is sent to MHX-2. The rest of vapour (stream 18) is expanded and further cooled down. Thus, more CO$_2$ can be recovered in D-7. The liquid CO$_2$ (stream 20) is pumped back to D-5 and mixed with the liquid CO$_2$ recovered from stream 15 in D-5. The CO$_2$-rich streams from D-5 and D-6 (stream 24 and 36 respectively) are also used as a coolant in MHX-1 and then expanded via the valves V-4 and V-5. A mixture of these two process streams is a CO$_2$ product at a pressure of 1 bar. On the other hand, the vapour stream leaving from D-7 (stream 21) is also advantageously used as a coolant in MHX-1 and then recycled to the compressor train. This

34

recycle stream improves the overall CO_2 recovery of the $CanCO_2$, but slightly decreases the CO_2 product purity. The impact of the recycle stream on the $CanCO_2$ capture performance is described in chapter 5. According to the flue gas composition shown in Table 3.2, the $CanCO_2$ achieves 88.7% CO_2 recovery and produce a CO_2 product stream with 95% purity, similar to the Air Products' CO_2CPU. It is noted that the only difference between flue gas specifications of the Air Products' CO_2CPU and the $CanCO_2$ is the mass flow rate. Everything else it pretty much the same. Also, the flue gas is assumed to be particulates-free.

Table 3.2 Flue gas specification for the $CanCO_2$ model

Temperature (K)	298.15
Pressure (bar)	1
Mass flow rate (kg/hr)	120
Composition (%mol)	
CO_2	74.3
O_2	6.1
Ar	2.4
N_2	15.0
H_2O	1.8
SO_2	0.3
NO	0.0

3.2 Basic equations for dynamic modelling

The conservation laws of mass and energy used to develop mathematical models for each unit operation are presented in this section in a general form for control volume analysis. The Peng-Robinson equation of state (EOS) used to calculate thermal and physical properties in the CO2CPU model is also described in this section.

3.2.1 Conservation of mass

As a quantity of mass flows across the boundary of a control volume, the conservation of mass can be expressed for one-dimensional flow model as follows (Moran and Shapiro, 2010):

$$\frac{dm_{CV}}{dt} = \sum_i \dot{m}_i - \sum_e \dot{m}_e \qquad (3.1)$$

Where m_{CV} is the mass within the control volume, and $\dot{m}_i$ and $\dot{m}_e$ are the instantaneous mass flow rate at the inlet and exit of the control volume (Figure 3.4) respectively.
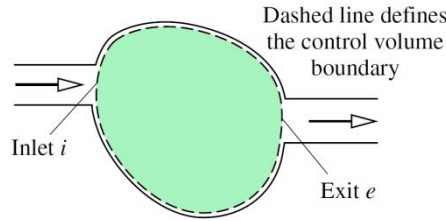
Figure 3.4 One-dimensional control volume (Moran and Shapiro, 2010)

Another form of conservation of mass can be illustrated by considering a quantity of mass flowing with velocity v across an incremental area dA in a time interval Δt. Then, the rate of mass flows across the control volume boundary is as follows:

$$\dot{m} = \int_A \rho v_n dA \qquad (3.2)$$

where the area integrals are over the areas through which the mass enters or exits the control volume and v_n denotes the relative velocity normal to dA in the direction of flow. The product ρv_n is known as the mass flux. The conservation of mass can be expressed in the integral form as follows:

$$\frac{d}{dt} \int_V \rho dV = \sum_i \left(\int_A \rho v_n dA \right)_i - \sum_e \left(\int_A \rho v_n dA \right)_e \qquad (3.3)$$

3.2.2 Conservation of energy

The conservation of energy for a control volume states that the rate of energy within the control volume equals the difference between the rates of energy transfer in and out across

the boundary. Thus, the control volume energy rate balance can be obtained by taking into account the rate of transfer of internal, kinetic and potential energy accompanying by the mass flow in and out of the control volume. For the one-dimensional flow, the conservation of energy is given as follows (Moran and Shapiro, 2010):

$$\frac{dE_{CV}}{dt} = \dot{Q} - \dot{W} + \dot{m}_i \left(u_i + \frac{v_i^2}{2} + gz_i \right) - \dot{m}_e \left(u_e + \frac{v_e^2}{2} + gz_e \right) \tag{3.4}$$

where E_{CV} denotes the energy of the control volume at time t. The terms $\dot{Q}$ and $\dot{W}$ represent the net rate of energy transfer by heat and work across the boundary of the control volume, respectively. The rate of work, $\dot{W}$, can be separated into two contributions which are the work associated with the fluid pressure and all other work effects associated with rotating shaft and electrical effects. Accordingly, the term $\dot{W}$ can be written as follows:

$$\dot{W} = \dot{W}_{CV} + \left(P_e A_e \right) v_e - \left(P_i A_i \right) v_i \tag{3.5}$$

Where the term PA represents the normal force at the control volume boundary. The product of the normal force multiplied by the fluid velocity is thus the work associated with the pressure at the inlet and exit of the control volume. The parameter $\dot{W}_{CV}$ accounts for the remaining energy transfers by work across the boundary of the control volume. Equation (3.5) can be rewritten as follows:

$$\dot{W} = \dot{W}_{CV} + \dot{m}_e \left(P_e V_e \right) - \dot{m}_i \left(P_i V_i \right) \tag{3.6}$$

where V_i and V_e are the specific volumes evaluated at the inlet and exit, respectively. Combining equations (3.4) and (3.6) yields

$$\frac{dE_{CV}}{dt} = \dot{Q} - \dot{W}_{CV} + \dot{m}_i \left(u_i + P_i V_i + \frac{v_i^2}{2} + gz_i \right) - \dot{m}_e \left(u_e + P_e V_e + \frac{v_e^2}{2} + gz_e \right) \tag{3.7}$$

37

with the definition of enthalpy, $h = u + PV$, the conservation of energy for a control volume becomes

$$\frac{dE_{CV}}{dt} = \dot{Q} - \dot{W}_{CV} + \sum_i \dot{m}_i \left(h_i + \frac{v_i^2}{2} + gz_i \right) - \sum_e \dot{m}_e \left(h_e + \frac{v_e^2}{2} + gz_e \right) \tag{3.8}$$

3.2.3 Peng-Robinson Equation of State

The equation of state (EOS) that determines the relationship between pressure (P), temperature (T) and molar volume (V_m) of substances is a key fundamental aspect for process modeling since it is used to predict the physical properties of the system. The equation of state has to be selected based on the nature of the process. The more rigorous the equation of state, the more accurate the predictions will be. A number of equations of state have been developed for gas and liquid systems. One of these equations of state is the Peng-Robinson EOS which is well suited for gas processing that contains non-polar or mildly polar components. The Peng-Robinson equation of state is presented in equation (3.9). This equation is relevant for this project since it will be used to simulate the CO_2CPU process (Peng and Robinson, 1976).

$$P = \frac{RT}{\left(V_m - b_i \right)} - \frac{a_i}{V_m \left(V_m + a_i \right) + b_i \left(V_m - b_i \right)} \tag{3.9}$$

where
$$a_i = \alpha_i 0.45724 \frac{R^2 T_{ci}^2}{P_{ci}} \tag{3.10}$$

$$b_i = 0.07780 \frac{RT_{ci}}{P_{ci}} \tag{3.11}$$

$$\alpha_i = \left[1 + m_i \left(1 - T_{ri}^{1/2} \right) \right]^2 \tag{3.12}$$

$$m_i = 0.37464 + 1.54226 \omega_i - 0.26992 \omega_i^2 \tag{3.13}$$

The acentric factor, ω_i, is a parameter used to characterize the shape of a molecule. The parameters, T_{ci} and P_{ci}, represent the critical temperature and pressure whereas T_{ri} is the

38

reduced temperature of each substance (i.e. T/T_{ci}). Another form of the Peng-Robinson EOS can be written in term of compressibility factor, Z, as follows:

$$Z^3 - (1-B)Z^2 + (A - 3B^2 - 2B)Z - (AB - B^2 - B^3) = 0 \tag{3.14}$$

where

$$A = \frac{aP}{RT^2} \tag{3.15}$$

$$B = \frac{bP}{RT} \tag{3.16}$$

$$Z = \frac{PV_m}{RT} \tag{3.17}$$

In a mixture, the mixing rule is applied to calculate the parameters a and b as follows:

$$a = \sum_{i=1}^{n} \sum_{j=1}^{n} x_i x_j \sqrt{a_i a_j} \left(1 - k_{ij}\right) \tag{3.18}$$

$$b = \sum_{i=1}^{n} x_i b_i \tag{3.19}$$

In equation (3.18), k_{ij} is a binary parameter to determine the binary interaction between component i and component j. This parameter can be obtained from the regression of phase equilibrium data.

3.3 Mathematical modelling

The CO_2CPU is comprised of compressors, expanders, flash drums, heaters, coolers and multi-stream heat exchangers, as shown in Figure 3.1 and 3.3. Mathematical models of each unit operation are provided below. Sizing equations are also described for the flash drum and the heat exchanger models.

3.3.1 Compressor

A compressor model was developed based on the polytropic real gas compression method proposed by Schultz (1962). The main consideration of compressor modeling is to determine the total work required for process operation. Thus, the present model analysis assumes infinitely fast dynamics; negligible hold-up and inertia of gases within the compressor; and no heat input. Also, changes of potential and kinetic energy are considered negligible in this unit. The theoretical work of compressor, or compressor head, can be obtained from the relationship between the measurable process variables, P and V, as follows:

$$W_P = \int_{P_1}^{P_2} V dP \tag{3.20}$$

Polytropic compression is a reversible process with heat transfer and variable entropy. The relationship between P and V can be determined using (3.21) while the compressor head can be calculated as shown in (3.24).

$$PV^n = const \tag{3.21}$$

$$P_1 V_1^n = P_2 V_2^n = const \tag{3.22}$$

Rearranging (3.22) and substituting V into (3.20) yields:

$$W_P = \int_{P_1}^{P_2} V_1 \left(\frac{P_1}{P} \right)^{1/n} dP \tag{3.23}$$

Integrating equation (3.23) results in

$$W_P = \left(\frac{n}{n-1} \right) Z_1 R T_1 \left[\left(\frac{P_2}{P_1} \right)^{(n-1)/n} - 1 \right] \tag{3.24}$$

The polytropic exponent, n, depends on the design and operation of the compressor. It can be approximated as a slope of a plot of log P versus log V observed from the polytropic compression. In this work, the real gas compression theory proposed by Schultz (1962) was used to develop a compressor model. To calculate the value of n for the real gas system, Schultz proposed two generalized compressibility functions, X and Y, as follows:

$$X = \frac{T}{V}\left(\frac{\partial V}{\partial T}\right)_P - 1 \tag{3.25}$$

$$Y = -\frac{P}{V}\left(\frac{\partial V}{\partial P}\right)_T \tag{3.26}$$

Recalling a general equation of state for any gas

$$PV = ZRT \tag{3.27}$$

The two derivative terms in equation (3.25) and (3.26) can be found by differentiation of equation (3.27) as shown in equation (3.28) and (3.29) respectively.

$$\left(\frac{\partial V}{\partial T}\right)_P = \frac{R}{P}\left[Z + T\left(\frac{\partial Z}{\partial T}\right)_P\right] \tag{3.28}$$

$$\left(\frac{\partial V}{\partial P}\right)_T = \frac{R}{P}\left[T\left(\frac{\partial Z}{\partial P}\right)_T - \frac{V}{R}\right] \tag{3.29}$$

At this point, the cubic form of Peng-Robinson EOS (equation 3.14) was used to derive the two derivative terms of the compressibility factor, Z, in equation (3.28) and (3.29). Solutions of the Peng-Robinson EOS for $\left(\frac{\partial Z}{\partial T}\right)_P$ in equation (3.28) is:

$$\left(\frac{\partial Z}{\partial T}\right)_P = \frac{(B-Z)\left(\frac{\partial A}{\partial T}\right)_P + \left(-Z^2 + 2Z + 6BZ + A - 2B - 3B^2\right)\left(\frac{\partial B}{\partial T}\right)_P}{3Z^2 - 2(B-1)Z + \left(A - 2B - 3B^2\right)} \qquad (3.30)$$

where
$$\left(\frac{\partial A}{\partial T}\right)_P = \frac{P}{R^2 T^2}\left(a' - \frac{2a}{T}\right) \qquad (3.31)$$

$$\left(\frac{\partial B}{\partial T}\right)_P = \frac{-bP}{RT^2} \qquad (3.32)$$

$$a' = \frac{-m_i a_i}{\sqrt{\alpha_i T \cdot T_{ci}}} \qquad (3.33)$$

The derivative term, $\left(\dfrac{\partial Z}{\partial P}\right)_T$, in equation (3.29) is:

$$\left(\frac{\partial Z}{\partial P}\right)_T = \frac{(B-Z)\left(\frac{\partial A}{\partial P}\right)_T + \left(-Z^2 + 2Z + 6BZ + A - 2B - 3B^2\right)\left(\frac{\partial B}{\partial P}\right)_T}{3Z^2 - 2(B-1)Z + \left(A - 2B - 3B^2\right)} \qquad (3.34)$$

where
$$\left(\frac{\partial A}{\partial P}\right)_T = \frac{a}{R^2 T^2} \qquad (3.35)$$

$$\left(\frac{\partial B}{\partial P}\right)_T = \frac{b}{RT} \qquad (3.36)$$

Note that A, B, a, a_i, b and α_i are Peng-Robinson EOS coefficients provided in section 3.2.3.

Two generalized compressibility functions, X and Y, proposed by Schultz can be used not only for calculating the polytropic exponent, n, but also to determine a polytropic temperature exponent, m, for calculating the outlet temperature, as follows:

$$T_2 = T_1 \left(\frac{P_2}{P_1} \right)^m \tag{3.37}$$

where
$$m = \frac{ZR}{C_P} \left(\frac{1}{\eta_P} + X \right) \tag{3.38}$$

The polytropic efficiency can be calculated as follows:

$$\eta_P = \frac{\text{Polytropic work}}{\text{Actual work required}} = \frac{\int_{P_1}^{P_2} V dP}{h_2 - h_1} \tag{3.39}$$

Thus, the polytropic exponent can be calculated from

$$n = \frac{1}{Y - m(1 + X)} \tag{3.40}$$

Because T, V, P, C_p, and Z used in equation (3.25)-(3.36) are mean values, a trial-and-error solution shown in Figure 3.5 was implemented in gPROMS in order to predict the compressed gas outlet temperature and the polytropic work required by the compressor. The initial polytropic exponent, m^0, was calculated using the heat capacity ratio, k, and the initial guess of polytropic efficiency and then used in equation (3.37) to calculate the initial outlet temperature, T_2^0. The mean pressure and temperature required for calculating V, C_p, X, Y and Z can be obtained afterwards. The iterative calculation is repeated until the outlet temperature is matched between the previous and current iteration.
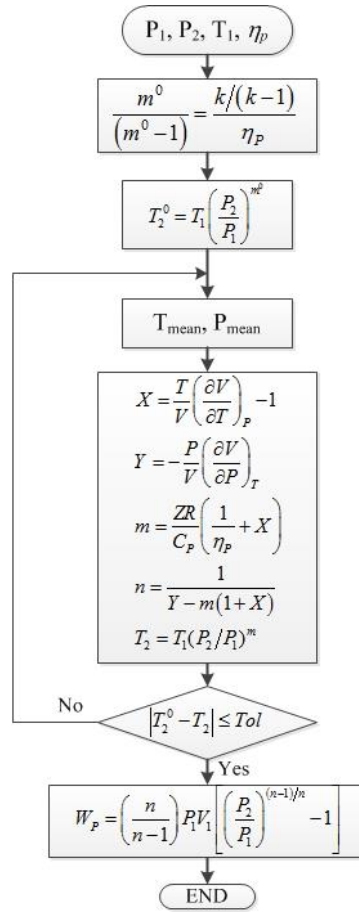
Figure 3.5 Real gas compression calculation flow chart

3.3.2 Expander

An expander model was developed using the same approach as the one implemented in the compressor model. The differences between an expander model and a compressor model are the equations to calculate the polytropic efficiency and the polytropic temperature exponent m. For expansion, the polytropic efficiency is defined as (Sinnott,, 2005):

$$\eta_P = \frac{\text{Actual work obtained}}{\text{Polytropic work}} \tag{3.41}$$

Consequently, the polytropic temperature exponent m can be obtained from equation (3.42) rather than equation (3.38) which is used for the compression system (Sinnott,, 2005)

44

$$m = \frac{ZR}{C_P}\left(e + X\right)$$
(3.42)

3.3.3 Flash drum

After compression and cooling, the flue gas is partially condensed and fed to a vapour-liquid separator where the liquid stream containing mainly CO_2 is separated from the vapour stream. A mathematical model and sizing equation of the flash drum are provided below.

3.3.3.1. Mathematical model

It was assumed that the vapour and liquid phases are in equilibrium, and tha tthere is no vapour hold-up in the drum. In addition, the flash drum was assumed to be operating isothermally at its inlet stream's temperature and pressure; i.e. no additional heating or cooling is required to separate the CO_2 from the flue gas. A separator is considered as a control volume that has one inlet stream and two outlet streams, i.e. vapour stream and liquid stream. Since there is no chemical reaction occurring inside the separator, equation (3.1) can be written on a molar basis as follows.

$$\frac{d(M_{cv})}{dt} = F - V - L$$
(3.43)

M_{cv} is the liquid molar hold-up while F, V and L are molar flow rates of feed stream, vapour product stream and liquid product stream, respectively. The M_{cv} can be obtained from equation (3.44) while L is calculated using the Bernoulli and continuity equations for ideal liquid flow through a pipe, as shown in equation (3.45) (Chalupa et. al., 2012). Thus, the liquid level of the drum can be monitored and the level control can be developed for safe operation.

$$M_{cv} = \frac{\rho \times A \times h}{MW}$$
(3.44)

$$L = \frac{c_v \times A_v \times \rho \times \sqrt{2gh}}{MW}$$
(3.45)

Where c_v is a flow coefficient and A_v is the flow area related to the valve position as:

$$A_v = s \cdot A_{v,\max} \qquad (3.46)$$

Where s is the stem valve position and $A_{v,max}$ is the maximum flow area of the valve.

In addition, the component balance given in equation (3.47) is also required in a separator model in order to calculate the compositions of the vapour and liquid streams.

$$\frac{d(M_{cv} \cdot x_i)}{dt} = F \cdot z_i - V \cdot y_i - L \cdot x_i \qquad (3.47)$$

In a vapour-liquid separator model, the relation between vapour phase composition (y_i) and liquid phase compositions (x_i) is determined by the vapour-liquid phase equilibrium. Phase equilibrium is required for the design of all separation processes that depend on differences in concentration between phases. The criterion for thermodynamic equilibrium between two phases of a multicomponent mixture is that for every component, i:

$$f_i^V = f_i^L \qquad (3.48)$$

where f_i^V and f_i^L are the vapour-phase and liquid-phase fugacity of component i, respectively. For a pure, ideal gas, the fugacity equals the pressure, and for a component in an ideal gas mixture, the fugacity of component i equals its partial pressure. Due to the close relationship between fugacity and pressure, it is convenient to define the ratio of fugacity to pressure as a fugacity coefficient, ϕ_i.

$$\phi_i^V = \frac{f_i^V}{y_i P} \qquad (3.49a)$$

$$\phi_i^L = \frac{f_i^L}{x_i P} \qquad (3.49b)$$

The superscripts V and L refer to the vapour and liquid phases, respectively. Substituting equations (3.49a) and (3.49b) into equation (3.48):

$$\phi_i^V y_i = \phi_i^L x_i \qquad (3.50)$$

The ratio between vapour phase composition (y_i) and liquid phase compositions (x_i) at equilibrium condition is defined as a *K*-value. Thus, the *K*-value can be calculated from liquid and vapour fugacity coefficients, as expressed in equation (3.52). In this work, the fugacity coefficient of each phase is provided by the Multiflash™ property package based on the Peng-Robinson equation of state.

$$K_i \equiv \frac{y_i}{x_i} \qquad (3.51)$$

$$K_i = \frac{\phi_i^L}{\phi_i^V} \qquad (3.52)$$

3.3.3.2. Equipment sizing

In this study, all vapour-liquid separators in the CO_2CPU are oriented vertically and have a demister pad installed. A separator diameter depends on the maximum vapour velocity in a disengagement section which is calculated from the following equation (Hall, 2012).

$$u_{V,max} = K_V \left(\frac{\rho_L - \rho_V}{\rho_V} \right)^{0.5} \qquad (3.53)$$

Where K_v is a factor for vertical separator design obtained from (Barton, 1974):

$$K_V = \exp\left(-1.94 - 0.815X - 0.179X^2 - 0.0124X^3 + 0.0039X^4 + 0.00026X^5\right) \qquad (3.54)$$

where $\qquad X = \ln\left(\frac{W_L}{W_V} \sqrt{\frac{\rho_V}{\rho_L}} \right) \qquad (3.55)$

W_L *and* W_V represent the mass flow rates of liquid phase and vapour phase, respectively. Once the maximum vapour velocity in the disengagement section is determined, the minimum cross-sectional area and diameter of the separator can be calculated as follows.

$$A_{\min} = \frac{W_L}{\rho_V u_{V,\max}}$$

(3.56)

$$D_{\min} = \sqrt{\frac{4A_{\min}}{\pi}}$$

(3.57)

The minimum diameter obtained from equation (3.57) may be adjusted to the next higher standard increments. In this study, diameters in 6-inch increments which are normally fabricated in the US were considered (Hall, 2012). The aspect ratio (the vertical height divided by diameter) of the separator can be up to 4:1 depending on the design operation (Hall, 2012). In this study, the aspect ratios of all separators were designed to be 2:1.

3.3.4 Heat exchanger

A number of heat exchangers are used in the CO_2CPU, the models of which were categorized as either simple heat exchangers or multi-stream heat exchangers. This section described a mathematical model and sizing of a simple heat exchanger used for modelling coolers and heaters that have only one hot stream and one cold stream flowing counter-currently; and do not encounter two phase flow. To reduce the complexity of the entire dynamic model of CO_2CPU, a spatial variation along the exchanger length was not taken into account in a simple heat exchanger model. Ordinary differential equations were solved in a simple heat exchanger to determine the outlet stream temperatures of various process streams. The transfer coefficients were calculated using average fluid properties. Details of the mathematical model are given below.

3.3.4.1. Mathematical model

This model was developed based on shell-and-tube configuration. A fluid that has high pressure is assigned to flow through the tube while a fluid with lower pressure flows counter-currently through the shell. Heat losses and thermal resistance of the tube wall were neglected and the mass flow rates were assumed constant. Effects of kinetic and potential energy were also ignored. Thus, the energy equation shown in equations (3.7) was simplified

48

to solve for the outlet temperatures at each side of the heat exchanger, as expressed in equation (3.58).

Tube-side:
$$\rho_t C_{p_t} V_t \frac{dT_t}{dt} = \rho_t F_t C_{p_t}(T_{t,in} - T_{t,out}) - Q \qquad (3.58a)$$

Shell-side:
$$\rho_s C_{p_s} V_s \frac{dT_s}{dt} = \rho_s F_s C_{p_s}(T_{s,in} - T_{s,out}) + Q \qquad (3.58b)$$

where Q is the rate of heat transfer between shell and tube which is calculated from the following equation.

$$Q = UA\Delta T_{LMTD} \qquad (3.59)$$

$$\Delta T_{LMTD} = \frac{(T_{t,out} - T_{s,in}) - (T_{t,in} - T_{s,out})}{\ln \dfrac{(T_{t,out} - T_{s,in})}{(T_{t,in} - T_{s,out})}} \qquad (3.60)$$

U and A in equation 3.59 represent the overall heat transfer coefficient and the heat transfer area, respectively. ΔT_{TLMD} is the log-mean temperature difference depending on flow arrangements in the heat exchanger. Equation 3.60 presents ΔT_{TLMD} of the counter-current flow arrangement in a shell-and-tube heat exchanger. As stated previously, the effect of tube wall is negligible, thus the overall heat transfer coefficient, U, per unit area can be obtained from:

$$U = \frac{1}{\left(\dfrac{1}{h_t} + \dfrac{1}{h_s}\right)} \qquad (3.61)$$

where h_t and h_s are heat transfer coefficients of fluids in tube-side and shell-side respectively. The general correlations of tube-side heat transfer coefficients used in this work are as follow (Sinnott, 2005).

If $Re > 2300$:

$$Nu = C \cdot \mathrm{Re}^{0.8} \cdot \mathrm{Pr}^{0.33} \left(\frac{\mu}{\mu_w} \right)^{0.14} \tag{3.62}$$

If $Re < 2300$:

$$Nu = 1.86 \left(\mathrm{Re} \cdot \mathrm{Pr} \right)^{0.33} \left(\frac{d}{L} \right)^{0.33} \left(\frac{\mu}{\mu_w} \right)^{0.14} \tag{3.63}$$

where $Nu = $ Nusselt number $= (hd/k)$

$Re = $ Reynolds number $= (\rho v d / \mu)$

$Pr = $ Prandtl number $= (c_P \mu / k)$

d is the tube diameter and L is the tube length. The value of C in equation (3.62) depends on the type of the fluid flowing through the heat exchanger. In this case, the C value equals to 0.023, which is the number recommended for gases (Sinnott, 2005). For the shell-side, the local heat transfer coefficient is based on Kern's method (Sinnott, 2005), as shown in (3.64).

$$Nu = \frac{h_s d_e}{k} = j_h \cdot \mathrm{Re} \cdot \mathrm{Pr}^{1/3} \left(\frac{\mu}{\mu_w} \right)^{0.14} \tag{3.64}$$

where $d_e = $ hydraulic mean diameter $= \dfrac{4 \left(p_t^2 - \dfrac{\pi}{4} d^2 \right)}{\pi d} \tag{3.65}$

$p_t = $ Tube pitch

j_h is a correction factor depending on the fluid Reynolds number, baffle cut, and tube arrangement. The value of j_h is obtained from a chart presented in (Sinnott, 2005), and assumed to be constant.

3.3.4.2. Equipment sizing

The tube diameters were selected based on the standard provided in textbooks (Kern, 1950; Sinnott,, 2005; Hall, 2012). Diameters in range 5/8 inch to 1 inch are preferable for most designs because the exchanger will be more compact, and therefore cheaper than using

bigger tube diameters. There are three patterns of tube arrangement that are usually found in an exchanger, i.e. triangular, square, or rotated square pattern, as shown in Figure 4.3. It is necessary to consider the tube arrangement because it determines the tube pitch (distance between tube centres) that is used to calculate the hydraulic mean diameter and heat transfer coefficient as expressed in equation (3.64). In this study, the triangular tube arrangement was selected, as it provides high heat transfer rate (Sinnott, 2005).
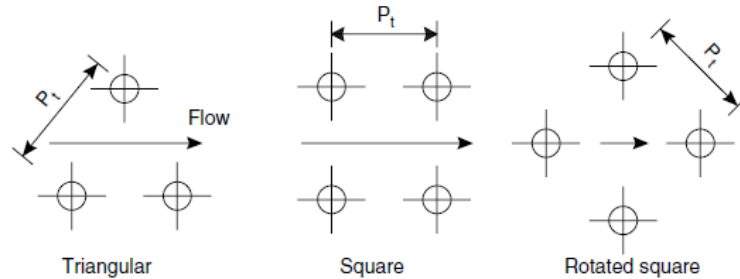
Figure 3.6 Tube patterns in shell and tube heat exchanger (Sinnott, 2005)

The recommended tube pitch is normally 1.25 times the outside tube diameter (Sinnott, 2005; Hall, 2012). In addition, the segmental baffle is considered in exchanger sizing. The baffle is usually installed in the shell as shown in Figure 3.7 in order to increase the fluid velocity and improve the heat transfer rate of an exchanger. The dimension of the baffle is usually referred to the baffle cut which is a height of the segment removed expressed as a percentage of the baffle disc diameter. A typical range of baffle cut is 15%-45%, but a general optimum range is 20%-25% (Sinnott, 2005). The distance between baffles is called baffle spacing. The shorter the baffle spacing used, the higher the heat transfer rate obtained. The baffle spacing can be 0.2-1.0 times the shell diameter, and generally an optimum spacing is 0.3-0.5 times the shell diameter (Sinnott, 2005). Therefore, in this study the baffle cut is specified at 20% while the baffle spacing is 0.25 times the shell diameter.
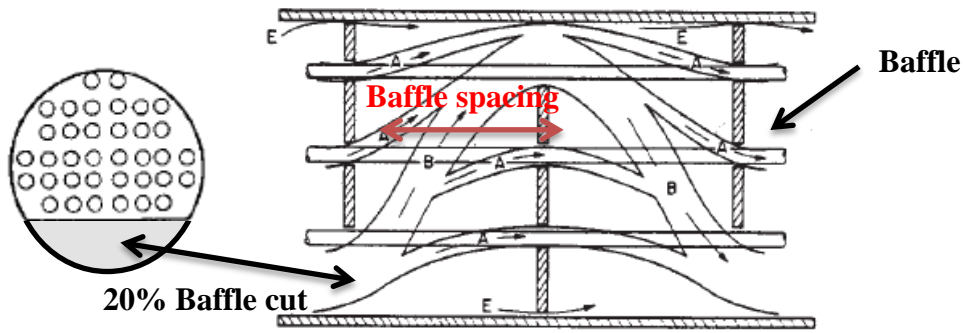
Figure 3.7 Baffle configuration (Sinnott, 2005)

The shell diameter must be selected to give as a close fit to the tube bundle as is practical. The bundle diameter depends on the number of tubes and the number of tube passes, and can be obtained from the following equation (Sinnott, 2005).

$$D_b = d_0 \left(\frac{N_t}{K_1} \right)^{1/n_1}$$

(3.66)

where

N_t = Number of tubes
D_b = Bundle diameter (mm)
d_0 = Tube outside diameter (mm)

The constants used in equation (3.66) are provided in Table 3.3. The bundle diameter obtained from equation (3.66) is used to select the shell diameter from the standard shell size which can be found in several textbooks (Kern, 1950; Perry, 2008). The number of tubes that can be accommodated in the standard shell size can also be found in textbooks.

Table 3.3 Constant for use in equation (3.66) (Sinnott, et al, 2005)

Triangular pitch, $p_t = 1.25d_0$

No. passes	1	2	4	6	8
K_1	0.319	0.249	0.175	0.0743	0.0365
n_1	2.142	2.207	2.285	2.499	2.675

Square pitch, $p_t = 1.25d_0$

No. passes	1	2	4	6	8
K_1	0.215	0.156	0.158	0.0402	0.0331
n_1	2.207	2.291	2.263	2.617	2.643

3.3.5 Multi-stream Heat exchanger

The actual design of a multi-stream heat exchanger is done using a plate-and-fin heat exchanger which is widely used in process industries including gas processing and cryogenic application. Basically, a plate-and-fin heat exchanger consists of stacked layers of corrugated fins separated by parting sheets and sealed along the edge by bars as shown in Figure 3.8. The corrugated fins provide an extended surface for heat transfer, thus high thermal efficiency is obtained (ALPEMA, 2000).
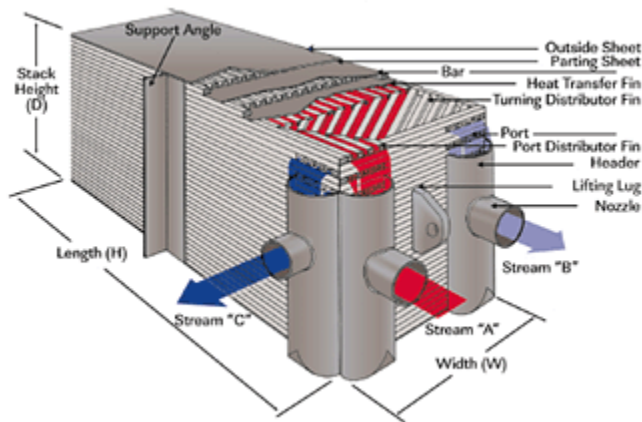
Figure 3.8 Plate-and-fin multi-stream heat exchanger (Process Cooling, 2000)

The steady-state behaviour of a plate-and-fin heat exchanger has been widely studied (Prasad and Gutukul, 1992; Lou et al, 2002; Boehme et al, 2003; Ghosh et al, 2006; Ghosh et al, 2007; Kohil et al, 2010). On the other hand, little efforts have been made to investigate the dynamic behaviour of a plate-and-fin heat exchanger. The complex flow patterns of a plate-and-fin heat exchanger that include cross-flow, counter-flow and parallel-flow arrangements make dynamic modelling very challenging. A simple and rapid dynamic model of plate-and-fin heat exchanger with reasonable accuracy is still required. Dynamic modelling of a plate-and-fin heat exchanger was initially proposed by Pingaud in 1989. Conservation laws of mass, energy and momentum of fluid flows were performed. The variation in parting sheet temperature and the phase change were also considered. However, the heat transfer area calculation and fluid flow direction used in Pingaud's model were not clearly stated. Correlations to calculate the void fraction in two phase region and heat transfer coefficients were not provided. Another dynamic model of plate-and-fin heat exchanger was presented in 1999 (Averous et al, 1999). In this study, a plate-fin heat exchanger was divided into two zones, i.e. distribution zone and exchange zone, and the heat balance was performed considering heat transfer between adjacent passages and conduction through the fins. This model was developed using a special dynamic simulator of brazed plate-fin heat exchangers, ProSec^{TM}. The heat transfer coefficients were evaluated with an in-house correlation linked with the manufacturer's data base. Two phase flow was not discussed in this study. A case study was performed to evaluate dynamic behaviour of the heat exchanger when one cold process stream of the heat exchanger was shut down. More recently, a generalized mathematical model for transient analysis in multi-stream heat exchangers was proposed (Luo et al, 2003). Four matching matrices were introduced to specify the boundary conditions of the spatial energy balance of the fluid flowing through the exchanger. Mathematical models were solved using Laplace transform and numerical inverse algorithm. The developed model was claimed by the authors to be capable for transient analysis in various types of multi-stream heat exchanger including a plate heat exchanger. However, two-phase flow is not valid in this model.

In the CO_2CPU, the multi-stream heat exchanger encounters both condensing and boiling two phase flows. The CO_2 in the flue gas was cooled and partially condensed while the liquid coolant from the flash drum was heated and partially vaporized. Furthermore, the two phase region does not exist across the entire exchanger length but occurs only partly in both the shell and tube sides. A combination between single phase and two phases governing equations is therefore required to model the multi-stream heat exchanger. Including complex flow patterns of the plate-and-fin heat exchanger and the two phase flow heat transfer phenomena in a dynamic model of multi-stream heat exchanger, a dynamic model of the CO_2CPU will become extremely elaborate and computationally intensive. Because the ultimate goal of this study is to develop a dynamic model of the entire CO_2CPU plant for control design purpose, a dynamic model that is not overly complicated to prevent extremely long dynamic simulation, but accurate enough to provide correct trends of temperature variation and time constants in the multi-stream heat exchanger is required. To simplify the multi-stream heat exchanger model and also the CO_2CPU model, the current model was developed based on a shell and tube configuration and employed the simplest spatial distributed two phase flow model, i.e. homogenous flow model, to model the two phase region in the multi-stream heat exchanger. The use of a shell and tube configuration allows for the assumption of one-dimensional flow which is preferred at this stage of modelling. Details of mathematical model and the shell-and-tube configuration considered in the multi-stream heat exchanger model are provided in the next section.

3.3.5.1. <u>Mathematical model</u>

To model the multi-stream heat exchanger, both single phase and two phase flow heat transfers were employed as described previously. This section provides details of the single phase and two phase governing equations. The following assumptions were made for both the single phase and the two phase regions in the dynamic model of multi-stream heat exchangers.

1) Fluid flow is one-dimensional.
2) Effects of kinetic and potential energy are neglected.

3) Pressure drop is negligible.

4) Liquid and vapour in the two-phase region are in thermal equilibrium.

5) Axial conduction is negligible.

6) Thermal resistance of the wall to heat transfer area is negligible.

Since the pressure drop is assumed negligible, the momentum equation can be eliminated. The mass and energy balances for the different regions can be simplified as follows.

1) Single phase region

Continuity and energy equations of one-dimensional fluid flow in a single phase region were developed using partial differential equations as shown in equations (3.67) and (3.68).

$$\frac{\partial \rho}{\partial t} + \frac{\partial}{\partial z}(\rho v) = 0 \qquad (3.67)$$

$$\frac{\partial(\rho h)}{\partial t} + \frac{\partial(\rho v h)}{\partial z} = \frac{4}{D} h_i \Delta T \qquad (3.68)$$

The right-hand side of equation (3.68) represents the rate of heat transfer from the hot stream to the cold stream. Equations (3.62)-(3.64) were used to calculate the heat transfer coefficients (h_t) in the single phase region. These equations are valid because the multi-stream heat exchanger is modelled based on a shell and tube configuration.

2) Two phase region

A number of two phase flow models have been proposed at different levels of complexity and accuracy. Generally, two phase flow models are divided into two main groups, lumped parameter and discretized models. A lumped parameter model, also known as a moving boundary model, is the most general two-phase flow model in which the entire two-phase flow region is considered as a single control volume that has constant properties. A lumped parameter model is relatively simple, and therefore, requires less computational effort and time. It, however, does not take in to account the spatial variation of fluid properties, thus the results obtained are less accurate and may lead to wrong decisions in the controller design.

Therefore, a more complicated discretized model was considered in this work. There are three types of discretized models commonly used in the literature (Levy, 1999; Faghri and Zhang, 2006):

a) Homogeneous model: This model assumes that the two phases flow at equal velocities and are well-mixed. The two-phase flow is discretized into a small control volume and modelled using averaged properties.

b) Separated flow model: This model considers different velocities between the two phases but assumes that only the velocities differ. The conservation equations are written for the combined flow and also solved using averaged properties. This is a simplified version of the two-fluid model (below).

c) Two-fluid model: The spatial governing equations are defined for each individual phase within a two-phase control volume. To solve this model, constitutive equations of mass, momentum and heat transfer across the phase boundary are required.

To reduce computational effort and complexity of the multi-stream heat exchanger model, a homogenous two phase flow model was used in this study. The vapour and liquid phases were assumed to be in thermal equilibrium, well-mixed and flowing through the exchanger at the same velocities. In this case, the two phase region was discretized into a small control volume and modelled using area-averaged properties. Studies on dynamic simulation and control of two phase flow heat exchangers, i.e., evaporators and condensers, which rely on homogenous flow model, are available in literature (Nyers and Stoyan, 1992; Jia et. al, 1995; Mithraratne et. al, 2000; Madsen et. al., 2012). The advantage of using a homogenous model is that the complicated interfacial phenomena can be avoided and all available analytical solutions or experimental correlations for single phase flow can be applied to the homogenous flow. One-dimensional continuity and energy equations of a homogeneous two-phase flow are shown in equations (3.69) and (3.70) (Faghri and Zhang, 2006).

$$\frac{\partial \langle \rho \rangle}{\partial t} + \frac{\partial}{\partial z}\left(\langle \rho \rangle \langle v \rangle\right) = 0 \qquad\qquad (3.69)$$

$$\frac{\partial(\langle\rho\rangle\langle h\rangle)}{\partial t} + \frac{\partial(\langle\rho\rangle\langle v\rangle\langle h\rangle)}{\partial z} = \frac{4}{D}h_{TP}\Delta T \tag{3.70}$$

The angle bracket, $\langle\ \rangle$, represents the area-averaged properties of the homogenous flow. If the angle bracket, $\langle\ \rangle$, was dropped for ease, the governing equations of homogenous flow become exactly the same as the single phase flow equations. This makes the computational coding easier, especially when the boundary of two phase region is unknown, since the decision-making algorithm (such as if-else conditions) to switch between sub-models is not required. Also, the entire simulation takes considerably less time to converge which is favoured when dynamically simulating the CO_2CPU. The homogenous properties were obtained from the following relations (Levy, 1999):

$$\langle\rho\rangle = \alpha\langle\rho_v\rangle + (1-\alpha)\langle\rho_l\rangle \tag{3.71}$$

$$\langle v\rangle = \frac{G}{\langle\rho\rangle} \tag{3.72}$$

$$\langle h\rangle = xh_v + (1-x)h_l \tag{3.73}$$

where α is the vapour void fraction defined as the ratio of cross-sectional area occupied by the vapour phase to the total cross-sectional area as shown in equation (3.74).

$$\alpha = \frac{\Delta z\int_{A_v} dA}{\Delta z\int_A dA} = \frac{A_v}{A_v + A_l} \tag{3.74}$$

Many void fraction models have been proposed for both general validity and specific flow regimes (Winkler et. al., 2012). In this work the Lockhart-Martinelli parameter-based void fraction model proposed by Abdul-Razzak et al. (1995) was used. It can be expressed as:

$$\alpha = \frac{1}{\left(1 + 0.49X_{tt}^{0.803}\right)} \tag{3.75}$$

where X_{tt} is a Lockhart-Martinelli parameter. For turbulent flow, X_{tt} is given by (Lockhart and Martinelli, 1949):

$$X_{tt} = \left(\frac{1-x}{x}\right)^{0.9} \left(\frac{\rho_v}{\rho_l}\right)^{0.5} \left(\frac{\mu_l}{\mu_v}\right)^{0.1} \tag{3.76}$$

The vapour quality (x), used in equations (3.73) and (3.76), is the ratio of the vapour mass flow rate to the total mass flow rate of the mixture given by (Mithraratne et. al., 2000):

$$x = \frac{(h - h_l)}{(h_v - h_l)} \tag{3.77}$$

Since homogenous flow was assumed, the two phase heat transfer coefficient (h_{TP}) can be calculated using single phase correlations shown in equations (3.62)-(3.64). But the Reynolds number, Prandtl number and Nusselt number were calculated using the density, viscosity and thermal conductivity of the homogenous flow defined by equations (3.71), (3.78) and (3.79) respectively (Levy, 1999).

$$\langle \mu \rangle = \alpha \langle \mu_v \rangle + (1 - \alpha)\langle \mu_l \rangle \tag{3.78}$$

$$\langle k_f \rangle = \alpha \langle k_v \rangle + (1 - \alpha)\langle k_l \rangle \tag{3.79}$$

Because the two phase region exists partly in both the shell and tube sides of heat exchanger and the location of phase boundary is unknown, a conditional calculation is implemented in the multi-stream heat exchanger model. If the temperature in a discretized element is lower than the dew point or higher than the bubble point of the fluid mixture, the homogenous flow model will be implemented. Discretized elements that are out of that temperature range will be modeled using single phase governing equations. Solving all discretized elements simultaneously, temperature profiles of each fluid flowing through the multi-stream heat exchanger are obtained.

3.3.5.2. Equipment sizing

Since actual design data of multi-stream heat exchangers in the CO_2CPU are not yet available and a simplified dynamic model is required, the current model was developed based on a shell and tube configuration as depicted in Figure 3.9. The hot stream was assigned to flow

inside the shell while a number of cold streams flowed counter-currently inside the tubes. The tube sheet is divided to accommodate each cold stream. The number of tubes per inlet was adjusted to obtain fully developed turbulent flows in which the Reynolds number (*Re*) greater than 4,000. This number is recommended in order to avoid the flow transition region in heat exchanger (Halman, 1997; Sinnott, 2005).
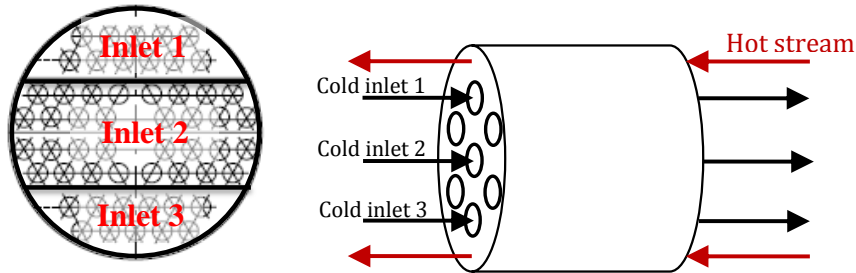
Figure 3.9 Multi-stream heat exchanger based on shell and tube design

The shell and tube diameters were selected based on the standard similar to the simple heat exchanger model described in section 3.3.4.2. The triangular tube arrangement with the tube pith of 1.25 times tube diameter was selected, while the 20% baffle cut was considered and the baffle spacing is 0.25 times the shell diameter. In addition, the tube length was adjusted to obtain desired heat transfer area and to validate the outlet temperatures with the plant data.

3.4 Dynamic modelling of the CO_2CPU

This section describes a procedure to integrate all unit operation models into the CO_2CPU plant model, namely convergence of the entire mechanistic process model. Two basic computational approaches can be used for solving plant simulation, i.e., sequential-modular approach and equation-oriented approach. In the sequential-modular approach, the unit operation models are solved one-by-one following a flowsheet sequence. To solve a recycled process simulation, the sequential-modular tears a recycle stream; provides initial guess of the tear stream, such as total flow, composition, temperature and pressure; and then solves each unit (module) in the recycled process model in sequence (Dimian, 2003; AspenTech, 2004). The iterative calculation is required to solve for the final steady state solution, thus the

sequential-modular approach can be very time-consuming for the recycled process simulation. On the other hand, the equation-oriented approach assembles all modelling equations and solves them simultaneously. The equation-oriented approach considers variables related to the recycle stream as unknowns which are solved simultaneously with other equations in each unit operation models to find the final steady state solution for the recycled process model. The equation-oriented approach is more efficient than the sequential-modular approach for process simulation with recycle stream (Barton, 2000; Dimian, 2003; AspenTech, 2004). Even though the use of equation-oriented approach does not require an iterative calculation, it requires good initial conditions; large storages and computer memory; and also a stable and reliable solver (Ku, 2013).

In this study, both the Air Products' CO_2CPU and the $CanCO_2$ plant models were developed using the efficient equation-oriented approach. The use of product streams from flash drum as coolants in the auto-refrigeration process makes the CO_2CPU plant model highly integrated, and imposes difficulty in flowsheet convergence to both plant models, especially in the $CanCO_2$ plant model in which a portion of the gas stream separated from the first flash drum is recycled back and mixed with the compressed flue gas upstream. The convergence of the recycle loop in the $CanCO_2$ is the most challenging part in this study. Due to the limited design data and the complexity of the process stream connections in the CO_2CPU plant, it is difficult to identify suitable initial conditions for each unit operation model, especially for the multi-stream heat exchanger models. Poor or inappropriate initial conditions may lead to convergence failure when all unit models are integrated into the CO_2CPU plant model. The procedure used to integrate all unit operations into a complete dynamic model of both CO_2CPU plants is described below.

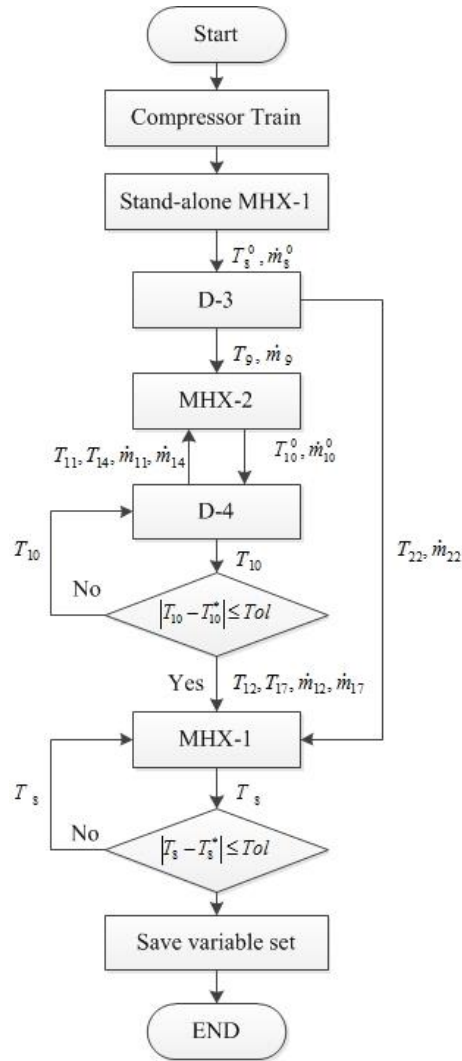### 3.4.1 Dynamic modelling of the Air Products' CO_2CPU

Dynamic models of both the Air Product's CO_2CPU and the $CanCO_2$ were developed using the gPROMS (Process System Enterprise, 2012) equation-oriented simulation software system. Physical and thermodynamic properties for this system were obtained from the Multiflash™ property package using Peng-Robinson EOS. The flue gas conditions, which

are input in the present model, are presented in Table 3.1. Initially, mathematical models of each unit operation provided in section 3.3 were coded and validated individually with the design data provided by Dillon et al. (2005). The partial differential equations in the multi-stream heat exchanger model were solved using a gPROMS built-in centred finite difference method with 30 discretized elements. Linear temperature profiles and their corresponding density profiles were calculated using the inlet and outlet temperatures provided in Dillon et al. (2005) as initial conditions for the multi-stream heat exchanger model. Boundary conditions were also specified at the inlet of each process stream using steady state data obtained from Dillon et al. (2005). Once all the stand-alone dynamic models were developed, the unit operation models were connected to describe the transient behaviour of the complete Air Products' CO_2CPU. The process stream connections were developed according to the flow diagram shown in Figure 3.1.

A dynamic model of the compressor train was first developed by connecting together the models for the units K-1, C-1, D-1, K-2, C-2 and D-2 according to the flow diagram shown in Figure 3.1. This step is straightforward since there is no recycle stream in the compressor train. Subsequently, a simulation procedure presented in Figure 3.10 was implemented. The moisture-free compressed flue gas obtained from a compressor train model (stream 7) was connected to a stand-alone MHX-1. The coolant streams 12, 17, and 22 were specified at this point using the steady state data provided by Dillon et al. (2005). The first trial was then simulated dynamically until the connected model reached steady state. The results obtained from the previous run were then used as an input for the next process units, and the connected model was again simulated dynamically until it reached a new steady state. The model connection proceeded according to the flow diagram shown in Figure 3.1. The process units were connected one at a time to facilitate the identification of potential failures in the simulation. Once streams 11 and 14 in the MHX-2 model were integrated to the model, the tube length of MHX-2 was adjusted to validate the outlet temperature of stream 10 with the data from Dillon et al. (2005). After the MHX-2 validation, data for streams 12, 17 and 22 obtained from the previous simulation were used in the MHX-1 model. Similarly, the tube length of MHX-1 was adjusted to validate the outlet temperature of stream 8 with the data

62

from Dillon et al. (2005). The dimensions of the multi-stream heat exchangers and the rest of the unit operations of the Air Products' CO_2CPU model are summarized in Appendix A. Once all the process unit models were connected and validated, a dynamic simulation of the Air Products' CO_2CPU was run over a certain period of simulation time to gather the initial steady state condition of the entire plant. These results were used as initial conditions for the Air Products' CO_2CPU model in the next run during transient analysis.

Figure 3.10 Procedure to develop the dynamic model of Air Products' CO_2CPU

3.4.2 Dynamic modelling of the CanmetENERGY's CO$_2$CPU (CanCO$_2$)

Similar to the Air Products' CO$_2$CPU model, stand-alone dynamic models of each unit operation included in the CanCO$_2$ were initially coded and validated in gPROMS. For the CanCO$_2$, the developed models were validated with the design data of CanCO$_2$ provided by CanmetENERGY. The flue gas conditions required as input for this model are presented in Table 3.2. The model connection started with the compressor train and then extended to include other process units as shown in Figure 3.11.
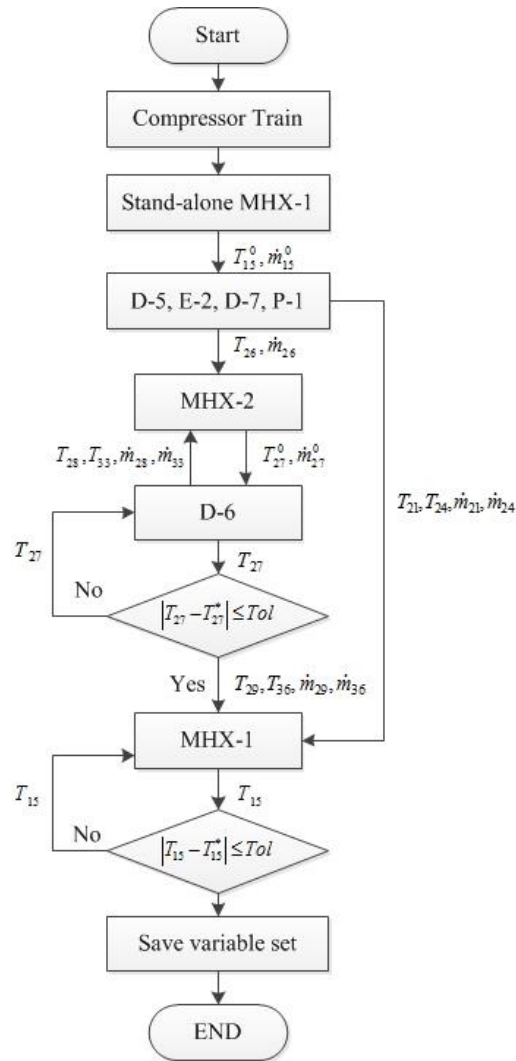
Figure 3.11 Procedure to develop the dynamic model of CanmetENERGY's CO$_2$CPU (CanCO$_2$)

64

First, the compressor train model was connected to the stand-alone MHX-1 model by stream 14, and then the connected model was simulated dynamically to determine stream 15's conditions. Afterwards, the connection was extended to include D-5, E-2, D-7 and P-1, and stream 26's conditions required for the MHX-2 model were determined. Subsequently, the MHX-2 was connected to the D-6 model and the tube length was adjusted to validate stream 27's temperature with the CanCO$_2$ design data. Once the MHX-2 was validated, streams 21 and 24 obtained from MHX-2 and streams 29 and 36 obtained from D-7 were connected to the MHX-1 model, and the tube length of MHX-1 was adjusted to validated stream 15's temperature with the CanCO$_2$ design data. The dimensions of the multi-stream heat exchangers and the rest of the unit operations included in the CanCO$_2$ plant model are summarized in Appendix B. The connected model was run over a certain period of time (360000 seconds) to gather the initial steady state conditions. These results will be further used as an initial condition for the CanCO$_2$ model. Note that stream 22 is not yet recycled to the compression train in the procedure described in Figure 3.11. As shown in Figure 3.3, the CanCO$_2$ is an integrated model that is very sensitive to the input change. Thus, the entire amount of gas present in stream 22 cannot be recycled to the compression train at once. The model should be slowly disturbed by a recycle stream; hence a purge valve was introduced to make a recycle gas flow rate adjustable as shown in Figure 3.12.
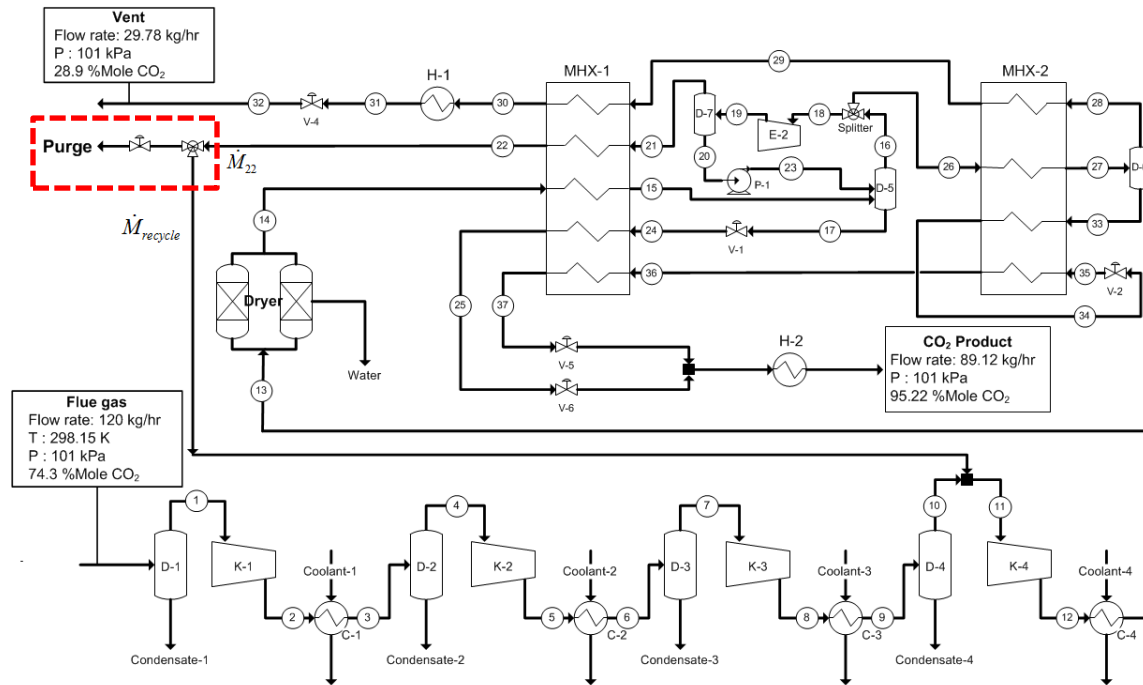
Figure 3.12 Purge valve addition to facilitate the $CanCO_2$ plant model convergence

The amount of gas recycled was determined by a recycle ratio, i.e. the ratio between the mass flow rate of gas recycled to the compressor train and the mass flow rate of stream 22.

$$\text{Recycle ratio} = \frac{\dot{M}_{recycle}}{\dot{M}_{22}} \qquad (3.80)$$

It should be noted that the purge valve was introduce to facilitate the flowsheet convergence of the $CanCO_2$ plant model, i.e., it does not exist in the actual plant. At the beginning of the model integration, the recycle ratio was kept constant at 0, i.e. the purge valve was fully open meaning and there is no recycle gas flowing to the compressor train. After the procedure presented in Figure 3.11 was completed and the initial steady state was obtained, the recycle ratio was gradually increased until the total mass flow rate of stream 22 was recycled to the compressor train (recycle ratio =1), that is the purge valve was fully closed . It was found that the ramp change in the recycle ratio from 0 to 1 within 72000 seconds (simulation time) is suitable for the $CanCO_2$ plant model. A faster change in the recycle ratio will cause

66

numerical instabilities in the CanCO$_2$ dynamic plant model. Even though the use of the purge valve is a simulation resource used to converge this plant, interesting results were observed while changing the recycle ratio, i.e. changing the recycle ratio changes the amount of gas recycled from D-5 to the compressor train and thus affect the operation of CanCO$_2$. The results obtained from this sensitivity analysis are presented in Chapter 5.

Chapter 4

Dynamic simulation results for the Air Products'CO_2CPU process

This chapter presents the simulation results obtained from both the Air Products' CO_2CPU model developed in chapter 3. The steady state validation of the Air Products' CO_2CPU model is firstly presented in section 4.1. Five transient analyses were performed on the Air Products' CO_2CPU model in order to examine the effect of operating conditions and potential disturbances on two key process performances, i.e. the CO_2 recovery and CO_2 product purity. Results obtained from these transient analyses are successively presented in sections 4.1-4.6.

4.1 Steady state validation

The model developed in section 3.4 was used to simulate the Air Products' CO_2CPU plant in gPROMS. The first initial steady state results obtained from the model were compared to the design data of the Air Products' CO_2CPU provided by an IEAGHG R&D report (Dillon et al, 2005) and shown in Table 4.1. It should be noted that the data provided by Dillon et al. are steady state data obtained from simulation using proprietary software. The product and vent streams refer to stream 27 and stream 15 in Figure 3.1, respectively. The CO_2 recovery is the ratio of the amount of captured CO_2 (CO_2 in stream 27) to the amount of CO_2 in the flue gas (CO_2 in stream 1). There is excellent agreement between the steady state model results and the design data presented in an IEAGHG R&D report (Dillon et al, 2005) with the exception of the O_2 content in the CO_2 product stream. The difference likely results from the use of a different physical property packages, not reported in Dillon et al. (2005). Nevertheless, the validation with this limited data set is very promising and acceptable to further perform transient analysis for the Air Products' CO_2CPU.

Table 4.1 Comparison between the simulation results and the Air Products' CO_2CPU design data (Dillon et al., 2005)

|	Simulation results		Dillon et al., 2005		Relative error (%)	
Process variables	Product	Vent	Product	Vent	Product	Vent
Temperature (K)	307.81	293.32	316.15	293.32	2.64	0.40
Pressure (bar)	110	1.01	110	1.01	-	-
Mass flow rate (kg/s)	128.06	40.68	126.97	38.61	0.86	5.37
Mole fraction						
CO_2	0.9534	0.2849	0.9584	0.2462	0.52	15.70
O_2	0.0158	0.1750	0.0105	0.1942	50.39	9.87
AR	0.0060	0.0692	0.0061	0.0712	2.16	2.73
N_2	0.0201	0.4714	0.0203	0.4872	0.94	3.25
H_2O	0	0	0	0	-	-
SO_2	0.0046	0	0.0045	0	2.41	-
NO	0.0001	0.0011	0.00013	0.00118	14.27	0.77
CO_2 recovery (%Wt)	88.96		91.13		2.39	
CO_2 purity (%mol)	95.34		95.84		0.52	

The temperature and vapour quality profiles of the multi-stream heat exchangers, MHX-1 and MHX-2, resulted from the homogeneous two phase flow model detailed in Chapter 3. To avoid confusion and make the results easy to follow, the flow arrangements of MHX-1 and MHX-2 are presented in Figure 4.1.
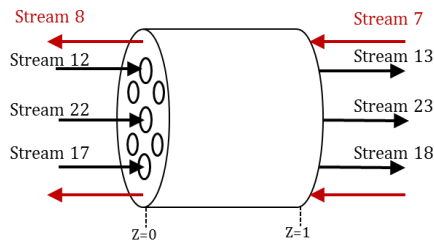

Figure 4.1 Flow arrangement in MHX-1

As shown in Figure 4.1, the hot flue gas enters the multi-stream heat exchanger, MHX-1, at the normalized length (z) equal to 1 and leaves to the flash drum, D-3, at z = 0, while the

three coolant streams enter MHX-1 at z = 0 and leave at z = 1. The temperature and vapour quality profiles of the MHX-1 are shown in Figure 4.2 and Figure 4.3, respectively. Very slight changes in the slope of flue gas temperature profile (stream 7-8) are observed in Figure 4.2 due to the fact that limited condensation is occurring. It is found from Figure 4.3 that the hot flue gas (streams 7-8) starts condensing near its outlet, at z ≈ 0.2, until it reaches a final quality of about 55% at the exit of the exchanger. Similarly, the slope of the coolant (stream 22-23) temperature profile changes as shown in Figure 4.2. This stream enters MHX-1 as a saturated liquid with slight vapour phase (x ≈ 0.06) and is totally vaporized by the middle of MHX-1 (z ≈ 0.5) as shown in Figure 4.3. Stream 17-18 also encounters a phase change but the vapour quality changed occurs rapidly between z=0 and z=0.1. Change in the slope of stream 17-18's temperature profile is not obviously shown, thus the phase change cannot be recognized in Figure 4.2. Instead, the location of phase boundary can be identified from the vapour quality profile shown in Figure 4.3. It is found that the phase boundary is at about z ≈ 0.1 where stream 17-18 was completely vaporized. Stream 12-13 did not encounter the two phase flow, thus its vapour quality was not shown in Figure 4.3. To avoid confusion, the arrows were added into Figures 4.2 and 4.3 to indicate the flow directions of each stream the multi-stream heat exchanger.
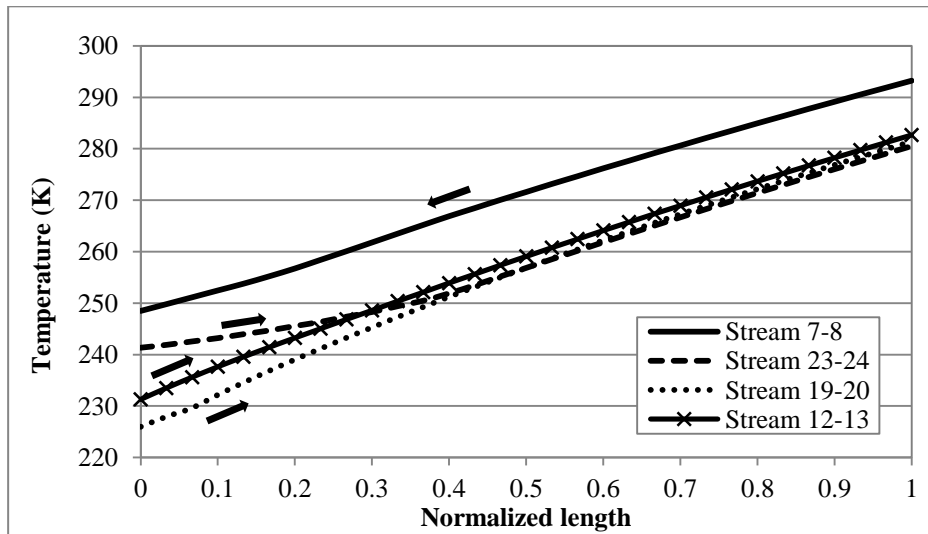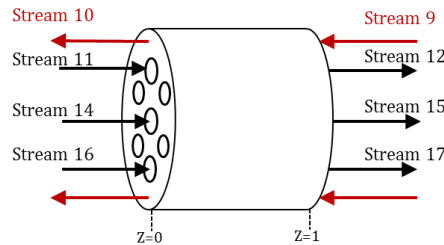

Figure 4.2 Temperature profile in MHX-1

70
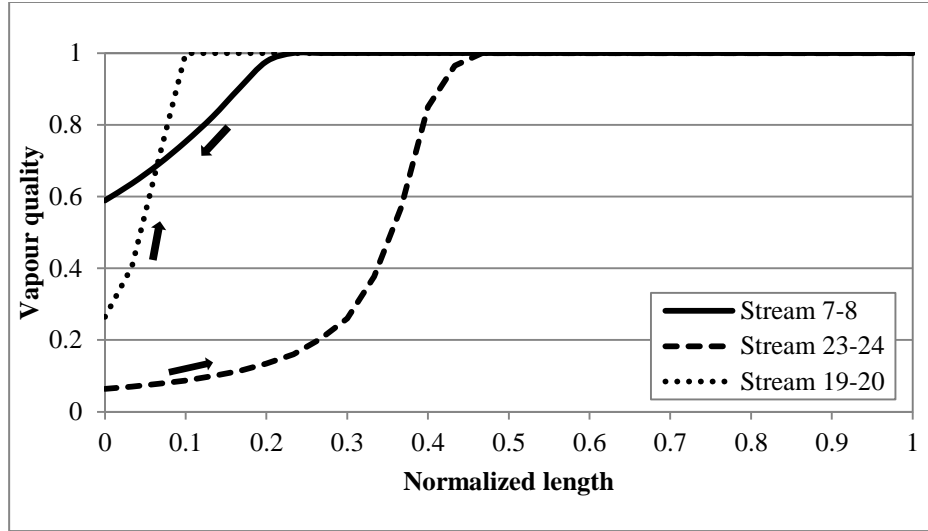
Figure 4.3 Vapour quality profiles in MHX-1

For the second multi-stream heat exchanger (MHX-2), the hot gas (stream 9-10) enters MHX-2 at $z = 1$ and leaves to the flash drum, D-4, at $z = 0$, while the other three coolants enter MHX-2 at $z = 0$ and leave at $z = 1$ as shown in Figure 4.4.

Figure 4.4 Flow arrangement in MHX-2

The heat transfer rate in MHX-2 was maximum at the hot stream inlet ($z=1$) where the largest temperature gradient was obtained as shown in Figure 4.5. The use of recycle streams from D-4 as coolants resulted in a dead zone between $z=0-0.2$ in MHX-2. In this zone, the heat transfer rate was very small resulting in constant temperature and vapour quality profiles in all process streams as shown in Figure 4.5 and Figure 4.6. The dead zone occurred because D-4 was operated isothermally at the outlet temperature of the hot gas (stream 10), thus the temperatures of the hot gas (stream 9-10) and the two coolants (stream 11-12 and stream 14-

71

15) at z = 0 are the same and no heat was exchanged between them. The hot gas (stream 9-10) exchanged heat with only one coolant (stream 16-17) within the dead zone and thus the temperature profile was not flat as much as stream 11-12 and stream 14-15 as shown in Figure 4.5.
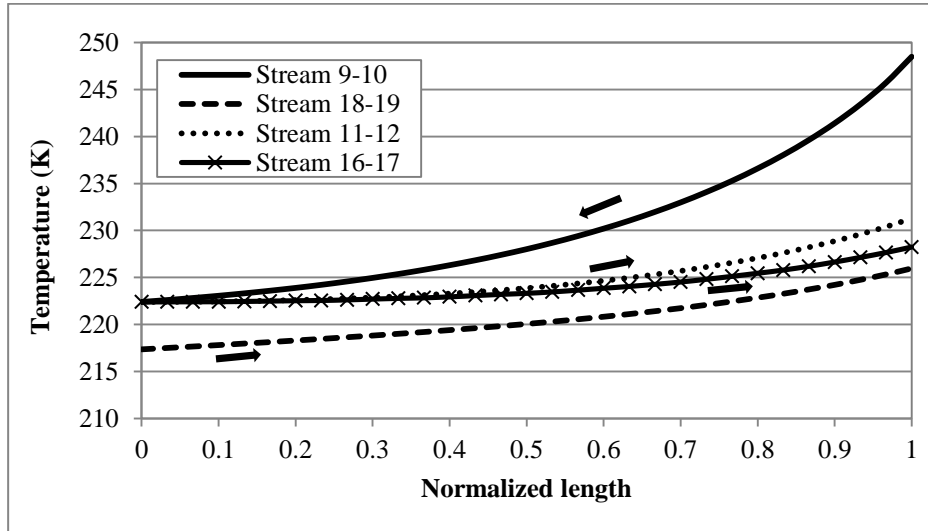
Figure 4.5 Temperature profile in MHX-2

The hot gas entering MHX-2 was saturated so it started condensing immediately upon entering MHX-2 at z=1 as shown in Figure 4.6. The vapour quality of the hot gas changes significantly within z=0.4-1 and gradually decreased within z=0-0.3 where the hot gas exchanged heat with only one coolant stream (stream 16-17). It reaches a final quality of about 40% at the exit of the exchanger. Only 10% vapour quality change was observed in stream 16-17, while stream 11-12, and stream 14-15 did not encounter the two phase flow, thus its vapour quality was not shown in Figure 4.6.
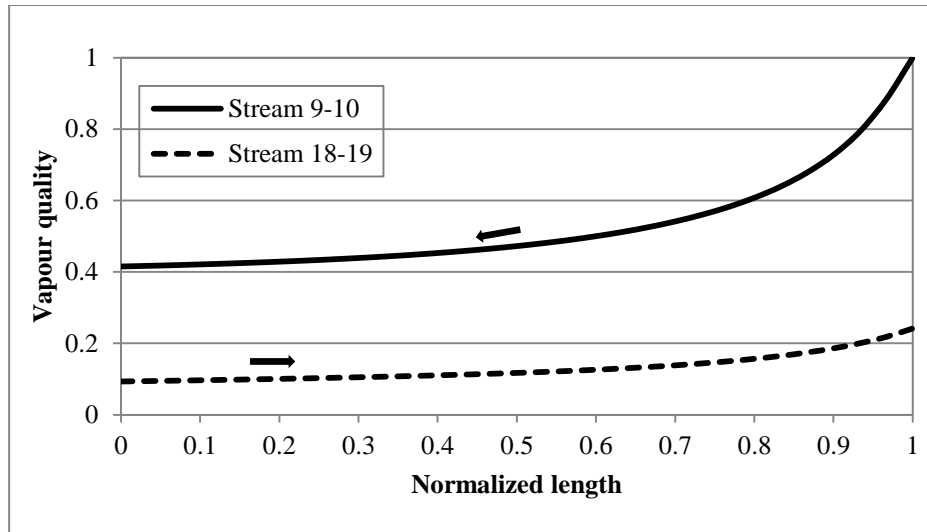
Figure 4.6 Temperature and vapour quality profiles in MHX-2

The model was now used to analyse the transient behaviour of the CO_2CPU. Several dynamic tests were applied to the inputs of the model and the outlet conditions of each unit operation were monitored. The focuses were on the CO_2 purity of the product stream (stream 27) and on the CO_2 recovery of the plant as these two variables represent the operating performance of the CO_2CPU.

4.2 Effect of compressor train outlet pressure

A compressor train refers to a combination between two compressors (K-1 and K-2), two coolers (C-1 and C-2), one knock-out drum (D-1) and one bed dryer (D-2) in the Air Products' CO_2CPU (see Figure 3.1 in chapter 3). In this section, the outlet pressure of the compressor train, that is K-2's discharge pressure, was examined. The test was applied to compressor K-2 by ramping up the discharge pressure from 30 bars to 33 bars within 300 seconds. As the discharge pressure increased, the inlet temperature of flue gas entering C-2 was increased resulting in an increase in stream 6's temperature as shown in Figure 4.7.
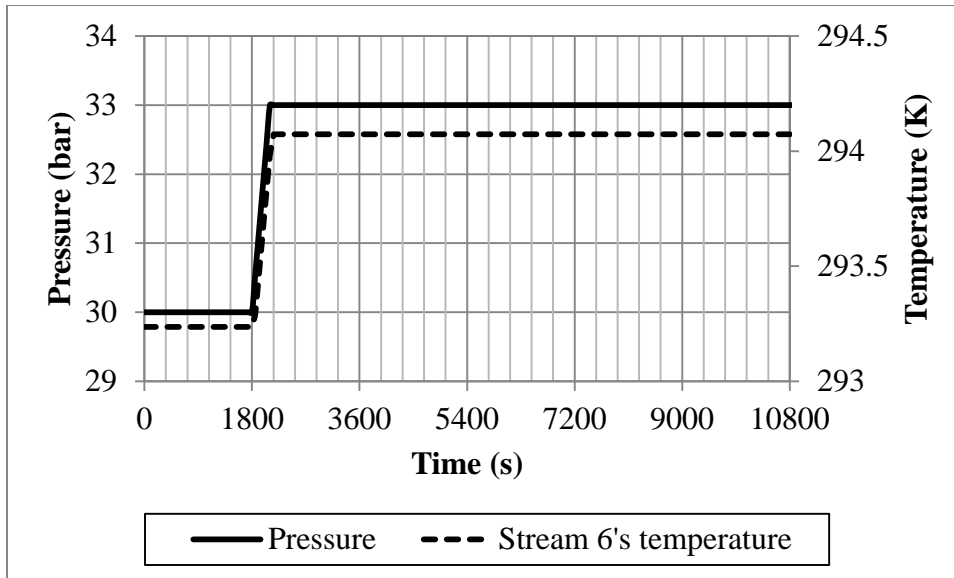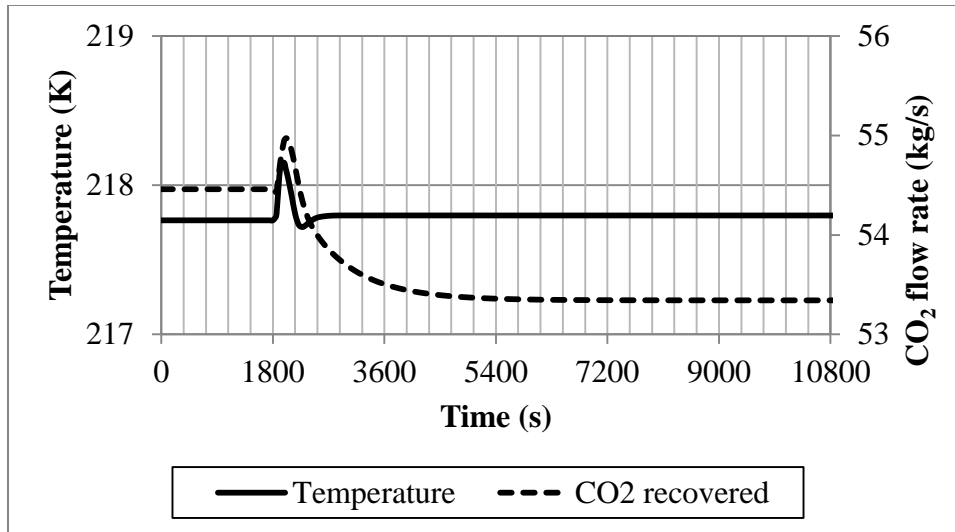
Figure 4.7 Stream 6's temperature in response to the ramp-up change in K-2 discharge pressure

Even though, the increased pressure enhanced the heat transfer coefficient of the hot gas flowing through MHX-1, by increasing the thermal conductivity and the Prandtl number, the effect of increasing stream 6's temperature was found to be more significant than increasing the heat transfer coefficient. Consequently, the temperature of stream 8 was increased, as shown in Figure 4.8. Since D-3 operates at the temperature and pressure of stream 8, changes in conditions of stream 8 affect the amounts of CO_2 separated from D-3, as also shown in Figure 4.8. Within the first 300 seconds, the rapid change in stream 8's temperature played a key role in the CO_2 condensation in D-3. Increasing the temperature reduced the CO_2 condensation, thus the liquid CO_2 recovered from D-3 was dropped initially. After 300 seconds, the stream 8's temperature is quite steady and the effect of increasing the operating pressure becomes significant for CO_2 condensation in D-3. Increasing pressure favours the CO_2 condensation, thus more liquid CO_2 was recovered from D-3 as shown in Figure 4.8.
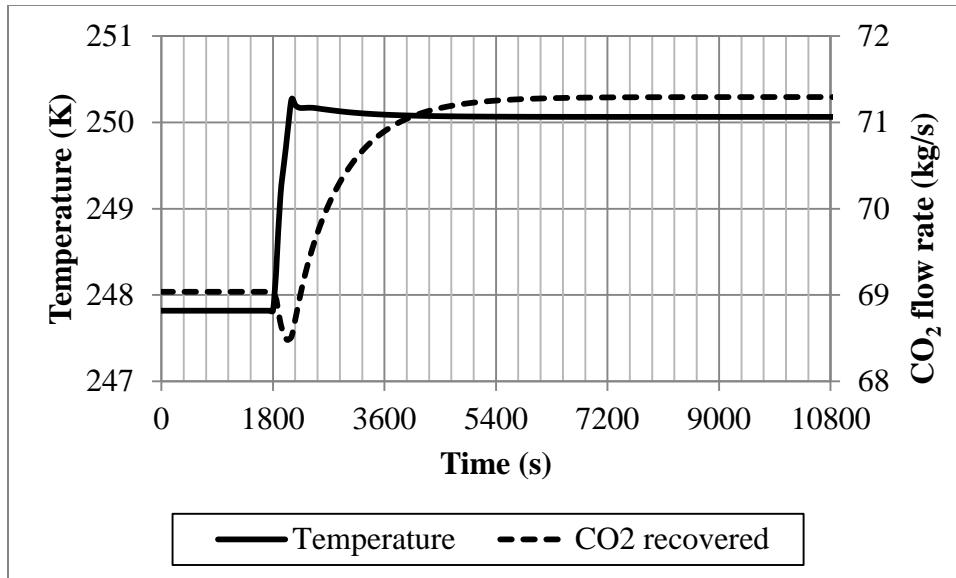
Figure 4.8 Stream 8's temperature and the CO_2 recovered from D-3 in response to the ramp-up change in K-2 discharge pressure

Consequently, the mass flow rate of stream 9, a gas stream leaving from D-3 to MHX-2, was decreased while its temperature was increased in accordance with increasing stream 8's temperature. The increase in stream 9's temperature caused an increase in stream 10's temperature but the temperature impact was balanced afterwards by the decrease in stream 9's mass flow rate. Therefore, the temperature of stream 10 was relatively steady, as shown in Figure 4.9. However, the amount of CO_2 separated from D-4 had the opposite trend compared to D-3. Since the CO_2 separated from D-3 decreased within the first 300 seconds, the amount of CO_2 carried over to D-4 increased initially. This then made the amount of CO_2 obtained from D-4 to increase within the first 300 seconds. Afterwards, the CO_2 fed to D-4 decreased, thereby decreasing the CO_2 in the liquid product stream, as shown in Figure 4.9. In other words, the amount of CO_2 recovered from D-4 was significantly determined by the amount of CO_2 carried over from D-3 rather than the temperature and pressure of stream 10.

Figure 4.9 Stream 10's temperature and the CO_2 recovered from D-4 in response to the ramp-up change in K-2 discharge pressure

The sum of liquid CO_2 obtained from D-3 and D-4 was used to calculate the total CO_2 recovery of the CO_2CPU, as shown in Figure 4.10. Because the increase in liquid CO_2 recovered from D-3 is more than the decrease in liquid CO_2 recovered from D-4, the total CO_2 recovery of the CO_2CPU was improved approximately by 1% when K02 discharge pressure increased by 3 bars.
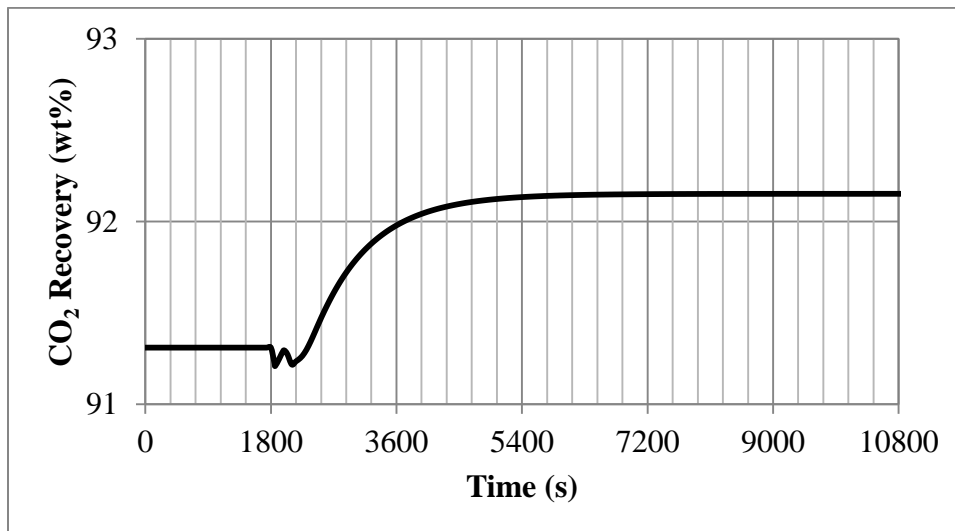
Figure 4.10 The CO_2 recovery in response to the ramp-up change in K-2 discharge pressure

76

While the CO_2 recovery was improved, the CO_2 purity was dropped by 0.5% as shown in Figure 4.11. This is because the operating conditions that favour CO_2 condensation also favour condensation of other (impurity) gases along with CO_2, thus the purity of CO_2 in the liquid stream had an opposite trend compared to the amount of liquid CO_2 recovered. Results obtained from this section show that the operating temperatures of D-3 and D-4 play a key role in the operation of CO_2CPU. It is noted that the amount of CO_2 captured and the purity obtained from D-3 were determined by its operating conditions (stream 8's pressure and temperature), while the amount of CO_2 captured and purity obtained from D-4 were determined by the amount of CO_2 carried over from D-3 to D-4. The CO_2 recovery responses to the change in operating pressure are slower than the CO_2 product purity. The CO_2 recovery took 3600 seconds while the CO_2 product purity took only 720 seconds to reach their new steady state values.
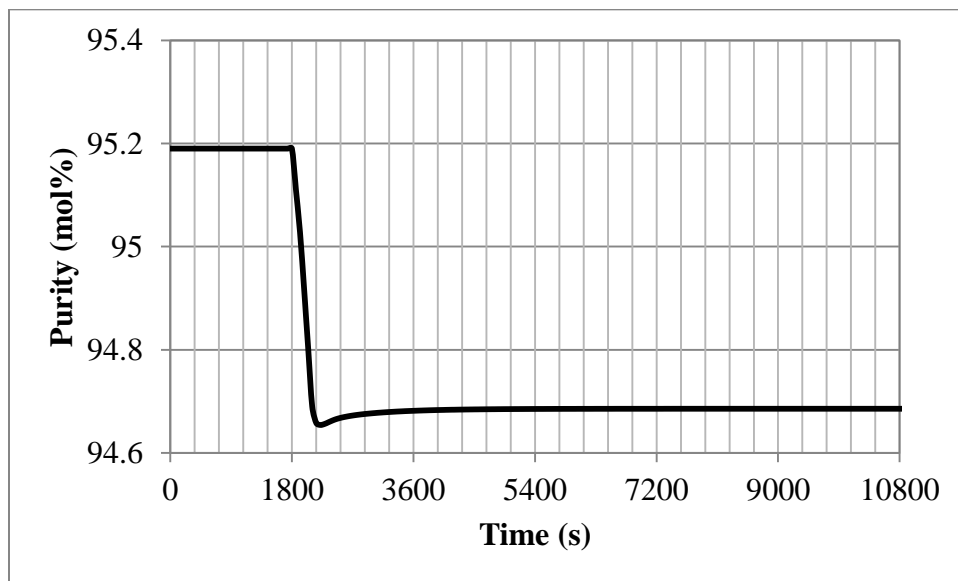

Figure 4.11 The CO_2 product purity in response to the ramp-up change in K-2 discharge pressure

The effect of decreasing pressure was also investigated by ramping down the discharge pressure of K-2 from 30 bars to 27 bars within 300 seconds. Opposite trends were observed in all process variables responses as expected. Because the operating pressure was decreased,

the amount of CO_2 condensation in D-3 was decreased. Thus, the amount of CO_2 carried over to MHX-2 was increased and more liquid CO_2 was separated from D-4 as shown in Figure 4.12.
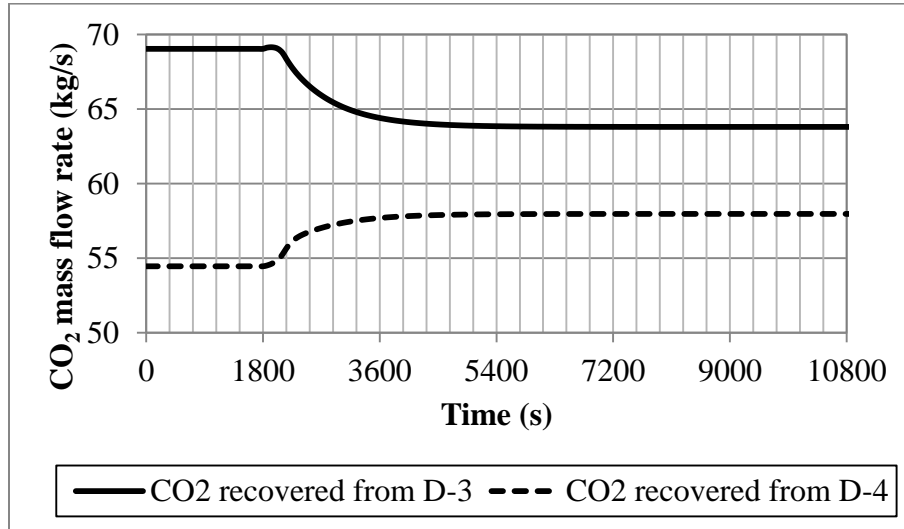
Figure 4.12 The amount of CO_2 recovered from D-3 and D-4 in response to the ramp-down change in K-2 discharge pressure

The total CO_2 recovery in response to the decrease in K-2 discharge pressure is presented in Figure 4.13. The CO_2 recovery results from the +10% ramp change is also shown in Figure 4.13 for comparison. Since the rate of increasing CO_2 recovered from D-4 is greater than the rate of decreasing CO_2 recovered from D-3, the CO_2 recovery initially increased, as can be seen in Figure 4.13. But since the increase in CO_2 recovered from D-3 is more than the decrease in CO_2 recovered from D-4, the total CO_2 recovery was dropped by about 1.3% when the K-2 discharge pressure was decreased by 3 bars. It should be noted that the +10% and -10% ramp changes in K-2 pressure return different changes in the CO_2 recovery.

On the other hand, the CO_2 product purity obtained for -10% ramp changes in K-2 pressure was increased because the lower pressure also reduces the condensation of inert impurities. Unlike the CO_2 recovery, the +10% and -10% ramp changes in K-2 pressure return almost the same changes in the CO_2 product purity which is about 0.5% mole as shown in Figure 4.14. It is also found that the CO_2 recovery responds to the decrease in K-2 discharge

pressure more significantly but is slower than for the CO_2 product purity, similar to the results obtained from the ramp-up change.
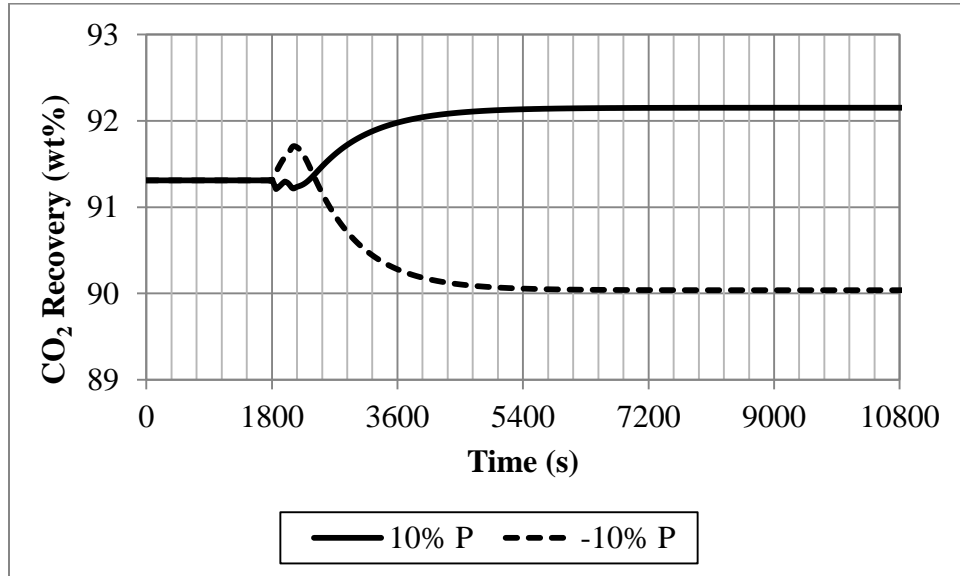

Figure 4.13 The CO_2 recovery in response to the changes in K-2 discharge pressure
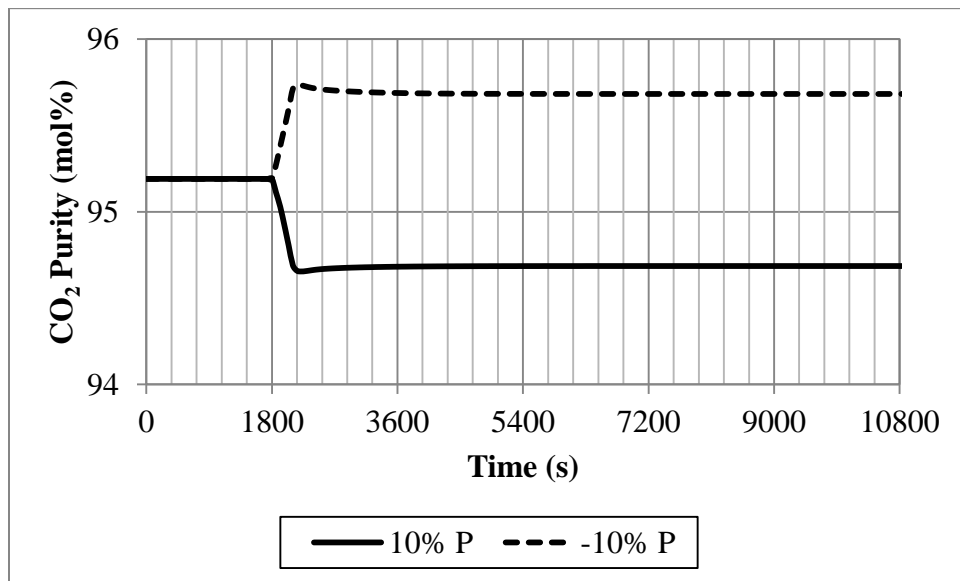

Figure 4.14 The CO_2 purity in response to the changes in K-2 discharge pressure

4.3 Effect of compressor train outlet temperature

In this section, the effect of the compressor train outlet temperature (stream 7's temperature) is examined. The mass flow rate of the coolant used in the cooler, C-2, was increased by 30% in a step manner. Increasing coolant flow rate reduced the hot gas outlet temperature in C-2 (stream 6's temperature). Consequently, the temperature of stream 7 decreased approximately by 2 K as shown in Figure 4.15.
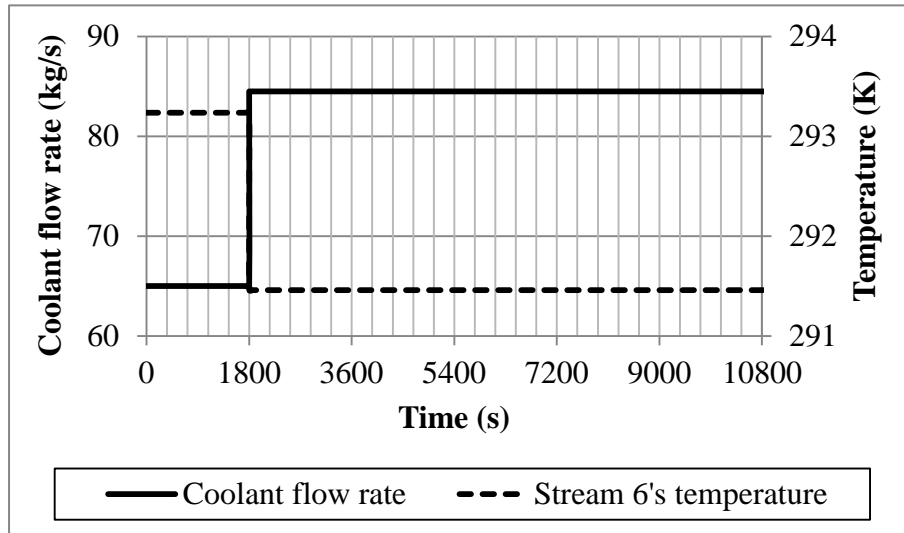
Figure 4.15 Stream 7's temperature in response to the step-up change in C-2 coolant flow rate

The rapid change in stream 7's temperature causes a decrease in stream 8's temperature by about 1 K within the first 120 seconds as shown in Figure 4.16. Consequently, more liquid was separated from D-3 and the amount of gas fed to MHX-2 and D-4 was decreased. Thus, the coolants flow rates of MHX-1 (streams 12 and 17) were decreased and caused the increase in stream 8's temperature afterwards. But since another coolant used in MHX-1, stream 22, was increased, the temperature of stream 8 was gradually decreased and finally reached a new steady state after 1 hour. The new steady state value of streams 8's temperature is approximately 0.7 K lower than its initial steady state value. However, this

condition favors the CO_2 condensation in D-3 therefore the amount of CO_2 recovered from D-3 was increased by 2.2 kg/s as shown in Figure 4.16.
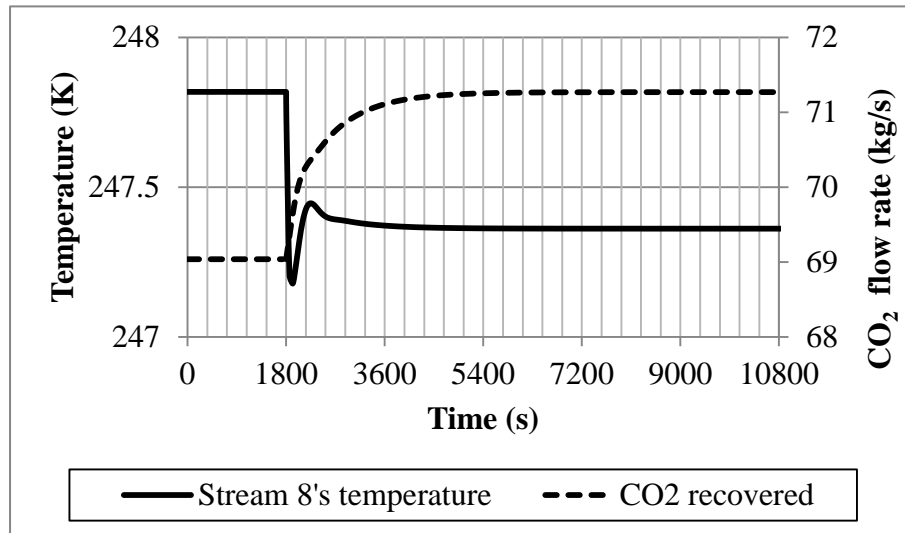
Figure 4.16 Stream 8's temperature and the CO_2 recovered from D-3 in response to the step-up change in the C-2 coolant flow rate

The CO_2 condensation in D-4 is affected by two variables, i.e. the temperature and flow rate of stream 10. The flow rate of stream 10 is determined by the operation in D-3. In this case, the flow rate of stream 10 decreased due to the decrease in D-3 operating temperature. The temperature of stream 10 in response to the step change in coolant flow rate is presented in Figure 4.17. Because the stream 10's temperature relies on the temperatures of streams 8 and 9, it was dropped according to the stream 8's temperature within the first 240 seconds. Subsequently, it was increased again because of decreases in the coolant flow rates in MHX-2 (streams 12, 14 and 16). The new steady state value of stream 10's temperature is only 0.3 K lower than its initial steady state value. This small decrease in the temperature did not help the CO_2 condensation along in D-4, and since the CO_2 carried over to D-4 was decreased, the CO_2 recovered from D-4 was dropped as also shown in Figure 4.17.
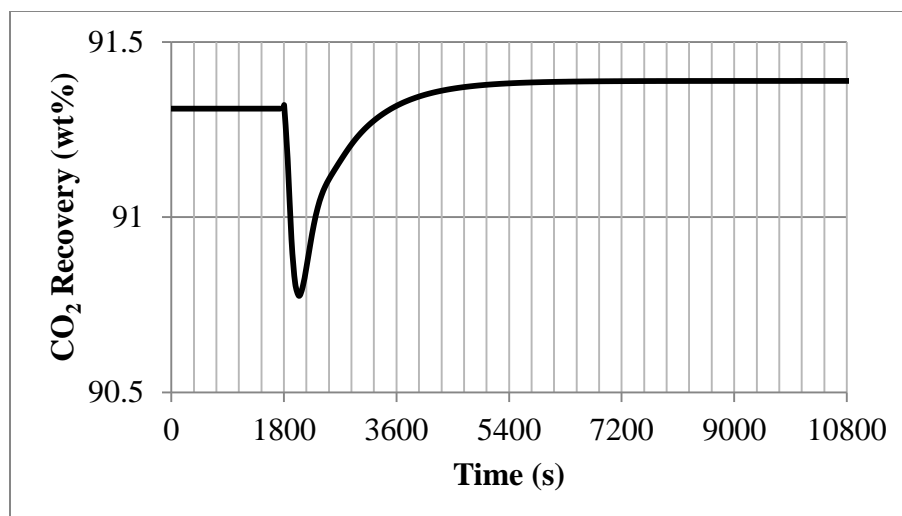
81
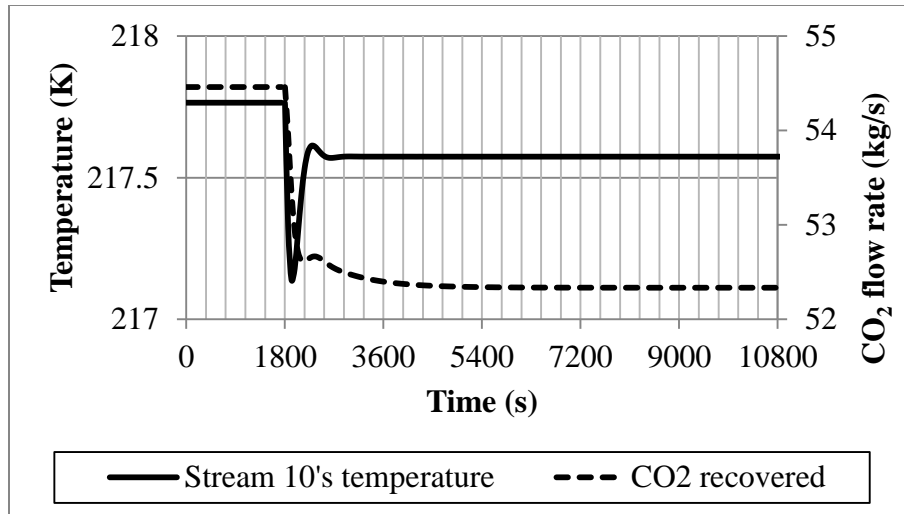
Figure 4.17 Stream 10's temperature and the CO_2 recovered from D-4 in response to the step-up change in the C-2 coolant flow rate

The sum of CO_2 obtained from D-3 and D-4 was used to calculate the CO_2 recovery. Figure 4.18 presents the total CO_2 recovery of the Air Product's CO_2CPU in response to the change in the C-2 coolant flow rate. Similar to the ramp change in pressure, an overshoot was found in the CO_2 recovery response. This is because the rate of decreasing CO_2 recovered from D-4 is more than the rate of increasing CO_2 recovered from D-3 at the beginning of responses. When the CO_2 condensed in D-4 reaches steady state, the amount of CO_2 condensed in D-3 starts playing a role on the CO_2 recovery, thereby increasing the CO_2 recovery as shown in Figure 4.18. Increasing 30% coolant flow rate in C-2 increased only by 0.1wt% the total CO_2 recovery.

Figure 4.18 CO_2 recovery in response to the step-up change in the C-2 coolant flow rate

Molar-averaged purities between the CO_2 recovered from D-3 and D-4 were calculated to determine the CO_2 purity in the product stream. In this case, the temperatures of streams 8 and 10 were decreased by less than 1 K while the pressure remained constant resulting in an insignificant change in the CO_2 product purity as shown in Figure 4.19. However, it was observed that the CO_2 purity was changed similarly to the operating temperature of each drum. This is because the liquid compositions obtained from the flash drum were calculated using the equilibrium K-value which is a function of temperature and pressure of the drum. Thus, the trend of CO_2 purity was matched the temperature trends streams 8 and 10 as shown in Figure 4.19.
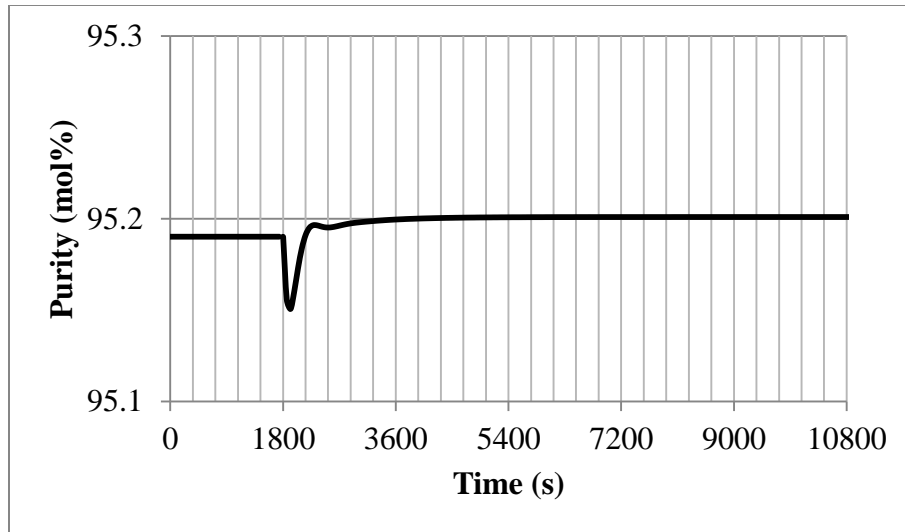
Figure 4.19 The CO_2 purity in response to the step-up change in the C-2 coolant flow rate

The effect of decreasing C-2 coolant flow rate was also evaluated. The mass flow rate of the coolant used in C-2 was decreased by 30% in a step fashion. In this case, the stream 6's temperature changed by 4.5 K. All process variables had opposite trends compared to results obtained from the +30% step change in coolant flow rate, but the magnitude of changes were different, as shown in Figure 4.20 and Figure 4.21.
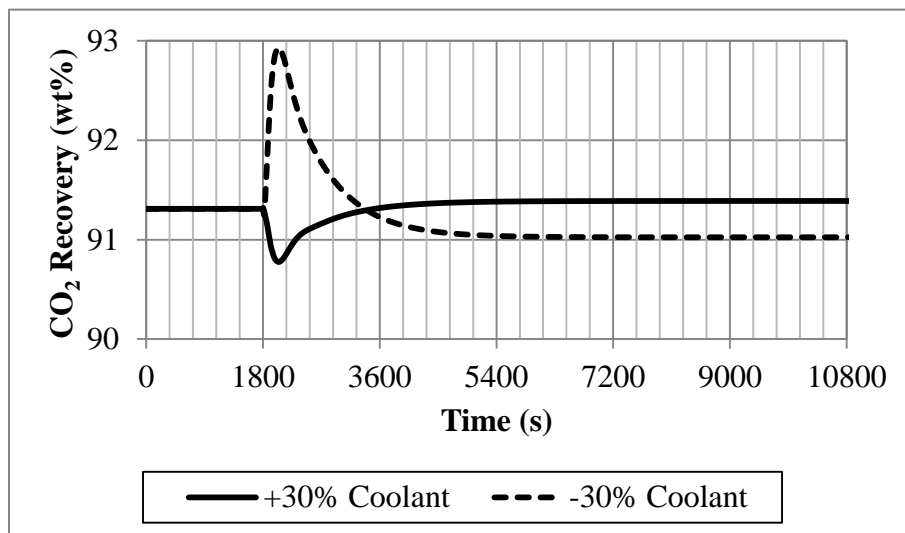
Figure 4.20 The CO_2 recovery in response to the changes in the C-2 coolant flow rate
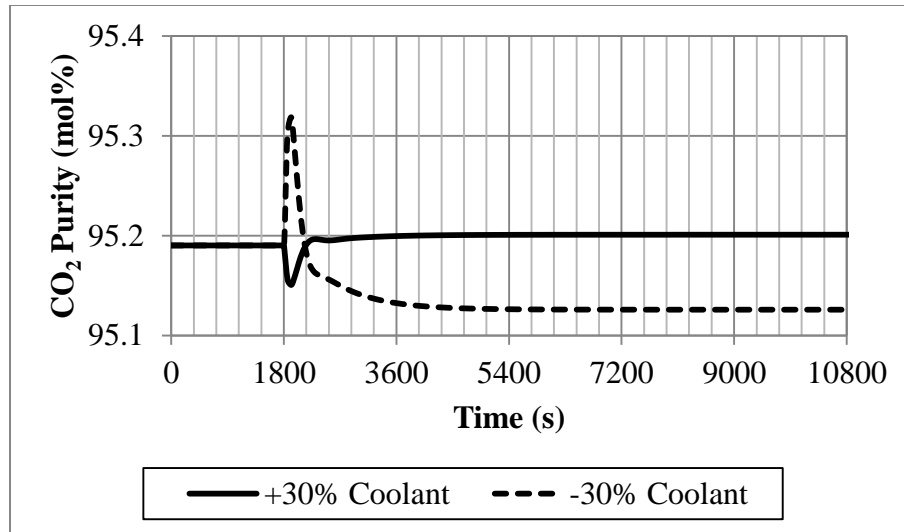
Figure 4.21 The CO_2 purity in response to the changes in the C-2 coolant flow rate

The CO_2 recovery decreased by 0.3% while the CO_2 product purity decreased by 0.07% in response to the -30% coolant flow rate in C-2, as shown in Figure 4.20 and Figure 4.21, respectively. It is noted that the changes in the amount of CO_2 captured and CO_2 purity observed in this section were very small due to the slight changes in temperatures of D-3 and D-4. The +30% and -30% changes in the coolant flow rate returns different changes in the CO_2 recovery and the CO_2 purity. Additionally, it was observed that the CO_2 recovery is more sensitive but slower to respond, to the operating conditions than the CO_2 purity, as also found in the previous section.

4.4 Effect of flue gas flow rate

The flue gas flow rate depends on the power plant load which is related to the electricity demand, and thus it may vary subject to the changes in the power plant operation. This section analyzes the effect of flue gas flow rate on the CO_2CPU capture performance. The mass flow rate of the flue gas was ramped up by 10% of the base case value presented in Table 3.1 (166.9 kg/s) within 1800 seconds while keeping the flue gas composition constant. Because the coolant flow rates used in C-1 and C-2 were constant while the amount of hot

flue gas increased, the flue gas left the cooler C-2 with a higher temperature as shown in Figure 4.22 (stream 7's temperature).
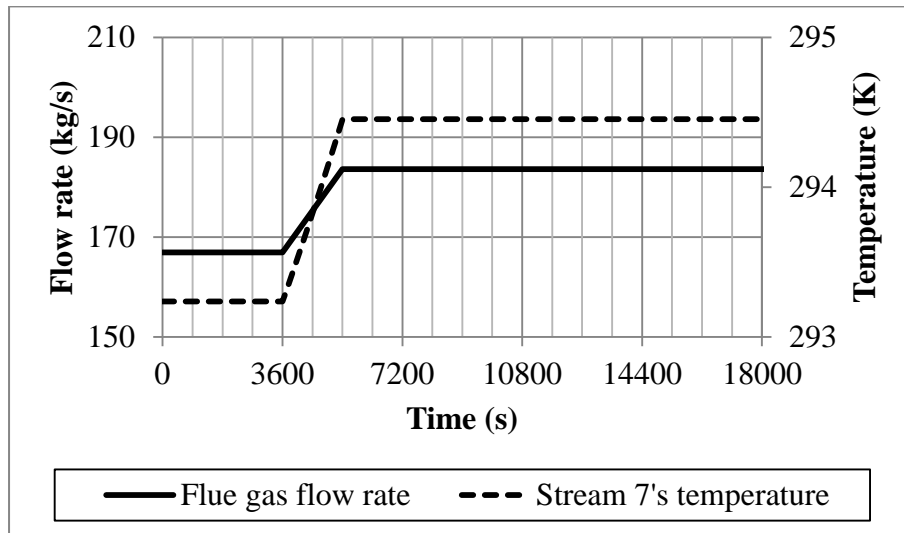
Figure 4.22 Stream 7's temperature in response to the ramp-up change in the flue gas flow rate

Increases in the temperature of stream 7 caused an increase in the temperature of stream 8 within the first 1800 seconds as shown in Figure 4.23. Increasing stream 8's temperature reduced the CO_2 condensation in D-3, thus the amount of gas leaving from D-3 to MHX-2 and then to D-4 increased. Because the amount of gas flowing to MHX-2 and D-4 increased, flow rates of streams 12 and 17 produced from D-4 were also increased. Streams 12 and 17 are used as coolants in MHX-1. Increasing coolant flow rates enhance the heat transfer rates resulting in decreasing hot gas temperature. Thus, the stream 8's temperature was dropped after 1800 seconds of ramp change because of increases in flow rates of streams 12 and 17 as shown in Figure 4.23. The stream 8's temperature was eventually steady at about 1.5 K higher than its base case value. Furthermore, the increase in stream 8's temperature affects the CO_2 condensation in D-3. The amount of CO_2 recovered from D-3 was initially dropped within 900 seconds due to the rapid increase in stream 8's temperature. Afterwards, the rate of change in stream 8's temperature was reduced and the amount of CO_2 recovered from D-3 was increased due to the effect of increasing flue gas flow rate. After 1800 seconds, the flue

86

gas flow rate became constant but still played a key role in D-3, such that the CO_2 recovered continued to increase, as shown in Figure 4.23. It should be noted that the total increase in the CO_2 recovered from D-3 is about 2 kg/s while the total increase of CO_2 in the flue gas flow rate is 13.5 kg/s.
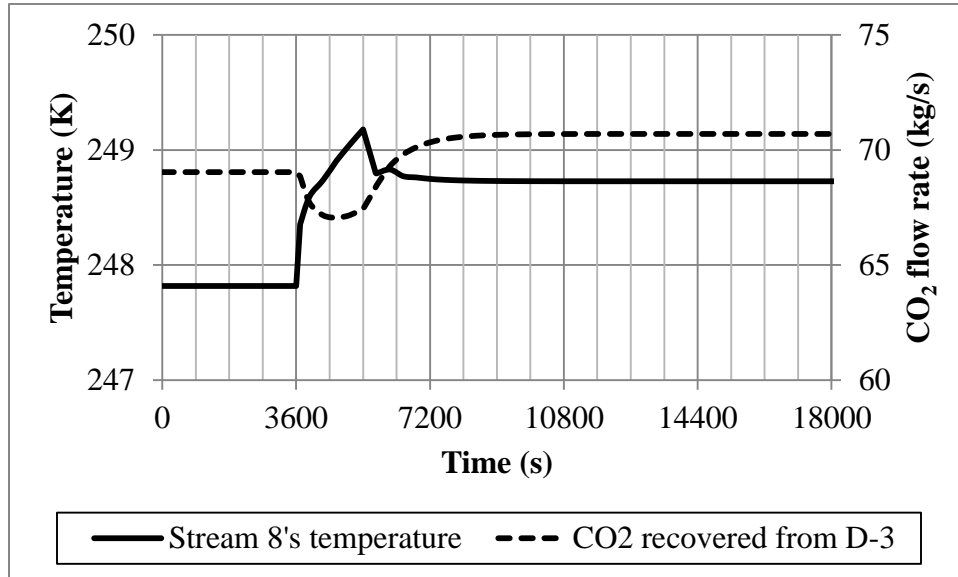
Figure 4.23 Stream 8's temperature and CO_2 recovered from D-3 in response to the ramp-up change in the flue gas flow rate

The temperature of stream 8 determined the inlet temperature of the hot gas flowing to MHX-2 and also the outlet temperature of hot gas (stream 10's temperature). Since stream 8' temperature increased, the stream 10's temperature also increased, as shown in Figure 4.24. It is found from Figure 4.24 that the stream 10's temperature has a similar trend to the stream 8's temperature. The stream 10's temperature was initially increased in accordance with stream 8's temperature within 1800 seconds, but dropped afterwards due to the effect of increasing flue gas. Increasing flue gas flow rate increased the flow rate of gas leaving from D-3 to MHX-2, as described previously. Consequently, the flow rates of streams 11 and 14 obtained from D-4 were increased. Streams 11 and 14 are used as coolants in MHX-2; therefore the hot gas outlet temperature (stream 10's temperature) was decreased because of increases in the flow rates of streams 11 and 14 after 1800 seconds. The temperature of

stream 10 decreased to a new steady state at about 218.5 K. Because D-4 operates at conditions determined by stream 10, increasing stream 10's temperature should decrease the CO_2 condensation in D-4. However, the liquid CO_2 recovered from D-4 was increased as a consequence of increasing flue gas flow in the CO_2CPU. This indicates that a change in the flue gas flow rate has a more significant impact on the CO_2 condensation in D-4 than the change in stream 10's temperature. The amount of CO_2 recovered from D-4 was increased approximately by 10 kg/s as shown in Figure 4.24.
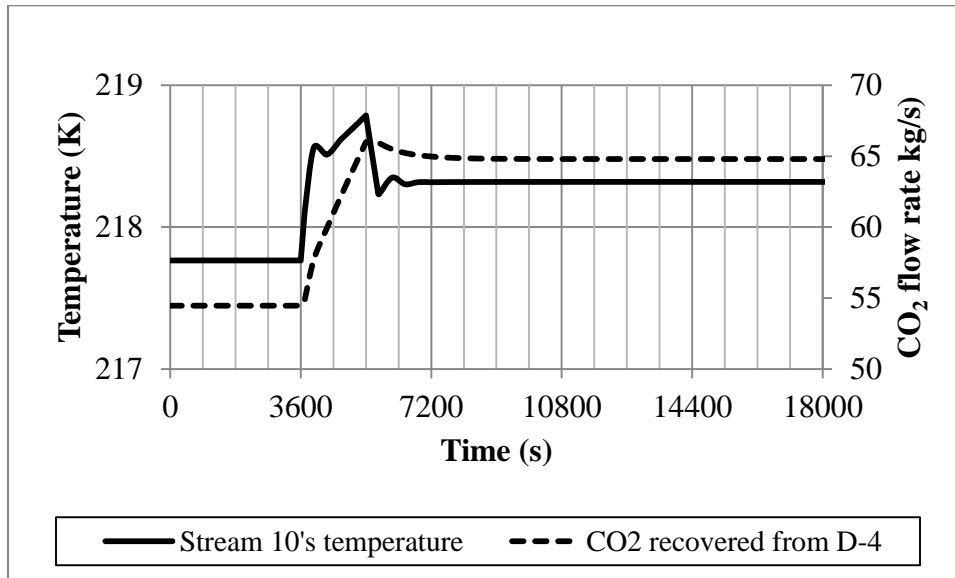
Figure 4.24 Stream 10's temperature and CO_2 recovered from D-4 in response to the ramp-up change in the flue gas flow rate

The ratio between the sum of CO_2 recovered from D-3 and D-4 and the amount of CO_2 in the flue gas was calculated to determine the total CO_2 recovery of the CO_2CPU, and the result is shown in Figure 4.25. The flue gas flow rate was continuously increased at constant flue gas composition, thereby increasing CO_2 in the flue gas within 1800 seconds. It was found that the rate of increasing CO_2 in the flue gas was faster than the rate of increase in the sum of CO_2 recovered from D-3 and D-4. Therefore, the CO_2 recovery initially dropped. After 1800 seconds, the flue gas flow rate was constant while the sum of CO_2 recovered from D-3 and D-4 was still increasing. Hence, the CO_2 recovery was increased back after 1800 seconds.

However, the total increase of liquid CO_2 (2 kg/s increased in D-3 and 10 kg/s increased in D-4) is still less than the total increase of the CO_2 in flue gas (13.5 kg/s). Hence, the overall CO_2 recovery dropped by approximately 0.3wt% when the flue gas mass flow rate was increased by 10% as shown in Figure 4.25.
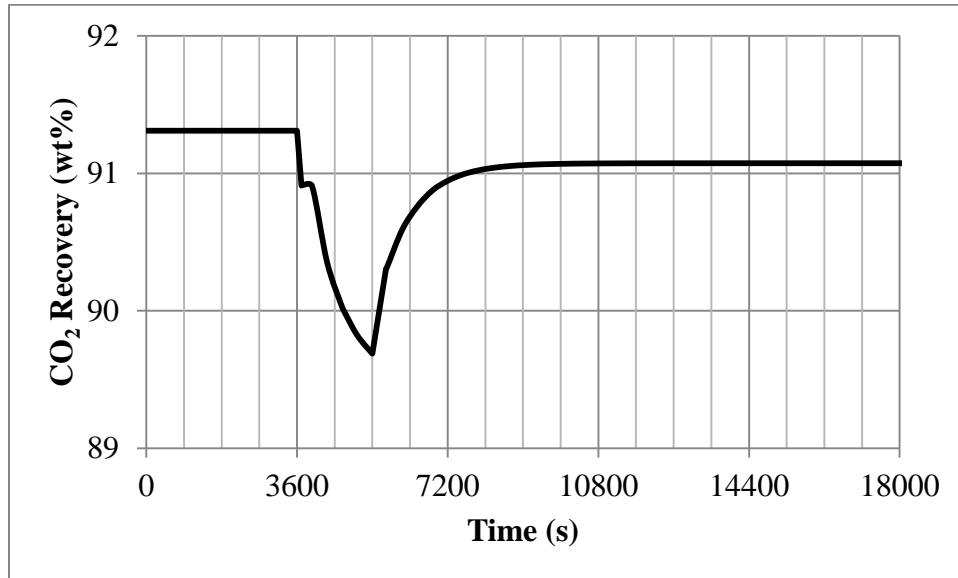
Figure 4.25 The CO_2 recovery in response to the ramp-up change in the flue gas flow rate

The mole fraction of CO_2 in the condensate obtained from D-3 and D-4 are presented in Figure 4.26. Because the liquid composition obtained from the flash drum is determined by the vapour-liquid equilibrium K-value, which is a function of operating temperature and pressure of the flash drum, the mass fraction of CO_2 in the condensate obtained from D-3 and D-4 followed the temperature trends of streams 8 and 10, respectively. Increasing the temperature reduces the inert impurities condensation, thus increasing the purity of liquid CO_2 recovered from D-3 and D-4, as shown in Figure 4.27. However, the molar-averaged between the CO_2 mole fractions obtained from D-3 and D-4, that is the overall CO_2 product purity, decreased, as shown in Figure 4.28. This is because the molar-average purity depends not only on the CO_2 mole fractions obtained from D-3 and D-4 but also the total amount of liquid condensates recovered from D-3 and D-4.

89
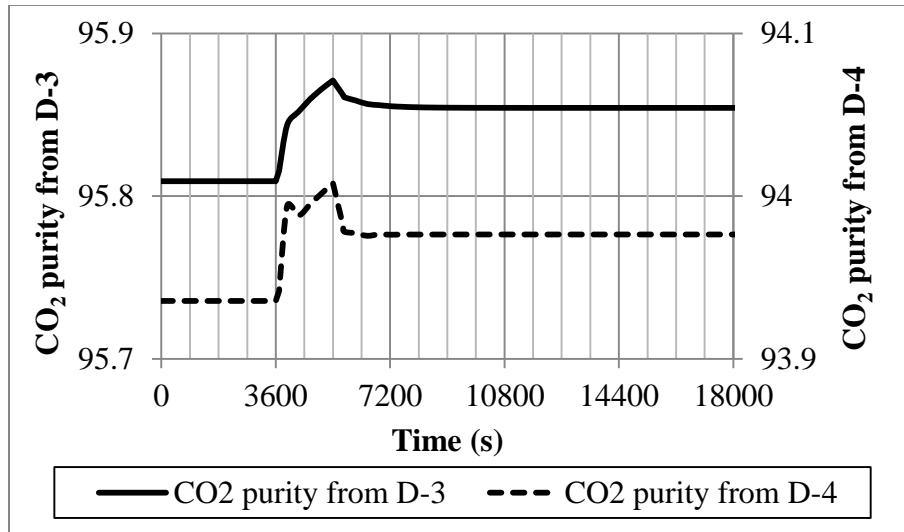
Figure 4.26 Purities of liquid CO_2 recovered from D-3 and D-4 in response to the ramp-up change in the flue gas flow rate

Within the first 360 seconds, rapid increases in the CO_2 mass fractions obtained from D-3 and D-4 are dominant, thus the CO_2 product purity increased correspondingly. Afterwards, increases in the amount of liquid condensates recovered from D-3 and D-4 were more significant than increases in the CO_2 mass fractions; thereby the molar-average purity of the CO_2 product stream decreased, as shown in Figure 4.28. After 1800 seconds, the operating temperatures of D-3 and D-4 were dropped fairly, resulting in decreases in the CO_2 mole fractions obtained from D-3 and D-4. The molar-average CO_2 product purity was then continuously decreased but the rate of decrease was relatively faster as can be recognized from the change in the slope of CO_2 product purity presented in Figure 4.28. Afterwards, the CO_2 mole fractions obtained from D-3 and D-4 were considerably constant while the amount of condensates recovered from D-3 and D-4 were slightly decreased; thereby the molar-averaged CO_2 product purity was slightly increased back after about 2160 seconds. The CO_2 product purity reached a new steady state at 95.17mol% (approximately 0.03mol% lower than its initial steady state value), as shown in Figure 4.28.
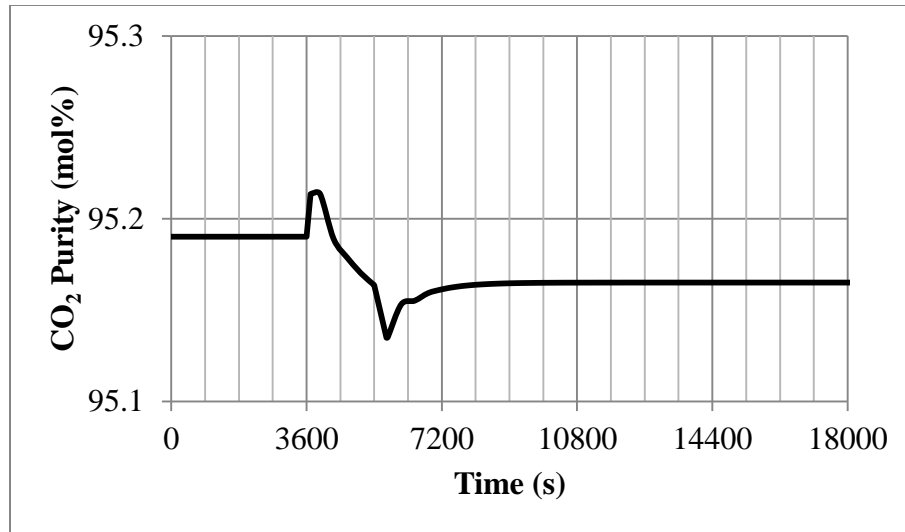
Figure 4.27 CO_2 product purity in response to the ramp-up change in the flue gas flow rate

Five more ramp changes were also performed, -10%, ±20% and ±30% on the flue gas flow rate within 1800 seconds. The ramp-down change returned opposite trends while the ramp-up changes at different magnitude of ramp change in the flue gas flow rate returned similar responses compared to the +10% change described above. However, it is observed that using the same magnitude of change but different direction, e.g., -20% and +20%, returned different changes in the CO_2 recovery and CO_2 product purity as shown in Figure 4.28 and Figure 4.29, respectively. The +20% flue gas changed the CO_2 recovery by 0.5wt% and the CO_2 product purity by 0.05mol%, while the -20% flue gas changed the CO_2 recovery by 0.3wt% and the CO_2 product purity by 0.01mol%. Although the changes are very small, they can indicate the nonlinearity of the Air Products' CO_2CPU design.
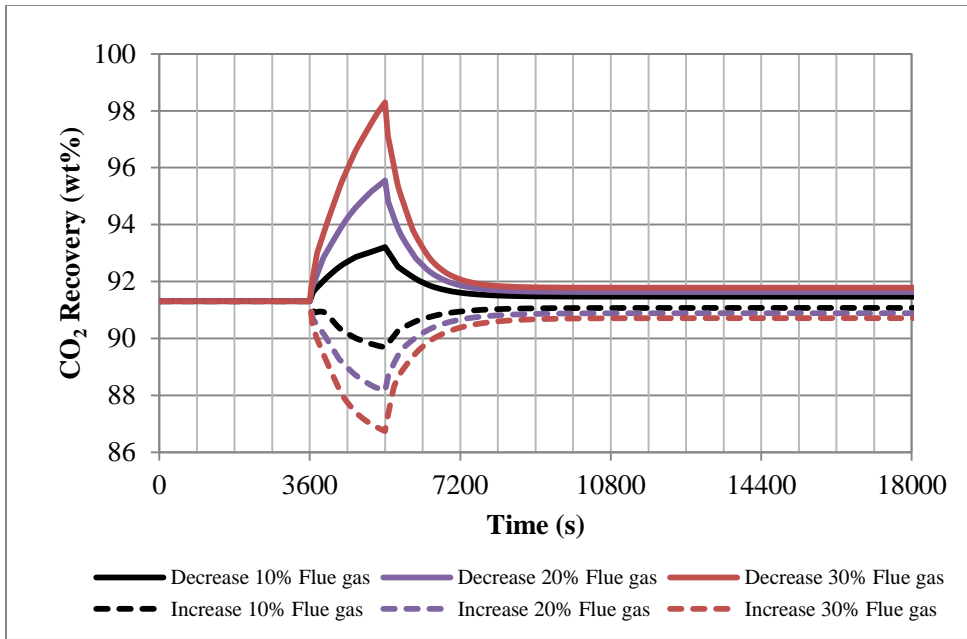
Figure 4.28 CO_2 recovery in response to the changes in the flue gas flow rate
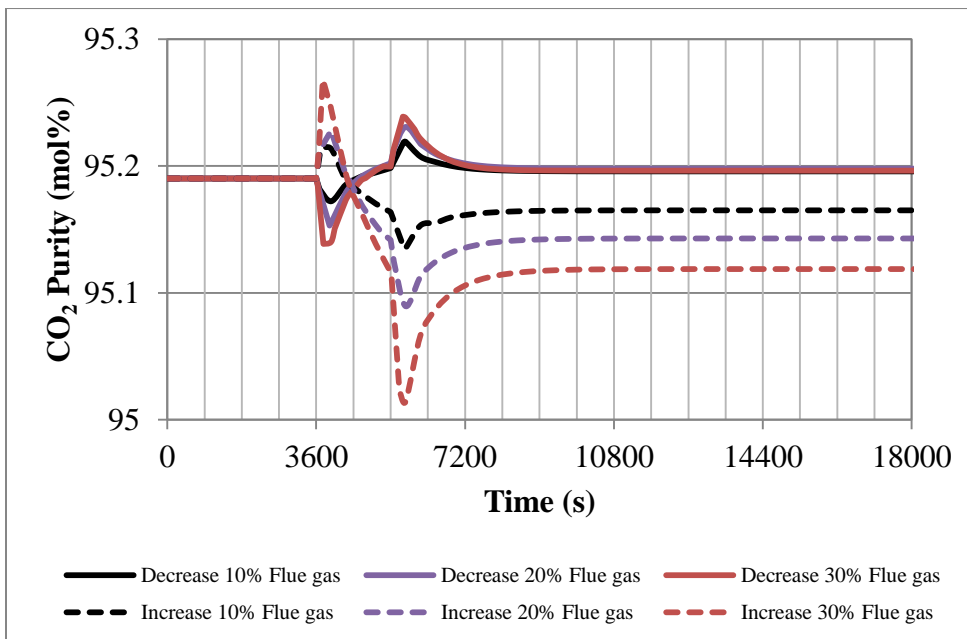
Figure 4.29 CO_2 product purity in response to the changes in the flue gas flow rate

4.5 Effect of flue gas composition

Flue gas flow rate and composition may vary subject to the changes in the power plant operation. The flue gas flow rate depends on the power plant load that relies on the electricity demand while the flue gas compositions depend on the fuel type and the purity of oxygen used for combustion. In this section, it was assumed that changes in power plant operation will affect mainly the amount of CO_2 in the flue gas. Ramp changes were applied to the mass flow rate of CO_2 in the flue gas while the mass flow rates of other impurities contained in the flue gas, i.e. O_2, Ar, N_2, H_2O, SO_2 and NO, were held constant. In this section, six ramp changes were performed, ±10%, ±20% and ±30% on the CO_2 mass flow rate within 1800 seconds. The final flue gas flow rate and composition after each ramp change are shown in Table 4.2 including the base case value before applying the ramp change.

Table 4.2 Flue gas conditions after ramp changes in CO_2 mass flow rate of the Air Products' CO_2CPU

Flue gas conditions	Percentage of the CO_2 flow rate change						
	Base case	-10%	-20%	-30%	10%	20%	30%
Total mass flow (kg/s)	166.92	180.44	193.97	207.49	153.39	139.87	126.34
Mass Flow (kg/s)							
CO_2	135.25	121.73	108.20	94.68	148.78	162.30	175.83
O_2	8.12	8.12	8.12	8.12	8.12	8.12	8.12
AR	3.98	3.98	3.98	3.98	3.98	3.98	3.98
N_2	17.35	17.35	17.35	17.35	17.35	17.35	17.35
H_2O	1.32	1.32	1.32	1.32	1.32	1.32	1.32
SO_2	0.85	0.85	0.85	0.85	0.85	0.85	0.85
NO	0.05	0.05	0.05	0.05	0.05	0.05	0.05
Mole fraction							
CO_2	0.743	0.723	0.699	0.670	0.761	0.777	0.790
O_2	0.061	0.066	0.072	0.079	0.057	0.053	0.050
AR	0.024	0.026	0.028	0.031	0.022	0.021	0.020
N_2	0.15	0.162	0.176	0.193	0.139	0.130	0.122
H_2O	0.018	0.019	0.021	0.023	0.016	0.015	0.014
SO_2	0.003	0.003	0.004	0.004	0.003	0.003	0.003
NO	0.000	0.000	0.000	0.001	0.000	0.000	0.000

Increasing the mass flow rate of CO_2 in the flue gas increases the total flue gas flow rate and the mass fraction of CO_2. Because the coolants used in coolers C-1 and C-2 were constant while the amount of hot flue gas flowing through them was increased, the outlet temperature of the flue gas (stream 6's temperature) was increased. Accordingly, the temperature of streams 8 was also increased, as shown in Figure 4.30.
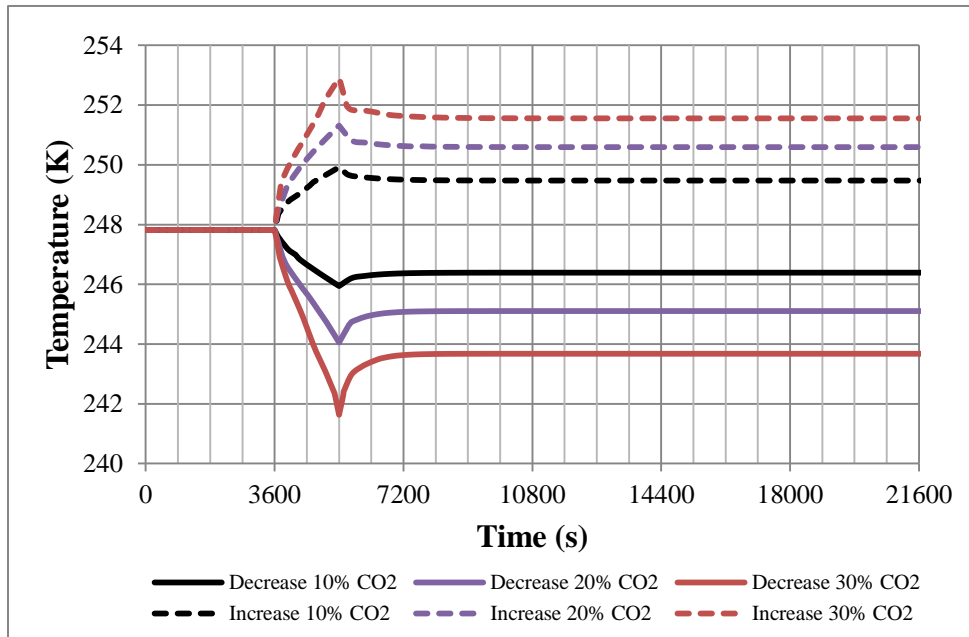
Figure 4.30 Stream 8's temperature in response to the ramp changes in the flue gas flow rate and compositions

The temperature of stream 8 changed rapidly at the beginning of the ramp change (within about 180 seconds) and then the rates of change dropped due to the effect of mass flow rate. For example, in the case of increasing CO_2 flow rate in the flue gas, the stream 8's temperature initially increased together with increasing CO_2 flow rate in the flue gas. On the one hand, increasing the temperature limits CO_2 condensation in D-3, and on the other hand increasing CO_2 in the feed increases the total amount of gas in the system; thus the flow rate of gas leaving from D-3 to MHX-2 was increased. Accordingly, flow rates of streams 12 and 17, which are coolants in MHX-1, were increased. Increasing coolant flow rates increases the rate of heat transfer in MHX-1, therefore the rate of increasing stream 8's temperature was

dropped after the first 180 seconds of ramp change. Afterwards, the CO_2 flow rate and the flue gas flow rate were held constant and the effect of increasing coolant flow rates become more significant. Hence, the temperature of stream 8 was dropped after 1800 seconds of ramp change, as shown in Figure 4.31.
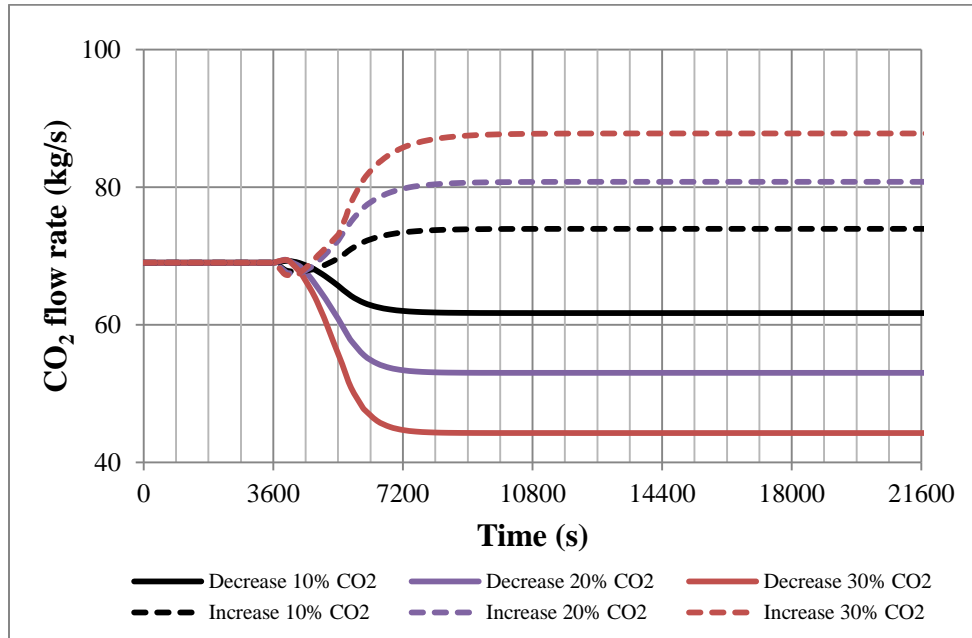
Figure 4.31 Amount of CO_2 recovered from D-3 in response to the ramp changes in the flue gas flow rate and compositions

Even though increasing stream 8's temperature should limit CO_2 condensation in D-3, the amount of CO_2 recovered from D-3 was increased, as shown in Figure 4.32, due to the influence of increasing CO_2 flow rate in the flue gas. The more CO_2 fed to the CO_2CPU, the more CO_2 recovered from D-3. It was observed that the amount of CO_2 recovered from D-3 was relatively constant within the first 900 seconds of ramp change. This is because the stream 8's temperature changed quickly within the first 900 seconds and thus the change in stream 8's temperature had a significant impact on the CO_2 condensation in D-3. However, the effect of stream 8's temperature was balanced by the effect of changing CO_2 flow rate in the flue gas; therefore the total amount of CO_2 recovered from D-3 was relatively constant within the first 900 seconds. Afterwards, the effect of change in mass flow rate of CO_2 in the

95

flue gas was dominant and the amount of CO_2 recovered from D-3 was changed according to the mass flow rate of CO_2, as shown in Figure 4.31.

Changing stream 8' temperature affects not only the CO_2 recovered from D-3 but also the operating temperature of D-4 since it determines the inlet temperature of the hot gas of MHX-2 (stream 9). When the temperature of stream 8 was increased, temperatures of streams 9 and 10 also increased. Because D-4 operates at the temperature of stream 10, the amount of liquid CO_2 recovered from D-4 is expected to change corresponding to stream 10's temperature. However, six ramp changes in CO_2 flow rate showed that the change in stream 10's temperature did not significantly influence the CO_2 condensation in D-4. Instead, the amount of CO_2 recovered from D-4 was changed in accordance with the amount of CO_2 carried over from D-3 to D-4. It was found from the simulation results that the amount of CO_2 carried over from D-3 to D-4 in this case greatly relied on the mass flow rate of CO_2 in the flue gas more than the operating temperature of D-3 (stream 8). The more CO_2 fed into the CO_2CPU, the more CO_2 carried over and the more CO_2 obtained from D-4. Thus, increasing the mass flow rate of CO_2 in the flue gas increased the amount of liquid CO_2 recovered from both D-3 and D-4. The sum of liquid CO_2 recovered from D-3 and D-4 is presented in Figure 4.32.
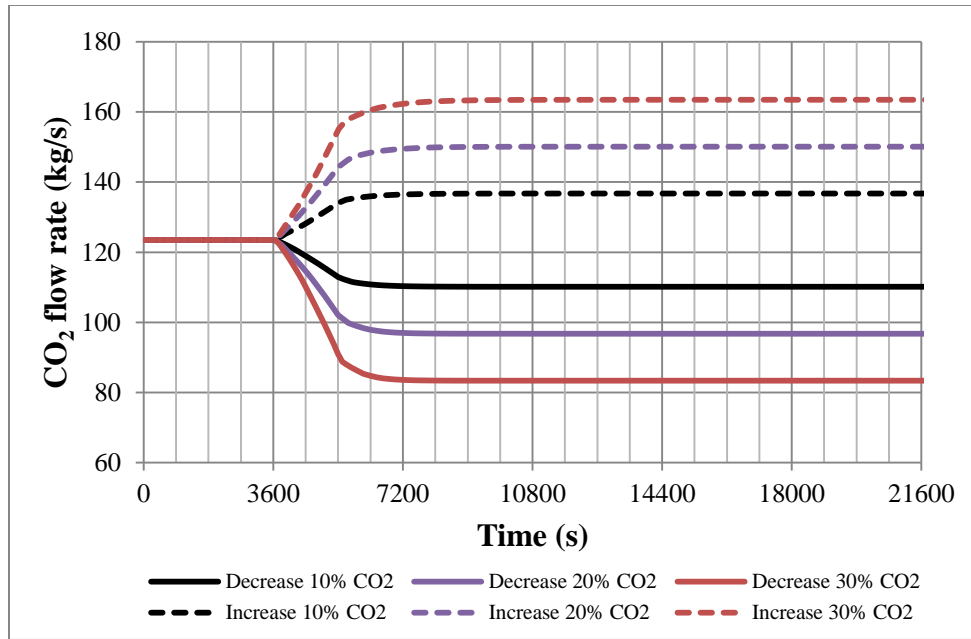
Figure 4.32 Sum of CO_2 recovered from D-3 and D-4 in response to the ramp changes in the flue gas flow rate and compositions

An overshoot or inverse response was observed when dividing the sum of liquid CO_2 obtained from D-3 and D-4 by the mass flow rate of CO_2 in the flue gas to calculate the CO_2 recovery, as shown in Figure 4.34. In the case of increasing CO_2 flow rate in the flue gas, the CO_2 recovery decreases initially because the rate of increasing flow rate of CO_2 in the flue gas was higher than the rate of increasing CO_2 recovered from D-3 and D-4. After 1800 seconds of ramp change, the flow rate of CO_2 in the flue gas was held constant and thus the CO_2 recovery increased with increasing the sum of liquid CO_2 obtained from D-3 and D-4. Opposite responses were obtained from the ramp-down tests. The CO_2 recoveries of six ramp changes are shown in Figure 4.33. The maximum change in the CO_2 recovery is about 3% when the mass flow rate of CO_2 in the flue gas was ramped down by 30% (CO_2 content reduced from 74% to 67% molar basis).
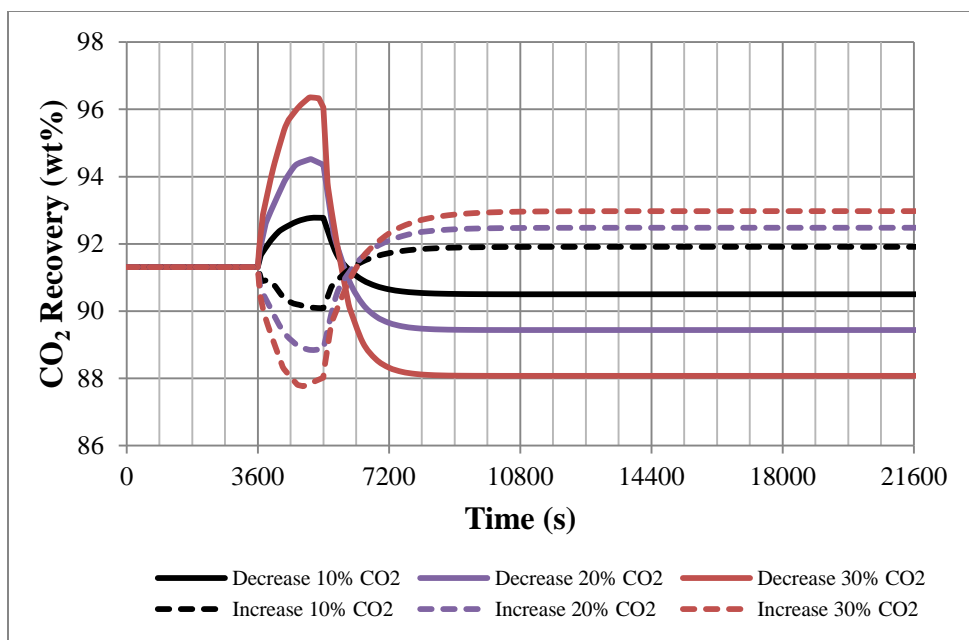
Figure 4.33 The CO_2 recovery in response to the ramp changes in the flue gas flow rate and compositions

The molar-averaged between the CO_2 mass fractions obtained from D-3 and D-4 was calculated to determine the CO_2 product purity. As described in the previous section, the molar-averaged purity depends on two factors, i.e. the CO_2 mass fractions and the total liquid condensates obtained from D-3 and D-4. Increasing mass flow rate of CO_2 in the flue gas increases the total flue gas flow rate and the mass fraction of CO_2, but decreases the mass fraction of impurities (O_2, Ar, N_2, H_2O, SO_2 and NO). Thus, the molar-averaged CO_2 purity is expected to increase when the CO_2 mass flow rate is increased, while the opposite response is expected in the case of decreasing the mass flow rate of CO_2. Results obtained from six ramp changes support this assumption, as shown in Figure 4.34. A slight drop in the CO_2 purity after 1800 seconds of ramp change was observed in Figure 4.34 when the mass flow rate of CO_2 in the flue gas was ramped up by 30%. This is because the vapour and liquid compositions obtained from the flash drum are determined by the equilibrium K-value, which is a function of temperature and pressure of the flash drum. If the temperatures of streams 8 and 10 (operating temperatures of D-3 and D-4) were significantly changed, the

change in CO_2 product purity would be observed accordingly. As shown in Figure 4.30, stream 8's temperature decreased after 1800 seconds of the +30% ramp change in the mass flow rate of CO_2. The trend of change in stream 8's temperature was already described above. Accordingly, the K-value and mole fraction of CO_2 in the condensate obtained from D-3 were decreased, thereby decreasing the CO_2 product purity after 1800 seconds of the +30% ramp change as shown in Figure 4.34. Similar results were obtained from the +10% and +20% ramp changes and the opposite trends were observed when the CO_2 flow rate in flue gas was ramped down as shown in Figure 4.34. The maximum change in the CO_2 purity is about 0.6mol% when the mass flow rate of CO_2 in the flue gas was ramped down by 30% (CO_2 content reduced from 74% to 67% molar basis).
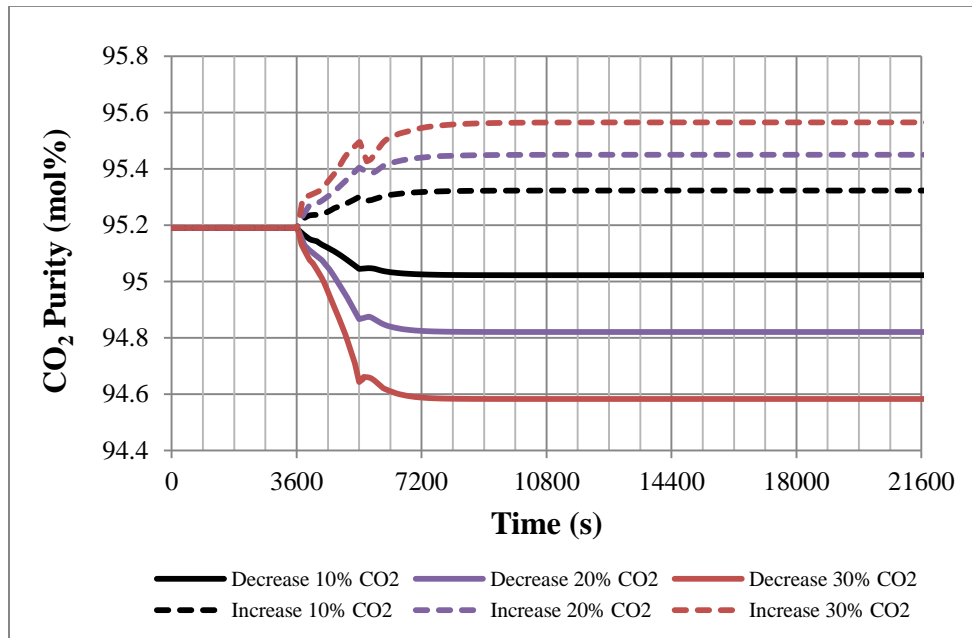

Figure 4.34 CO_2 purity in response to the ramp changes in the flue gas flow rate and compositions

It should also be noted that the +30% and -30% ramp changes in CO_2 mass flow rate returns different changes in the CO_2 recovery and CO_2 product purity. Similar results were observed from the other tests, as shown in sections 4.2-4.4. These results demonstrate the nonlinearity

of the CO_2CPU plant that will make the control system design for CO_2CPU more challenging.

4.6 Pilot plant flue gas compositions

In this section, the flue gas composition is subject to change in accordance with the oxyfuel pilot plant operation. Experimental data obtained from the Air Products Vattenfall Oxyfuel CO_2 Compression and Purification Pilot Plant (ACPP) was recently presented to the Oxyfuel combustion conference (White et al., 2013). The flue gas of the ACPP was taken from the Vanttenfall's 30 MW_{th} oxyfuel demonstration plant (OxPP) which periodically turned down the oxy-fired mode and allowed air ingress at night. Thus, the ACPP's CO_2 feed composition was alternated between two levels as shown in Figure 4.35. During the oxy-fired mode, the CO_2 concentration was approximately at 78% while the air ingress mode provided about 74% CO_2 concentration.
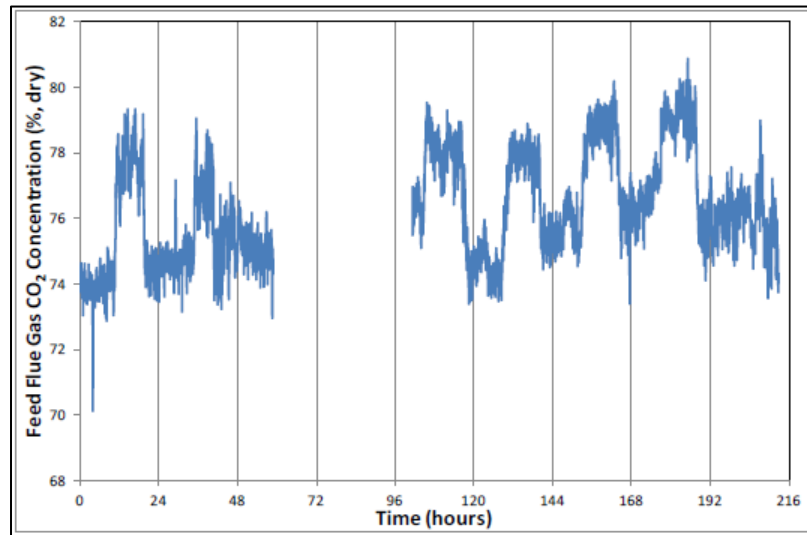
Figure 4.35 CO_2 content in the flue gas obtained from the Vattenfall's demonstration plant (White et al., 2013)

Because experimentation data rather than the trend of CO_2 concentration shown in Figure 4.35 were not provided, this section assumed that changes in the power plant operation affected mainly the amount of CO_2 in the flue gas similar to what was described in section

4.5. It was observed that the +10% CO_2 flow rate in section 4.5 returned the flue gas compositions closed to Figure 4.36 which are 75.6% dry basis at the base case and 77.7% dry basis at +10% CO_2 increased. Thus, in this section the mass flow rate of CO_2 in the flue gas feed was changed in a rectangular impulse fashion starting from the base case value and then ramped up by 10% to reach the CO_2 concentration of 77.7% and then ramp down with the same pace as shown in Figure 4.36. In addition, random noises were applied to the CO_2 flow rate in order to make the change in CO_2 composition similar to the demonstration plant trend presented in Figure 4.35. The mass flow rates of other impurities contained in the flue gas, i.e. O_2, Ar, N_2, H_2O, SO_2 and NO, were held constant. The total flue gas flow rate was calculated by summing up the component mass flow rates and thus it was changed in accordance with the CO_2 flow rate. The developed noised rectangular impulse CO_2 concentration of the flue gas which was used as an input of the model in this section is presented in Figure 4.37.
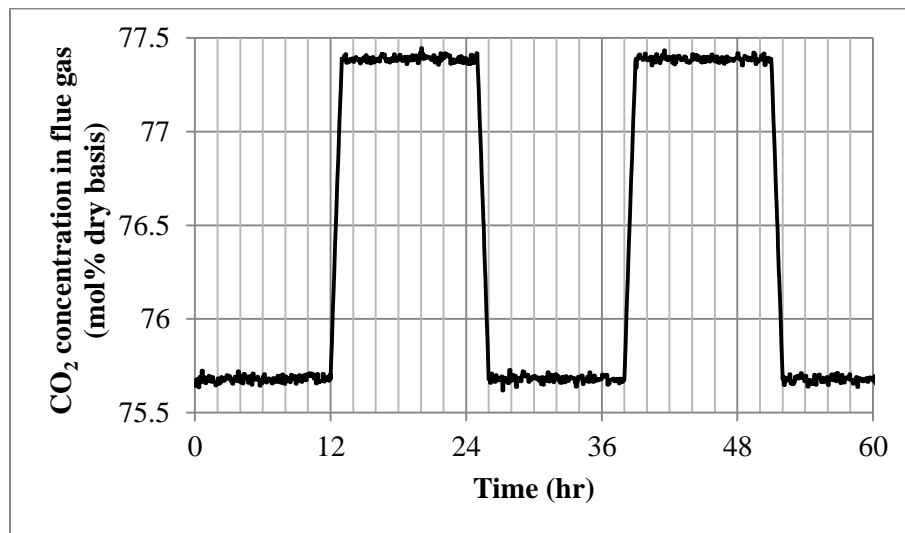
Figure 4.36 Developed noised rectangular impulse CO_2 concentration in flue gas feed

Since the Air Products' CO_2CPU operate near the saturation point of the fluid, more aggressive noises will dramatically disturbed the physical properties calculations in gPROMS model and thus it could not be implemented in this case. The noised CO_2 concentration presented in Figure 4.36 was calculated using random numbers sampled from a normal

distribution with mean 0 and standard deviation 1. Referring to results obtained from the +10% CO_2 flow rate in section 4.5, the CO_2 recovery increased with increasing CO_2 flow rate in the flue gas and the overshoot was observed at the beginning of the increase. Similar results were obtained from this section as shown in Figure 4.37. An overshoot still existed in the CO_2 recovery response. The CO_2 recovery increased with increasing CO_2 concentration and then decreased back to the initial value when the CO_2 concentration was dropped. The limited noises also had a significant impact on the CO_2 recovery. However, results indicated that the CO_2 recovery of the Air Products' CO_2CPU was stable in the presence of noise in the CO_2 concentration. The CO_2 recovery changed according to the change in CO_2 content in the flue gas without difficulty. With 75.6mol% CO_2 in flue gas, the CO_2 recovery was around 91.3wt% and then increased to about 92wt% when the CO_2 concentration was shifted to 77.7mol%. The CO_2 purity obtained for the noised rectangular impulse of the CO_2 concentration in flue gas feed is presented in Figure 4.38.
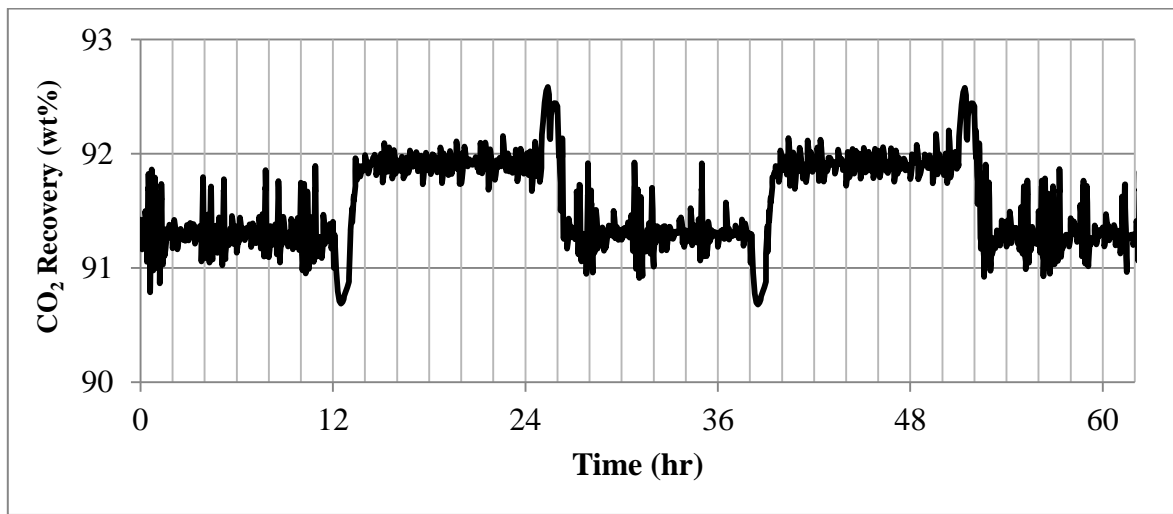
Figure 4.37 CO_2 recovery in response to the noised rectangular impulse CO_2 concentration in flue gas feed
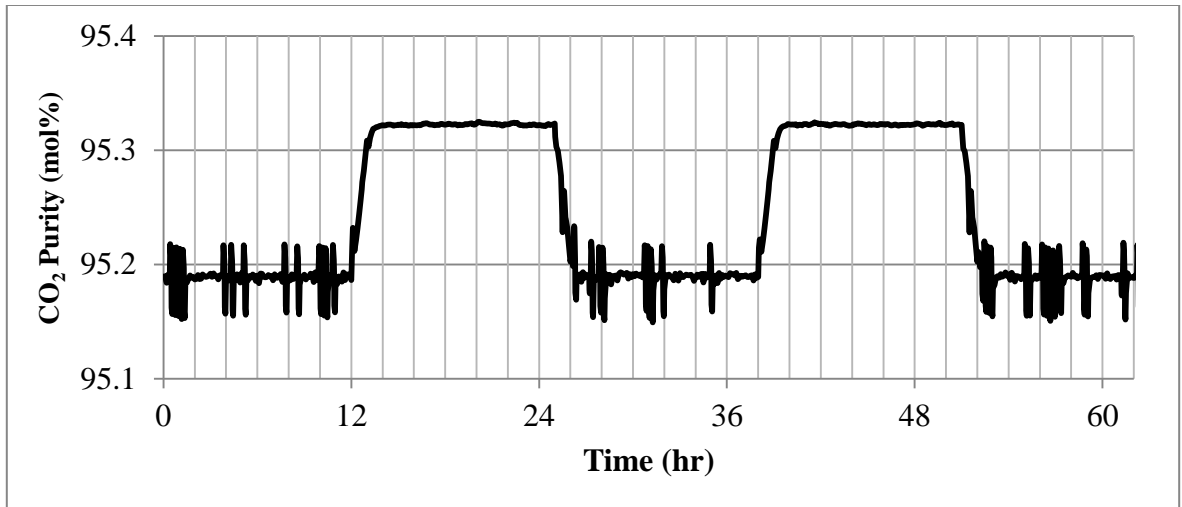
Figure 4.38 CO_2 purity in response to the noised rectangular impulse CO_2 concentration in flue gas feed

It was observed from Figure 4.38 that the noises had more significant impact on the CO_2 purity when the CO_2 content in the flue gas was around 75.6mol%. When the CO_2 content was increased to 77.7mol%, the CO_2 purity was considerably constant around 95.32mol%. Nevertheless, on the whole, the changes were small and the CO_2 purity was relatively steady compared to the change in CO_2 recovery. This result agrees well with the data presented by White et al. (2013).

Chapter 5

Dynamic simulation results for the CanCO$_2$ process

This chapter presents the simulation results obtained from the CanCO$_2$ model described in Chapter 3. The CanCO$_2$ is an extended design of the Air Products' CO$_2$CPU. The use of a recycle gas stream represents the major difference between the Air Products' CO$_2$CPU and the CanCO$_2$ process. As shown in Figure 3.3, a gas stream produced from the third separator, S-3, is recycled to the compressor train providing more CO$_2$ captured from the CanCO$_2$. As described in Chapter 3 (Section 3.5), the simulation were initially started with 0% gas recycled to the CanCO$_2$ plant, i.e., that the gas stream obtained from S-3 was assumed to be completely purged to the atmosphere after it was utilized as a coolant in MHX-1.The steady state results obtained from 0% gas recycled simulation are then used as the initial conditions for the next simulation in which a portion of gas recycle is slowly increased until 100% recycle is achieved, i.e., 0% purge. The simulation results obtained under the assumption of 100% gas recycled was validated with the design data of the CanCO$_2$ and it is presented here in the next Section. The role of the recycle ratio (defined in equation 3.80) on the CanCO$_2$ process observed during the 100% recycle CanCO$_2$ model development is presented in Section 5.2. Six case studies describing the transient operation of this process at100% recycle are presented in Sections 5.3-5.8 A summary of the CO$_2$CPU simulation is provided at the end of this Chapter.

5.1 Steady state validation

The steady state results obtained from the model with 100% gas recycled were compared to the design data of the CanCO$_2$ provided by CanmetENERGY. As shown in Table 5.1, the design data for the CanCO$_2$ is limited since the data is only available at some sample points within the CanCO$_2$ plant, e.g., stream 22, stream 26, vent gas and CO$_2$ product (see Figure 3.3), and only mass flow rate, pressure and temperature of each stream are provided. In addition, the CO$_2$ contents are provided only for the vent gas and the CO$_2$ product stream. The validation with this limited data set is very promising and was used to endorse our model

and justify the pursuit of additional simulation results including those resulting from dynamic simulations. Because the flue gas compositions used in the Air Product's CO_2CPU model and the $CanCO_2$ model are the same, it is expected that the CO_2 recovery and CO_2 purity obtained from the $CanCO_2$ will be higher than those obtained from the Air Product's CO_2CPU due to the recycle gas stream. However, the CO_2 recovery obtained from the $CanCO_2$ was slightly lower than the CO_2 recovery of the Air Product's CO_2CPU. With 74 mol% CO_2 in the flue gas (wet basis), the $CanCO_2$ achieved 88.7wt% CO_2 recovery while the Air Products' CO_2CPU achieved 91wt% CO_2 recovery. This is because the first flash drum in the $CanCO_2$ process (D-5) was operated at a temperature that is higher than the operating temperature of D-3 in Air Products' CO_2CPU. The liquid phase fraction in D-5 was about 20% and 40% in D-3. The CO_2 recovery of the $CanCO_2$ was therefore lower even though the recycle gas stream was introduced. However, the CO_2 purities obtained from the Air Product's CO_2CPU and the $CanCO_2$ were very similar due to the equivalent operating pressure (30 bars).

Table 5.1 Comparison between the simulation results and the $CanCO_2$'s design data obtained from CanmetENERGY

Process variables	Simulation results			CanCO$_2$ design's data		
	Product	**Vent**	**Stream 22**	**Product**	**Vent**	**Stream 22**
Temperature (K)	292.3	296.6	290.7	-	296. 5	293.2
Pressure* (bar)	1.01	110	14.8	1.01	110	14.8
Flow rate (kg/hr)	89.77	29.28	33.5	89.12	29.78	34.95
Composition (mol%)						
CO$_2$	95.2	29.0	65.9	≥95	≤30	-
O$_2$	1.6	17.3	8.7	-	-	-
Ar	0.6	6.9	3.4	-	-	-
N$_2$	2.1	46.9	20.7	-	-	-
H$_2$O	0	0	0	-	-	-
SO$_2$	0.5	0	0.1	-	-	-
NO	0	0.1	0.1	-	-	-
CO$_2$ recovery (wt%)	88.73					
Purity (mol%)	95.20					

* indicates an input to the model

The temperature and vapour quality profiles of the *multi-stream* heat exchangers, MHX-1 and MHX-2, resulted from the homogeneous two phase flow model, are shown below. To avoid confusion and make the results easy to follow, the flow arrangements of MHX-1 and MHX-2 as presented in Figure 5.1. The location of each stream in the $CanCO_2$ process can be seen in Chapter 3 (Figure 3.3).
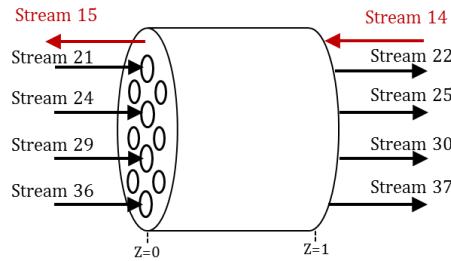
Figure 5.1 Flow arrangement in MHX-1 of the $CanCO_2$

The hot flue gas (stream 14-15) enters the *multi-stream* heat exchanger (MHX-1) at the normalized length (z) equal to 1 and leaves to the flash drum (D-5) at z=0; the other four coolants enter MHX-1 at z=0 and leave at z=1. The temperature and vapour quality profiles of the MHX-1 are shown in Figure 5.2 and Figure 5.3, respectively.
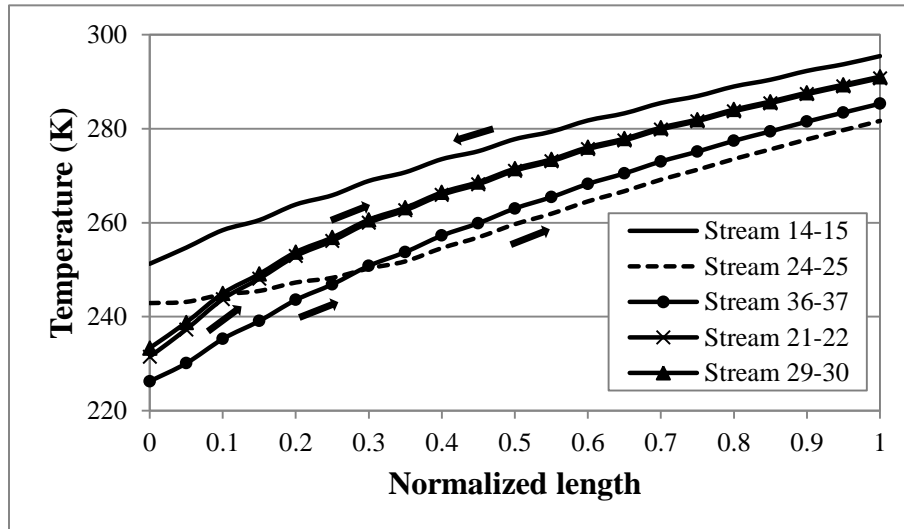
Figure 5.2 Temperature profile in MHX-1

106

Because partial CO_2 condensation is occurring in the shell side, the slope of the flue gas temperature (stream 14-15) is slightly changed as shown in Figure 5.2. As shown in Figure 5.3, the hot flue gas (stream 14-15) starts condensing near its outlet, at $z \approx 0.1$, until it reaches a final quality of about 78% at the exit of the exchanger. Similarly, the slope of the coolant temperature profile changes because these streams (streams 24-25 and 36-37) were vaporized in MHX-1.
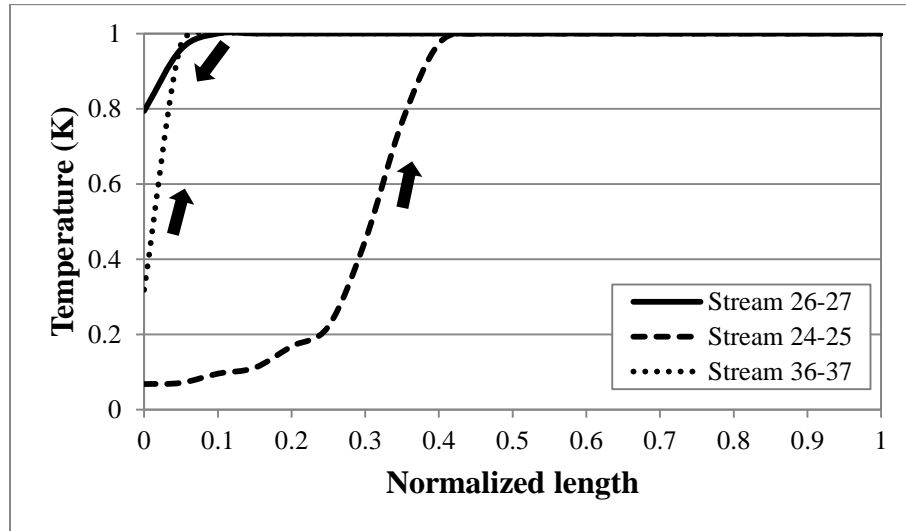
Figure 5.3 Vapour quality profiles in MHX-1

Stream 24-25 enter MHX-1 as a saturated liquid with lightly vapour phase ($x \approx 0.07$) and is totally vaporized ($x = 1$) near the middle of MHX-1 ($z \approx 0.4$) as shown in Figure 5.3. Stream 36-37 also encounters the phase change but the vapour quality changed rapidly between $z=0$ and $z=0.1$. The rest of coolants in MHX-1 (streams 21-22 and 29-30) do not change phases; i.e., changes in the slope of the temperature profiles are not observed. For the second *multi-stream* heat exchanger (MHX-2), the hot gas (stream 26-27) enter MHX-2 at $z = 1$ and leaves to the flash drum, D-6, at $z = 0$, while the other three coolants enter MHX-2 at $z = 0$ and leave at $z = 1$, as shown in Figure 5.4.
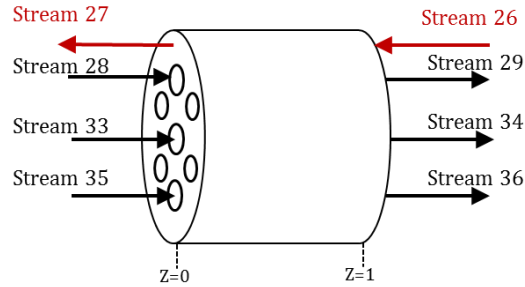
Figure 5.4 Flow arrangement in MHX-2

As shown in Figure 5.5, the heat transfer rate in MHX-2 was maximum at the hot stream inlet (z=1) where the largest temperature gradient is obtained. The use of product streams obtained from D-6 as coolants resulted in a dead zone between z≈0 and z~0.15 in MHX-2; this behaviour was also observed in the MHX-2 of The Air Products' CO_2CPU. Thus, heat was not exchanged between the hot gas (stream 26-27) and the two coolants obtained from D-6 (streams 28-29 and 33-34), but between the hot gas and the coolant stream 35-36.
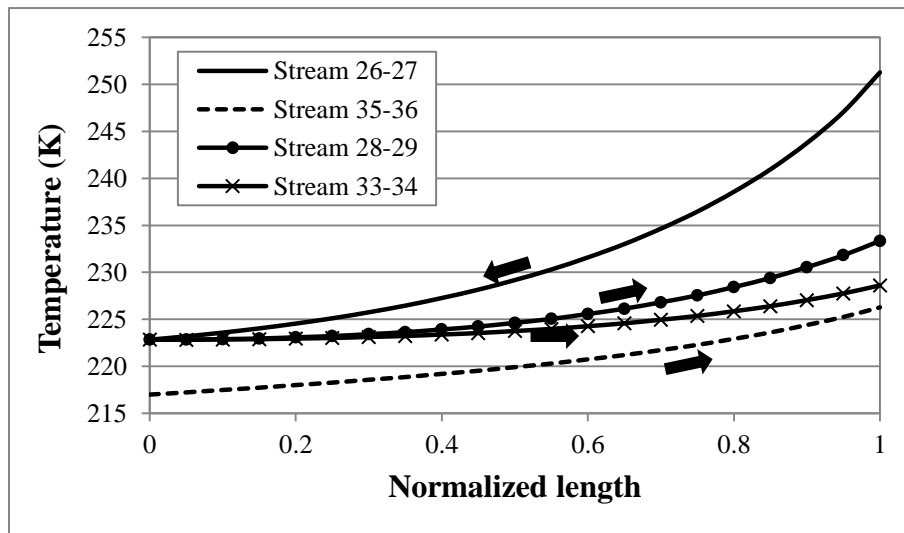
Figure 5.5 Temperature profile in MHX-2

The hot gas entering MHX-2 is saturated so it started condensing immediately upon entering MHX-2 at z=1 as shown in Figure 5.6. The vapour quality of the hot gas changes

significantly within z=0.4-1 and gradually decreased within z=0-0.3 where the hot gas exchanged heat with only one coolant stream (stream 35-36). The hot gas (stream 26-27) reaches a final quality of about 40% at the exit of the exchanger. The vapour quality of stream 35-36 changed by 20% while stream 28-29, and stream 33-34 did not encounter the two phase flow; thus, its vapour quality is not shown in Figure 5.6.

In this section, the results show that the operations of two multi-stream heat exchangers, MHX-1 and MHX-2, of both the $CanCO_2$ plant and the Air Products' CO_2CPU plant are very similar at steady state, even though the $CanCO_2$ process includes the recycle stream that is aimed to improve the CO_2 recovery. In the following section, the operation of these two multi-stream heat exchangers will be examined to determine the role of the recycle stream on the dynamic behaviour of the $CanCO_2$ process.
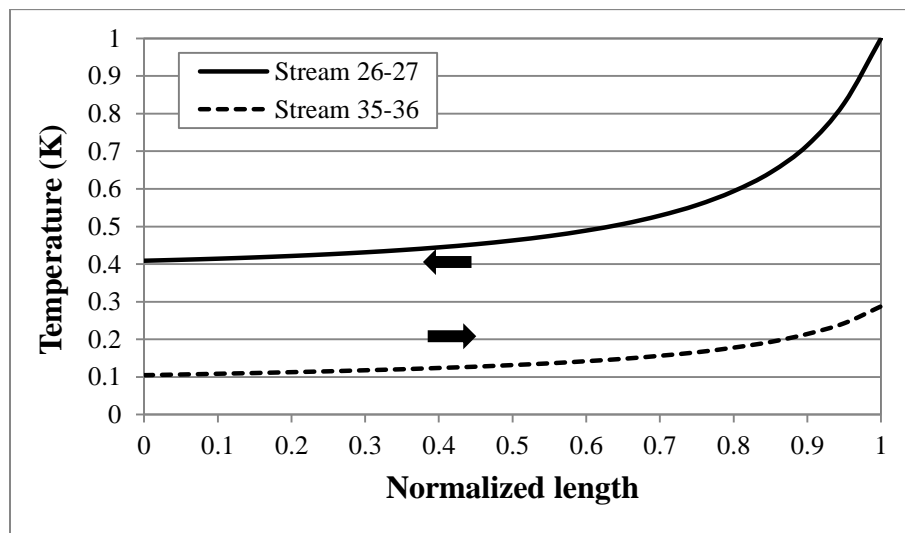
Figure 5.6 Temperature and vapour quality profiles in MHX-2

5.2 Effect of a recycle stream

This section examines the effect of the recycle gas stream on the operating performance of the $CanCO_2$ process. The amount of gas recycled was determined in the model using a recycle ratio, which is the ratio between the amount of gas recycled to the compressor train

and the total amount of gas collected on stream 22 (see Figure 3.3). To gain insight on the influence of the recycle stream over the $CanCO_2$, four ramp changes were applied, +0.25, +0.5, +0.75 and +1 to the recycle ratio within 72,000 seconds, which was initially specified at 0%. When a portion of gas stream leaving from S-3 to MHX-1 was recycled backed to the compressor train instead of being purged to the atmosphere, the total CO_2 in the process was increased providing more CO_2 captured from the $CanCO_2$. The CO_2 recovery obtained from each ramp change in the recycle ratio was shown in Figure 5.7.
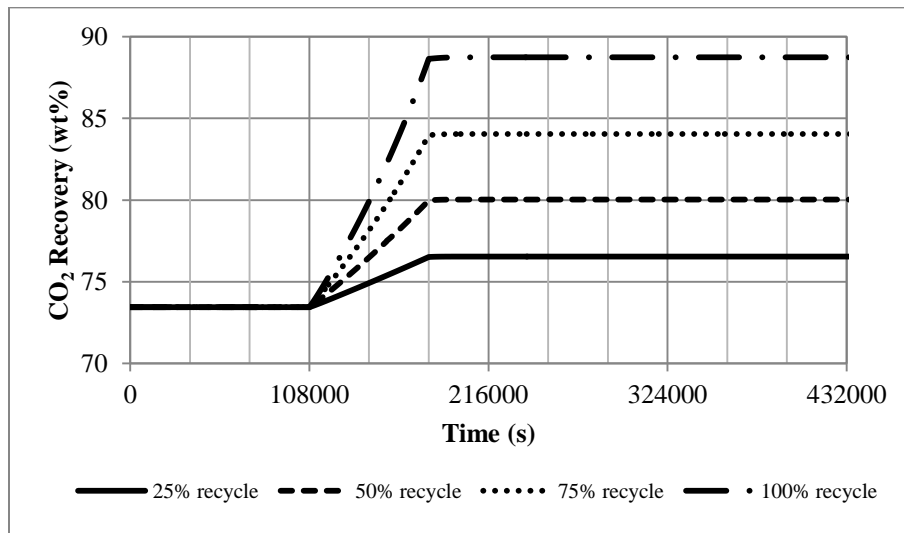
Figure 5.7 CO_2 recovery in response to the ramp change in recycle ratio

Because the ramp change in recycle ratio was occurred slowly, the process conditions were also slowly changed and the CO_2 recovery was slowly moved to the new steady state as shown in Figure 5.7. Figure 5.8 presents the CO_2 product purity of the $CanCO_2$ obtained from each ramp change at steady state. Since not only the CO2 but also the inert purities contained in the gas recycle stream (stream 22), the CO_2 purity in the product stream was dropped when the recycle ratio increased as shown in Figure 5.8. The CO_2 purity was moved slowly to the new steady state in accordance with the ramp change in recycle ratio as well.

110
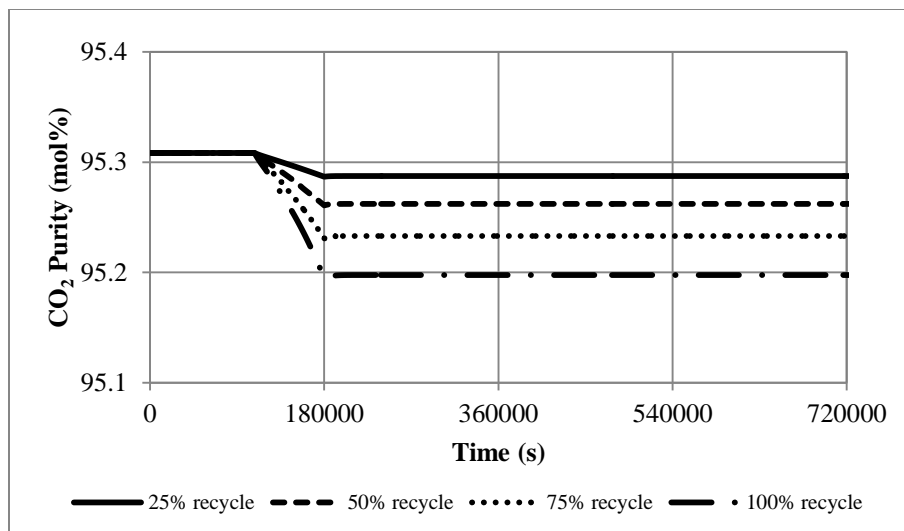
Figure 5.8 CO_2 purity in response to the ramp change in recycle ratio

In summary, it was observed that the recycle stream can improve the CO_2 recovery of the CO_2CPU process but reduce the CO_2 purity in the product stream. However, it was observed in the $CanCO_2$ model that, the decrease in CO_2 purity was very small and insignificant when compared to the increase in CO_2 recovery obtained (see Figure 5.9). Thus, the $CanCO_2$ is normally operated at 100% recycle (recycle ratio = 1). Results obtained from 100% recycle were considered as the base case values in this study.
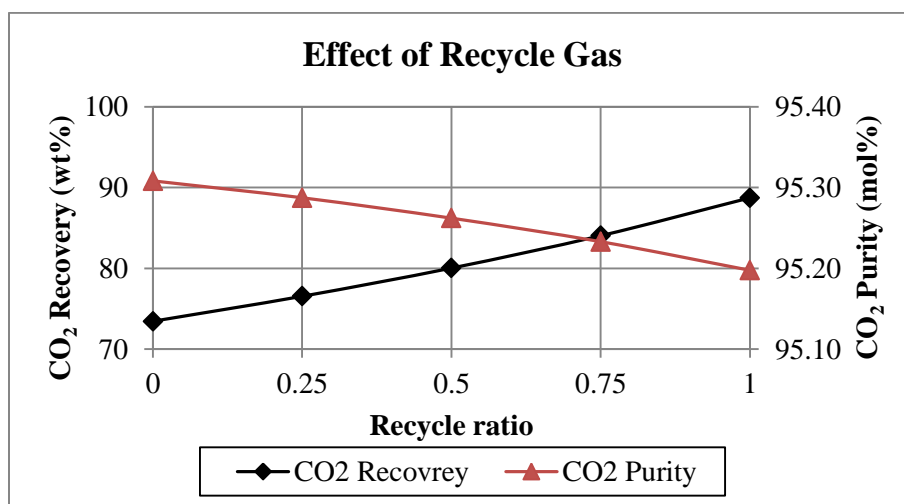
Figure 5.9 Effect of gas recycle stream on the $CanCO_2$ capture performance

111

In the following sections, several dynamic tests were applied to the inputs of the process; in these analyses, the recycle ratio was fixed at 1, which means that the purge stream is set to 0. The process outputs of each unit operation were monitored and recorded. As in the Air Products' CO_2CPU model, the focus is on the CO_2 recovery and the CO_2 product purity of the plant as these two variables represent the key operating performance metrics of the CO_2CPU process.

5.3 Effect of a compressor train outlet pressure

As shown in Figure 3.3, the compressor train in the $CanCO_2$ process includes four compressors (K-1 to K-4) and a connection between these four compressors, including four knock-out drums and four coolers. In this section, the outlet pressure of the compressor train, i.e., K-4's discharge pressure, was examined. The discharge pressure of compressor K-4 was ramped up from 30 bars to 33 bars within 720 seconds. Due to the addition of the recycle gas in the $CanCO_2$ model, this process is sensitive to sudden changes in the process inputs. Hence, ramp changes within 300 seconds similar to the Air Products' CO_2CPU are considered to be fast changes that affect the operability of this plant. As the discharge pressure increased, the inlet temperature of flue gas entering C-4 was increased resulting in an increase in stream 13's temperature (gas outlet temperature of C-4) as shown in Figure 5.10.
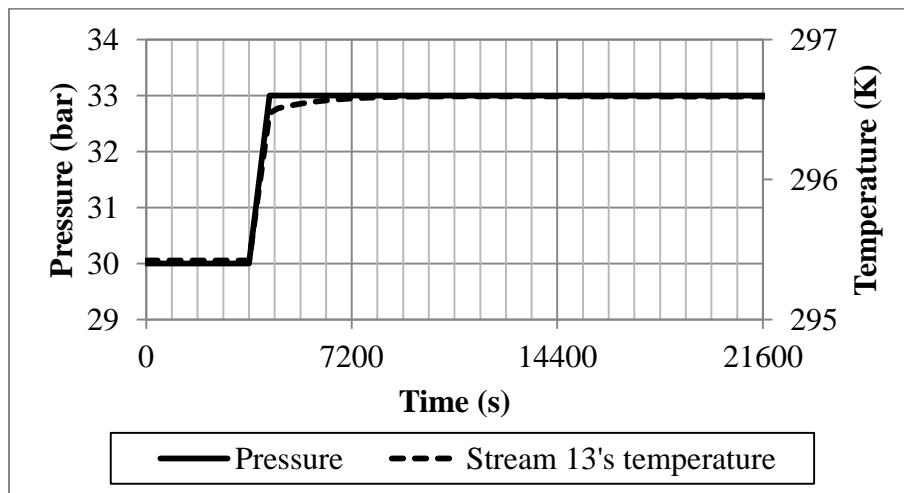
Figure 5.10 Stream 13's temperature in response to the ramped-up in K-4 discharge pressure

112

Increasing K-4 discharge pressure increased stream 15's pressure and enhanced the CO_2 condensation in D-5, thus increasing the overall amount of liquid recovered from the $CanCO_2$. Accordingly, the mass flow rate of recycle gas stream is decreased as more liquid is being produced at this operating condition. Decreasing the recycle gas flow rate reduced the mass flow rate of the hot gas entering MHX-1 thereby decreasing the heat transfer in MHX-1. Although an increase in the hot gas inlet temperature (stream 13's temperature) may increase the heat transfer in MHX-1 and decrease the hot gas outlet temperature (stream 15's temperature), the effect of decreasing the hot gas flow rate was found to be more significant than the effect of increasing hot gas inlet temperature. Consequently, the total heat transfer in MHX-1 was decreased by decreasing the hot gas flow rate. Hence, the hot gas outlet temperature (stream 15's temperature) of MHX-1 was increased as shown in Figure 5.11.
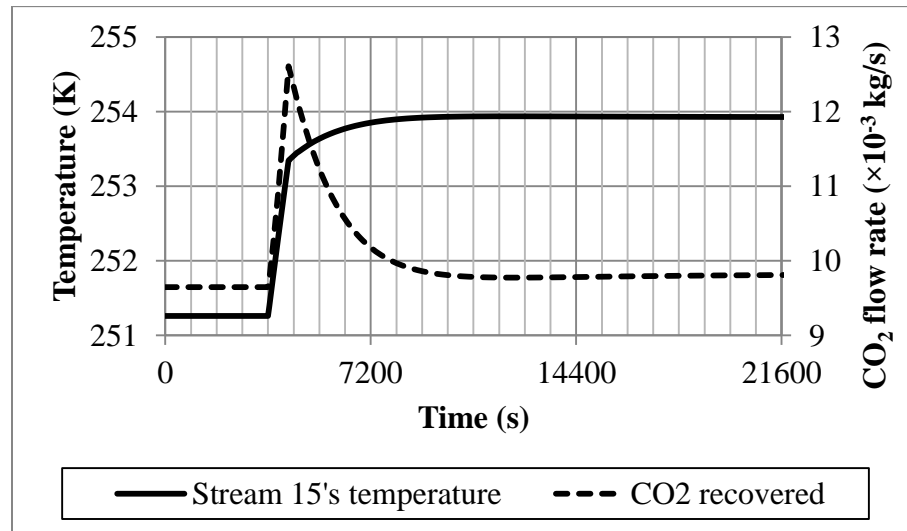
Figure 5.11 Stream 15's temperature and the CO_2 recovered from D-5 in response to the ramped-up in K-4 discharge pressure.

Since D-5 operates at the temperature and pressure of stream 15, a change in the operating conditions of stream 15 affect the separation of CO_2 in D-5. While the pressure was continuously increased in the first 720 seconds, the pressure played a key role in the CO_2 condensation in D-5. Increasing pressure enhances the CO_2 condensation, thus liquid CO_2 recovered from D-5 was initially increased within 720 seconds as is shown in Figure 5.11.

After 720 seconds of the ramp change, the operating pressure became constant while stream 15's temperature was still increasing due to impacts of two factors which are the stream 13's temperature and the coolants flow rate in MHX-1. Because the amount of CO_2 recovered from D-5 was significantly increased within 720 seconds, the amount of gas carried over to MHX-2 and S-3 was dropped. Consequently, flow rates of streams 21, 29 and 36 which are coolants in MHX-1 were decreased; therefore, stream 15's temperature was continuously increased after 720 seconds of ramp change. Since the flow rate of stream 21 was decreased, the flow rate of the recycle stream was decreased and thus the amount of hot gas fed to MHX-1 (stream 13) was decreased. Decreasing stream 13's flow rate while increasing stream 15's temperature prevent condensation of CO_2 in D-5. The amount of liquid CO_2 recovered from D-5 was therefore decreased after 720 seconds of ramp change as shown in Figure 5.11. Unlike the results obtained from the Air Products' CO_2CPU, the amount of CO_2 recovered from D-5 in the CanCO$_2$ is affected not only by the operating conditions in S-3 but also by the amount of recycle gas. Thus, an overshoot in the response of CO_2 recovered from D-5 was obtained as shown in Figure 5.11.

Increasing pressure also increases the heat transfer coefficient of the hot gas; unlike in MHX-1, the effect of increasing the heat transfer coefficient in MHX-2 was slightly more significant than the effect of increasing inlet temperature (stream 26's temperature). Hence, the temperature of stream 27 (hot gas outlet temperature) was fairly dropped within 720 seconds of the ramp change as shown in Figure 5.12. After 720 seconds, the pressure became constant while stream 15's temperature continued increasing, thus the effect of increasing stream 26's temperature became dominant and caused an increase in stream 27's temperature. On the other hand, a small overshoot of the CO_2 recovered from D-6 was observed in Figure 5.12.
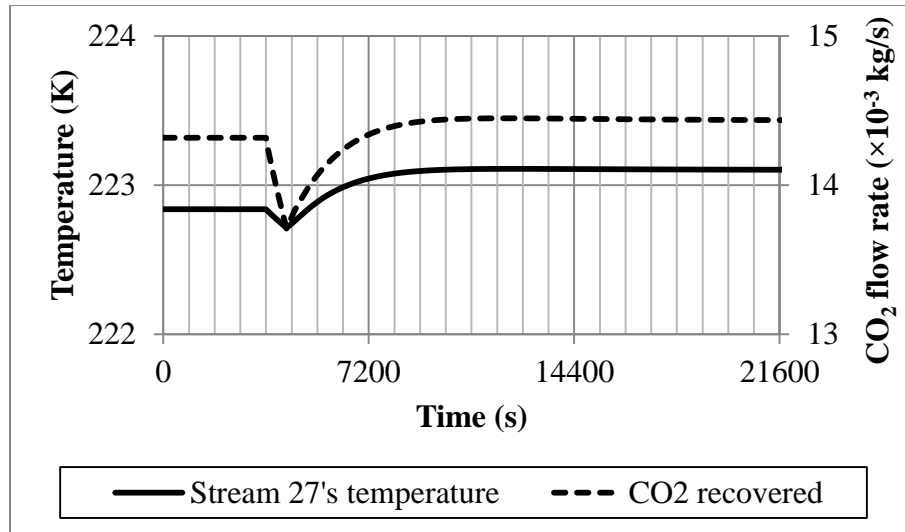
114

Figure 5.12 Stream 27's temperature and the CO_2 recovered from D-6 in response to the ramped-up in K-4 discharge pressure.

A small change in stream 27's temperature within 720 seconds did not affect significantly the CO_2 condensation in D-6. The amount of CO_2 recovered from D-6 was initially decreased and then increased in accordance with the change in CO_2 carried over from D-5 to MHX-2. Thus, the amount of CO2 recovered from D-6 in this case was determined by the amount of CO_2 carried over from D-5. The more CO_2 recovered from D-5, the less CO_2 carried over and thus the less CO_2 recovered from D-6 as illustrated in Figure 5.12.

The ratio between the total liquid CO_2 obtained from D-5 and D-6 and the amount of CO_2 in the flue gas was calculated to determine the total CO_2 recovery in the $CanCO_2$ process. Because the flow rate and compositions of the flue gas were held constant while the total liquid CO_2 collected from D-5 and D-6 was increased, the CO_2 recovery was eventually increased as shown in Figure 5.13. Moreover, since the increase of CO_2 recovered from D-5 was three times greater than the increase of CO_2 recovered from D-6, the response of the CO_2 recovery (a combination between the two liquid CO_2 recovered from D-5 and D-6) was increased and then decreased similar to the response in CO_2 recovered from D-5. It was observed that the CO_2 recovery was improved by approximately 1wt% when the discharge pressure of K-4 was increase by 3 bars. Figure 5.14 presents the response of the CO_2 product

115

purity due to the ramp change in pressure. Similar to the Air Products' CO_2CPU process, the CO_2 product purity was decreased with increasing pressure because the elevated pressure enhanced not only the CO_2 condensation but also the inert impurities (O_2, N_2, etc.) condensation. Thus, the CO_2 purity was decreased with increasing pressure. The CO_2 product purity was eventually reduced to about 94.7mol% (0.5% lower than its initial value) when the pressure was increased by 3 bars.
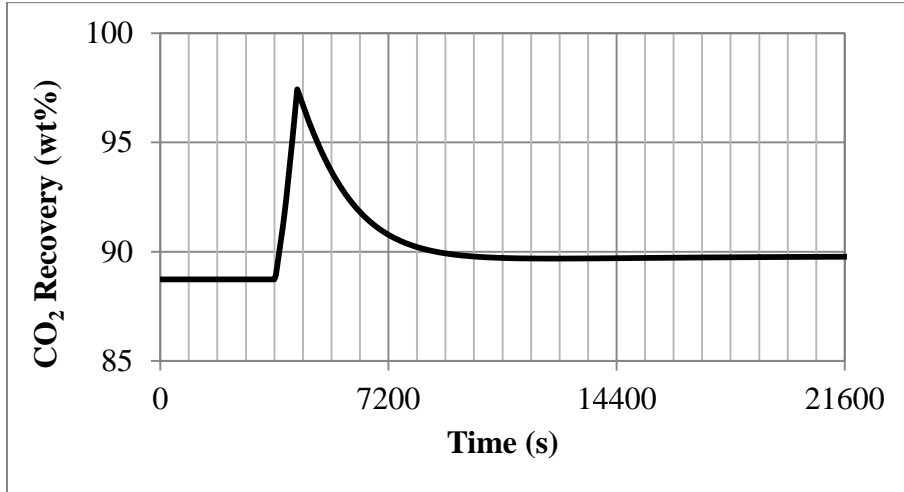
Figure 5.13 CO_2 recovery in response to the ramped-up K-4 discharge pressure
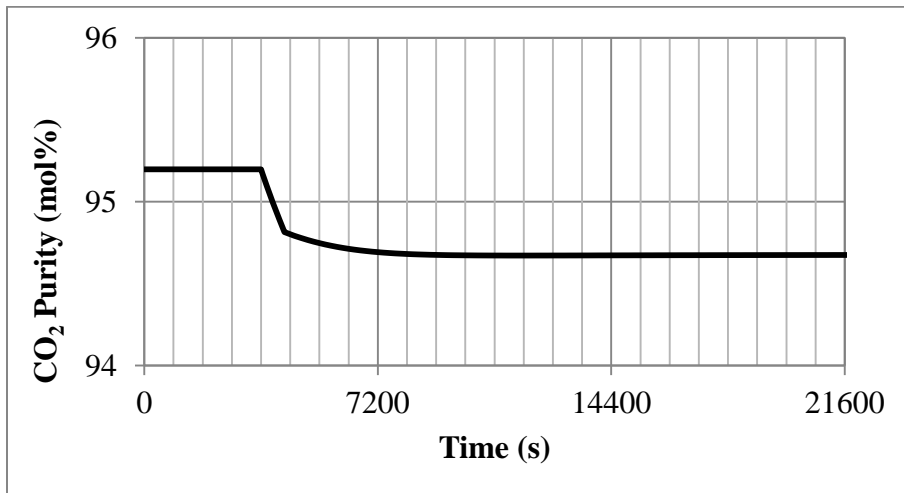
Figure 5.14 CO_2 purity in response to the ramp-up in K-4 discharge pressure

116

The ramp-down test on the K-4 discharge pressure was also performed. Results obtained from the ramp-down test showed that all process variables changed in the opposite direction compared to the ramp-up change described above. Decreasing pressure prevents the CO_2 condensation and other gas impurities in flash drums, thus reducing the CO_2 recovery but increasing the CO_2 product purity. The dynamic responses of the CO_2 recovery and CO_2 purity are presented in Figures 5.15 and 5.16, respectively.
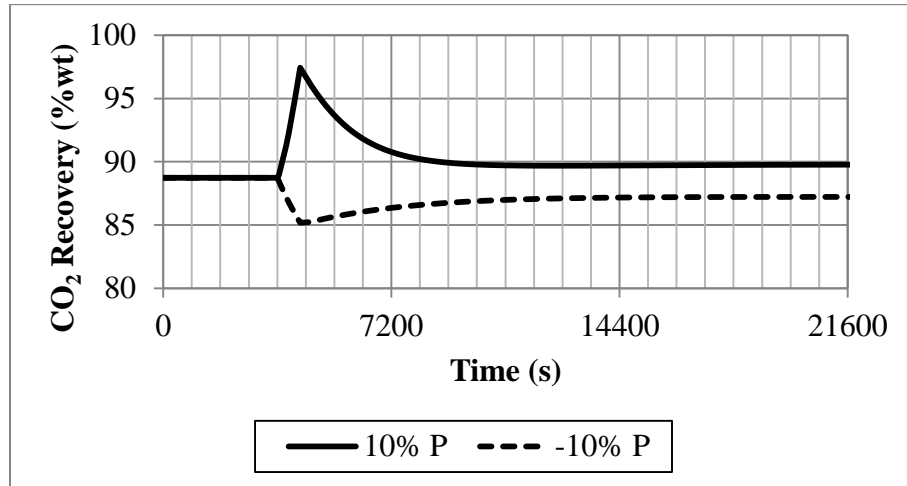
Figure 5.15 The CO_2 recovery in response to the ramp changes in K-4 discharge pressure
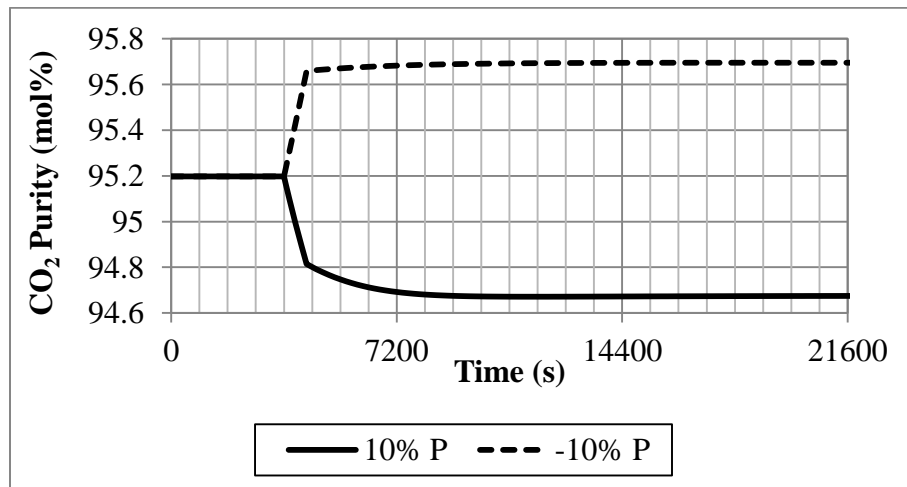

Figure 5.16 The CO_2 purity in response to the ramp change in K-4 discharge pressure

The results show that changing pressure within ±10% introduced a large overshoot at the initial times but did not change considerably the overall change in CO_2 recovery of the CanCO$_2$ process since the effect of changing pressure was balanced by the changes in recycle flow rate. A comparison between Figure 4.13 (ramp changes in the operating pressure in the Air Products' CO_2CPU) and Figure 5.15 also shows that a larger overshoot in the CO_2 recovery response was observed from the CanCO$_2$ process model while the Air Products' CO_2CPU process model returned a very small overshoot only for the -10% change in the K-4 discharge pressure. The CO_2 recovery response of the Air Products' CO_2CPU followed a first-order process response when the operating pressure was increased by 10% (3 bars). Unlike the CO_2 recovery, significant changes in the CO_2 purity are observed for the CanCO$_2$ as shown in Figure 5.16. A larger change of CO_2 purity was observed in the CanCO$_2$ when comparing Figure 5.16 with Figure 4.14, which was obtained from the Air Products' CO_2CPU process model. That is, the recycle stream makes the changes in CO_2 recovery and CO_2 purity in the CanCO$_2$ more sensitive to the outlet pressure of the compressor train. Although the use of recycle stream did not cause an overshoot in the CO_2 purity response, it reduced the overall purity of CO_2 in the product stream since other gas impurities (i.e. O_2, Ar, N_2, SO_2 and NO) were also recycled along with the CO_2. It should be noted that the +10% and -10% ramp changes considered here returned different changes in both CO_2 recovery and CO_2 purity, which reflects the nonlinearity of the CanCO$_2$ process.

5.4 Effect of a compressor train outlet temperature

This section examines the effect of temperature of the hot gas leaving from compressor train to MHX-1. The flow rate of the coolant used in the cooler C-4 was increased by +20% in a step fashion. Since the flue gas flow rate is constant while the coolant flow rate was increased, the gas outlet temperature (stream 13's temperature) was decreased. Increasing the coolant flow rate by 20% reduced the temperature of stream 13 by 1.5 K as shown in Figure 5.17.
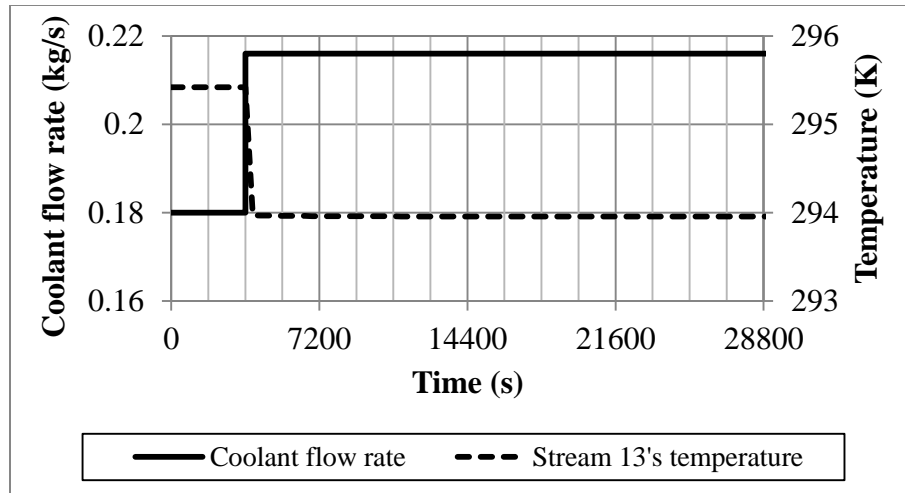
Figure 5.17 Stream 13's temperature in response to the step up coolants in C-4

Figure 5.18 presents the dynamic responses of stream 15's temperature and the amount of CO_2 recovered from D-5. As shown in that Figure, a fast change in stream 15's temperature at the beginning was observed; this is caused by a step decreased in stream 13's temperature. Decreasing stream 13's temperature favours the CO_2 condensation in D-5, thus more liquid CO_2 was recovered from D-5. Because the liquid recovered from D-5 (stream 17) is a coolant in MHX-1, increasing stream 17's flow rate increases the heat transfer in MHX-1. Thus, the temperature of stream 15 was gradually decreased afterwards as illustrated in Figure 5.18.

Moreover, a decrease in stream 15's temperature affects the flow rate and temperature of the hot gas feed (stream 26) of MHX-2, thus affecting the temperature of stream 27 (see Figure 5.19). The temperature of stream 27 was quickly decreased after the step change was introduced into the system and then gradually decreased until it reached a new steady state that is 0.2 K lower than its initial temperature value. Because the change in stream 27's temperature was not significant, it did not have a major impact on the CO_2 condensation in D-6. The amount of liquid CO_2 recovered from D-6 was determined by the amount of CO_2 carried over from D-5. Since more liquid CO_2 was recovered in D-5, the amount of CO_2 carried over to D-6 was decreased. Therefore, the amount of CO_2 recovered from D-6 was decreased as shown in Figure 5.19.
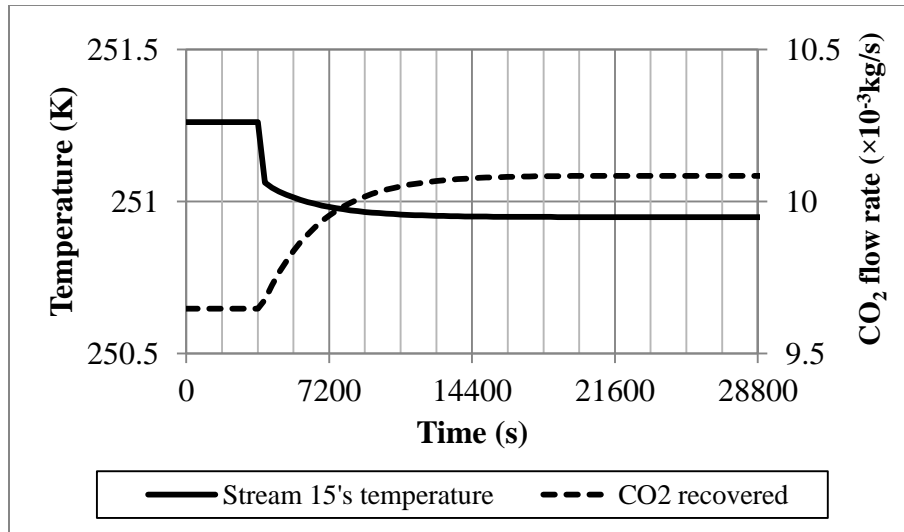
Figure 5.18 Stream 15's temperature and the CO_2 recovered from D-5 in response to the step up coolants in C-4
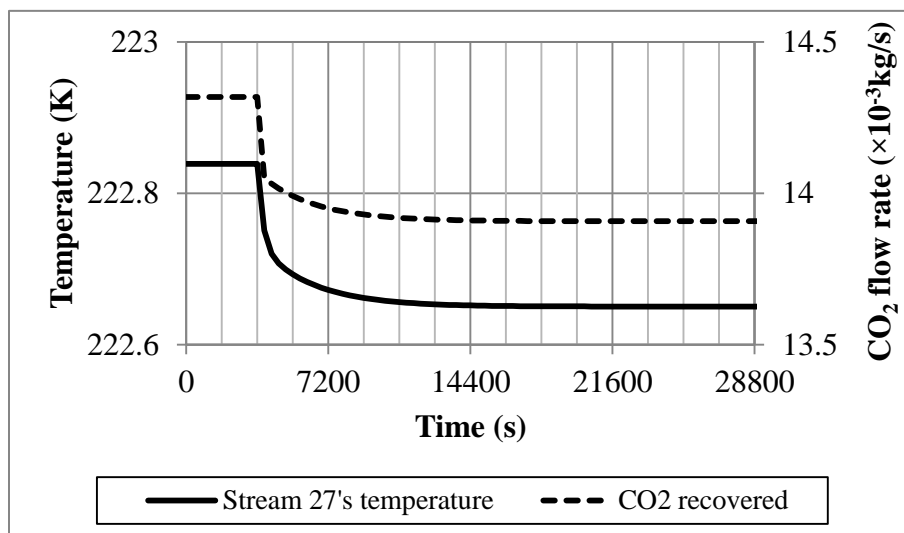
Figure 5.19 Stream 27's temperature and the CO_2 recovered from D-6 in response to the step up coolants in C-4

Since the flue gas flow rate and compositions were constant, the CO_2 recovery was determined in this case by the total liquid CO_2 obtained from D-5 and D-6. The rate at which the liquid CO_2 obtained from D-6 decreases was faster than the rate of increasing liquid CO_2

obtained from D-5 within the first 360 seconds after the step change in temperature; thus, the CO_2 recovery initially dropped as shown in Figure 5.20.
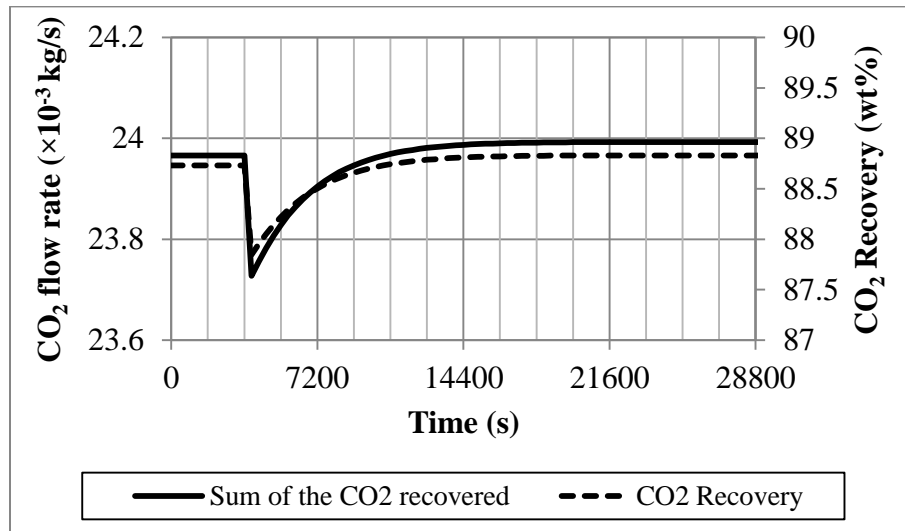
Figure 5.20 The sum of liquid CO_2 recovered from D-5 and D-6; and the CO_2 recovery in response to the step up coolants in C-4

Subsequently, the rate of decreasing liquid CO_2 obtained from D-6 was decreased and thus the rate of increasing liquid CO_2 in D-5 became dominant, and the CO_2 recovery was increased accordingly. Generally, the decrease in stream 13's temperature increases the CO_2 recovery; since stream 13's temperature was decreased only 1.5 K in this case, a small increase in the CO_2 recovery was observed (~ 0.1 wt%). It should be noted that in the Air Products' CO_2CPU process, a 0.1wt% CO_2 recovery improvement was obtained when the hot gas temperature was dropped by 2 K due to a +30% step change in C-2 coolant flow rate (section 4.3). A smaller change in the hot gas temperature was obtained in the CanCO2 but the increase in CO_2 recovery achieved was the same as in the Air Products' CO_2CPU. Even though the change is very small, this comparison shows that the use of recycle gas can improve the CO_2 recovery of the plant. In addition, the molar-averaged purities between the liquid CO_2 obtained from D-5 and D-6 were calculated to determine the CO_2 product purity. In this case, the temperatures of streams 15 and 27 were decreased by less than 1 K while the

pressure remained constant resulting in a slight change in the CO_2 product purity as shown in Figure 5.21(a).

(a)   (b)
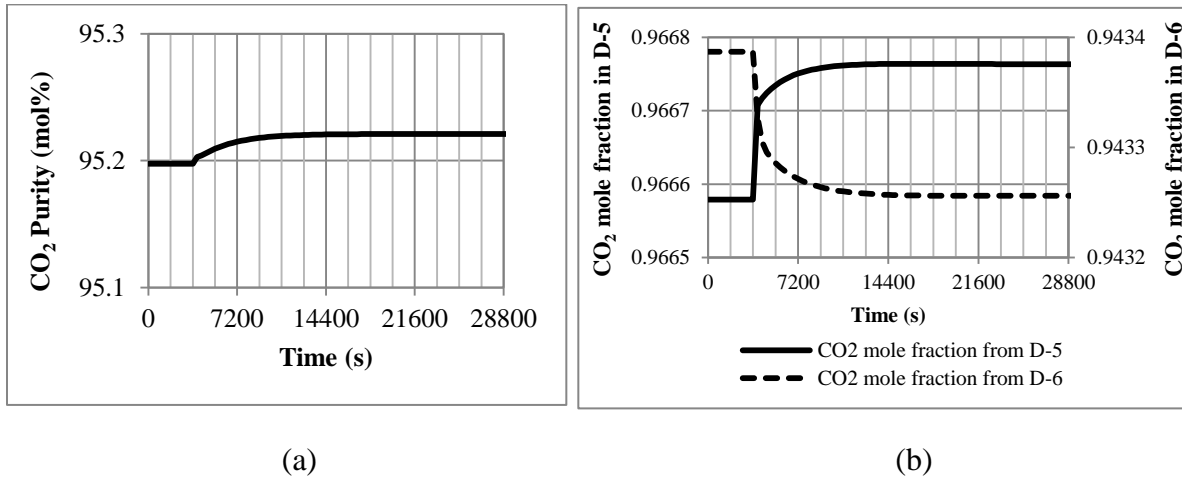
Figure 5.21 The CO_2 purity in (a) product stream (b) liquid CO_2 recovered from D-5 and D-6, in response to the step up coolants in C-4

As shown in Figure 5.18, the operating temperature of D-5 was decreased only by 0.3 K which was not enough to favour the condensations of other inert gas impurities in D-5. Thus, the liquid mole fraction of CO_2 obtained from D-5 was increased along with the amount of CO_2 recovered. Consequently, the gas leaving from D-5 to D-6 contained more gas impurities but less CO_2 content. Because the operating temperature of D-6 is much lower than the temperature of D-5, the condensation of gas impurities can be easily obtained from D-6 when the impurity contents in the gas stream carried over from D-5 increases. Therefore, the mole fraction of CO_2 obtained from D-6 was decreased as shown in Figure 5.21 (b). Because the increase of CO_2 mole fraction obtained from D-5 is more than the decrease of CO_2 mole fraction obtained from D-6, the molar-averaged CO_2 product purity was increased in accordance with increasing CO_2 mole fraction from D-5. In this case, the CO_2 product purity was increased by only 0.02mol% due to a small decrease in the operating temperatures of D-5 and D-6.

The effect of decreasing C-4's coolant flow rate was also evaluated. In this case, the mass flow rate of the coolant used in the C-4 unit was decreased by 20% in a step fashion. This change resulted in a change in stream 13's temperature by 2.3 K. All process variables had opposite trends compared to the +20% step change results; however, the magnitude of the changes were different as shown in Figure 5.22 and Figure 5.23.
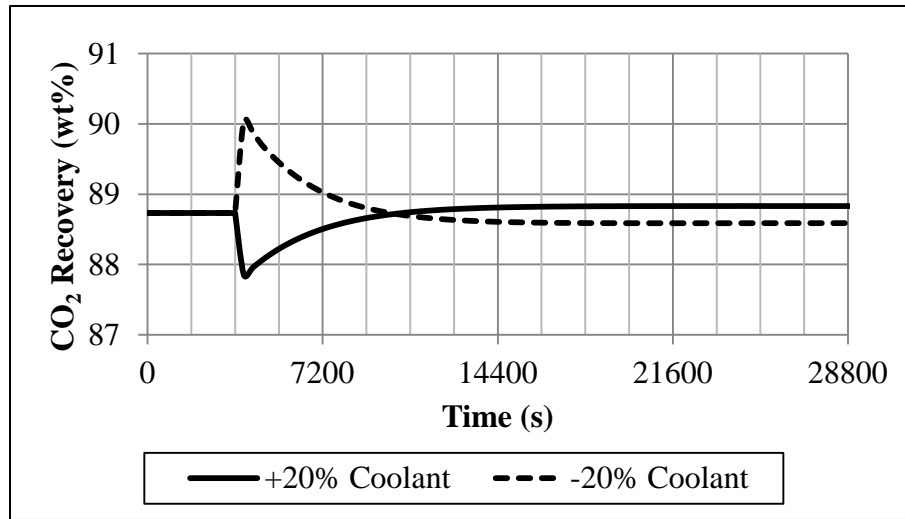
Figure 5.22 The CO_2 recovery in response to the step changes in coolant flow rate in C-4
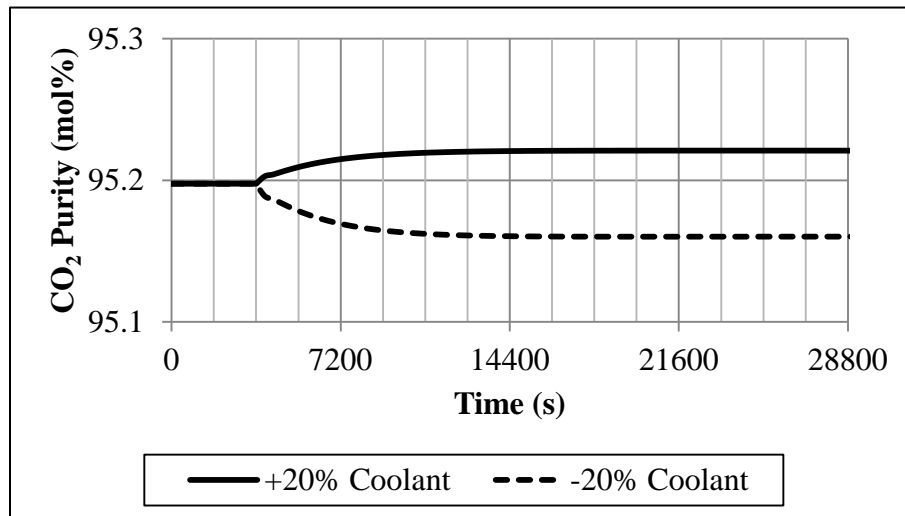
Figure 5.23 The CO_2 purity in response to the step changes in coolant flow rate in C-4

123

The CO_2 recovery decreased by 0.14% whereas the CO_2 product purity decreased by 0.04% in response to the decrease of 20% in the coolant flow rate in C-4 as shown in Figure 5.22 and Figure 5.23, respectively. It is noted that the changes in the amount of CO_2 capture and CO_2 purity observed in this section were relatively small due to slight changes in the operating temperatures of D-5 and D-6. The +20% and -20% changes in the coolant flow rate returns different changes in the CO_2 recovery and the CO_2 purity, thus demonstrating the nonlinearity of the $CanCO_2$.

5.5 Effect of gas splitter

In the $CanCO_2$ process, the mass flow rate of gas flowing from D-5 to MHX-2 (stream 26) can be adjusted by using the gas splitter (SF). It was assumed that the mass flow rate of stream 26 is directly proportional to the mass flow rate of stream 15 and can be calculated using the split fraction, which is the ratio of mass flow rates of streams 26 and 16 and is as follows (see Figure 3.3 for location of each process stream).

$$SF = \frac{\text{Total mass flow rate of stream 26}}{\text{Total mass flow rate of stream 16}} \tag{5.1}$$

In the base case simulation, the split fraction was fixed at 0.7 to match the simulation results obtained with the design data of the $CanCO_2$ process. In this section, the split fraction was ramped down within 720 seconds in order to examine the effect of the gas splitter operation on the $CanCO_2$ process. Since the flue gas conditions were held constant, decreasing split fraction reduced the mass flow rate of stream 26 flowing to MHX-2 but increased the mass flow rate of recycle stream (stream 22) as shown in Figure 5.24. Increasing the recycle flow rate increased the mass flow rate of the hot gas entering the cooler C-4. Because the coolants in C-4 remained constant, the outlet temperature of the hot gas (stream 13's temperature) was increased. Nevertheless, the total increase of stream 13's temperature was only 0.4% with respect to the initial temperature while the total increase of the recycle flow rate was almost

50% with respect to the initial recycle flow rate. Thus, the effect of increasing mass flow rate of stream 13 was dominant in MHX-1.
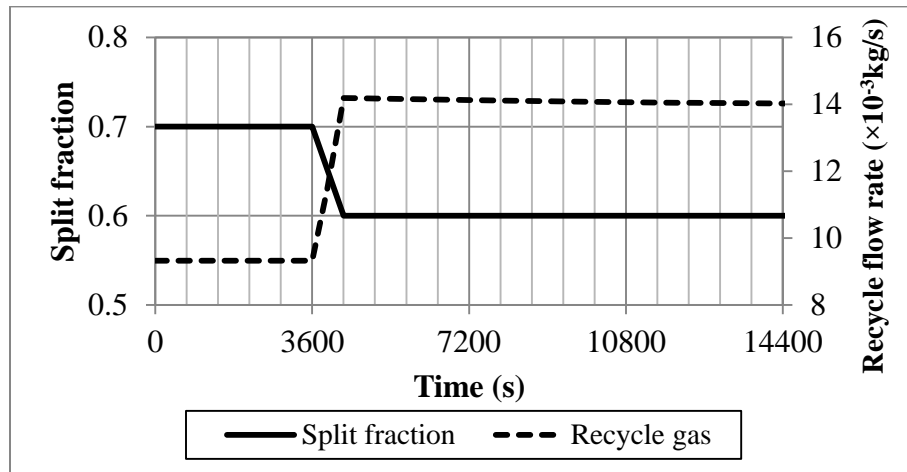
Figure 5.24 The ramp-down split fraction and the mass flow rate of recycle stream

Increasing the mass flow rate of the hot gas enhances the heat transfer in MHX-1; thus the temperature of the hot gas leaving from MHX-1 (stream 15's temperature) decreases. In addition, decreasing stream 15's temperature promotes CO_2 condensation; therefore, the amount of CO_2 recovered from D-5 was increased as shown in Figure 5.25.
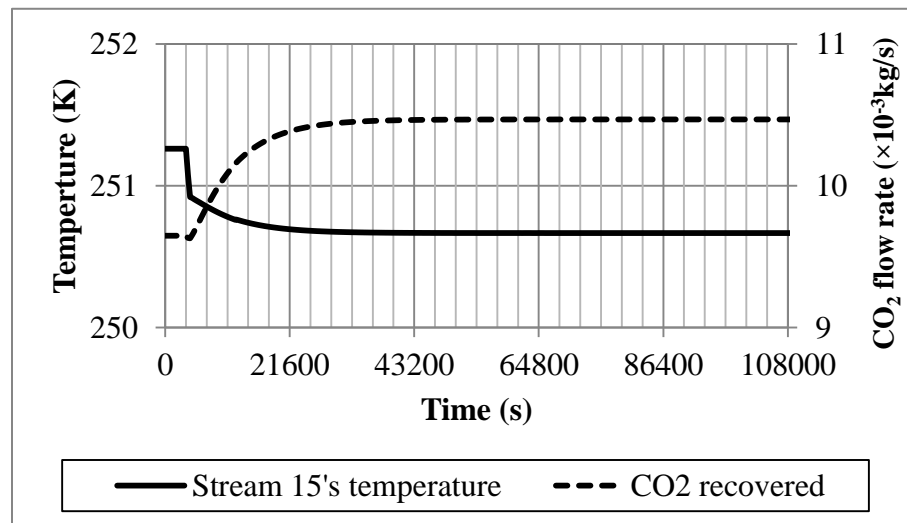
Figure 5.25 The stream 15's temperature and the CO_2 recovered from D-5 in response to the ramp-down change in split fraction

In the MHX-2 unit, the hot gas inlet flow rate was reduced due to the ramp-down change in the split fraction while the hot gas inlet temperature (stream 26) was also reduced according to stream 15's temperature. Decreasing the mass flow rate of the hot gas also decreases the heat transfer and the fluid velocity in MHX-2. Decreasing the velocity increases the residence time of the hot gas in MHX-2, which favours the heat transfer in the heat exchanger. These two effects were balanced and finally stream 27's temperature slightly dropped in accordance with stream 26's temperature as shown in Figure 5.26. Even though the decrease in stream 27's temperature favours the CO_2 condensation in MHX-2, the amount of liquid CO_2 obtained from D-6 was reduced. This is because more liquid CO_2 was recovered from D-5; hence, the amount of CO_2 carried over to D-6 was decreased thereby decreasing the amount of liquid CO_2 recovered from D-6 (see Figure 5.26). Thus, the amount of CO_2 obtained from D-6 in this case was determined primarily by the amount CO_2 carried over from D-5.
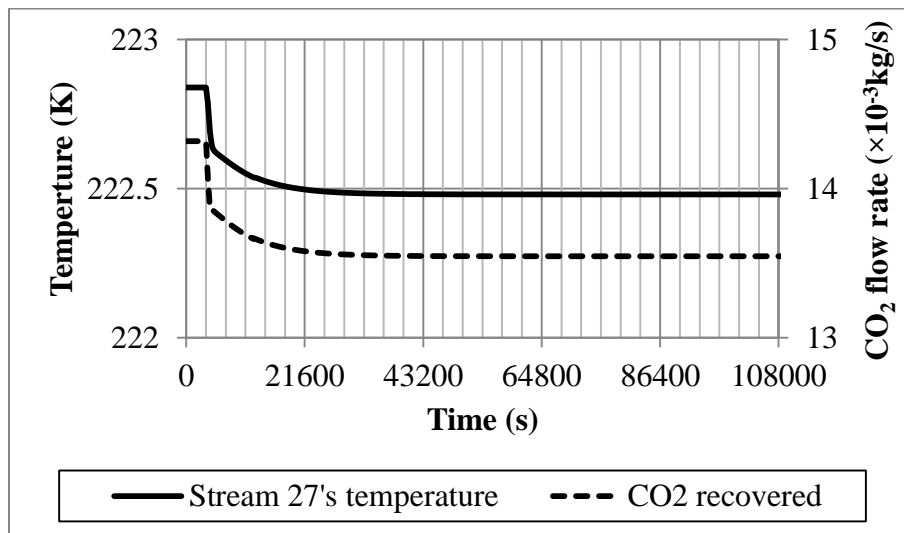
Figure 5.26 The stream 27's temperature and the CO_2 recovered from D-6 in response to the ramp-down change in split fraction

Figure 5.26 presents the response of CO_2 recovery due to the change in the split fraction. Note that an overshoot occurs in the CO_2 recovery response. Because the rate of decreasing liquid CO_2 recovered from D-6 was more than the rate of increasing CO_2 recovered from D-5

within the first 720 seconds of ramp change, the CO_2 recovery initially dropped. Afterwards, the liquid CO_2 obtained from D-6 decreased slowly, thus the CO_2 recovery increased with increasing liquid CO_2 obtained from D-5 and reached the new steady state at which the CO_2 recovery was improved by 0.2wt%. A -10% ramp change in slit fraction was also performed. The CO_2 recovery obtained from the -10% split fraction is also shown Figure 5.27 for comparison. As can be seen, the CO_2 recovery obtained from the -10% was opposite to the +10% ramp change in split fraction. It is noted that the final CO_2 recovery obtained from both ramp changes were very close to the initial CO_2 recovery because the change in liquid CO_2 recovered from D-5 was balanced by the opposite change in liquid CO_2 recovered from D-6.
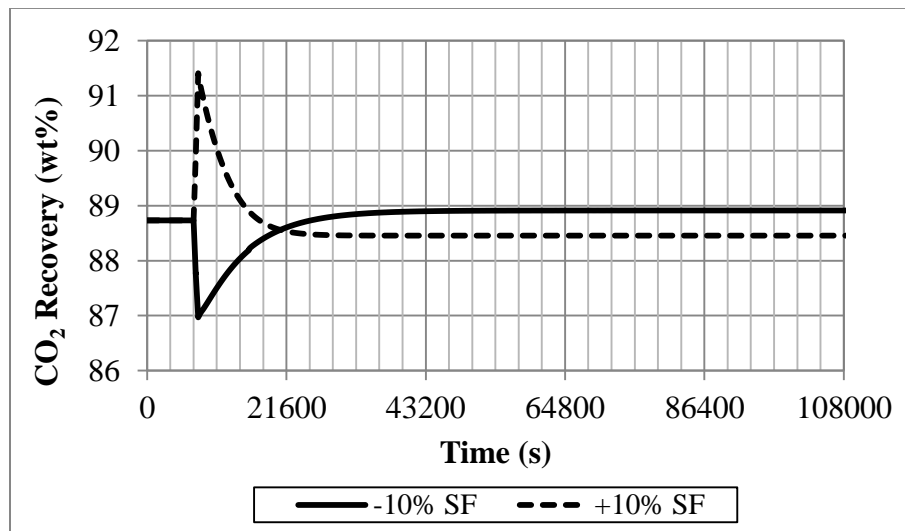
Figure 5.27 The CO_2 recovery in response to the ramp changes in split fraction

Figure 5.28 shows the CO_2 product purity obtained from the +10% and -10% ramp changes on the split fraction. As shown in that Figure, the CO_2 purity increased when more gas was fed to the MHX-2 rather than recycled back to the compressor train. Increasing the recycle gas flow rate increases not only the CO_2 but also other gas impurities in the process, which also increases the CO_2 recovery but decreases the CO_2 product purity.
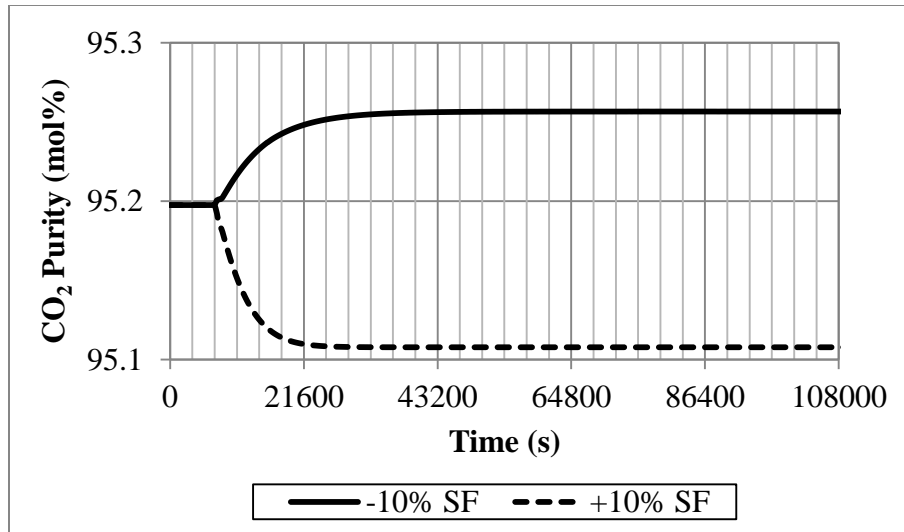
Figure 5.28 The CO_2 purity in response to the ramp changes in split fraction

5.6 Effect of flue gas flow rate

The effect of the flue gas flow rate on the CanCO2 process is studied in this section. The flue gas flow rate was ramped up by 30% within 1,800 seconds while the flue gas compositions were held constant. Similar to the Air Products' CO_2CPU plant, increasing flue gas flow rate increases the flue gas outlet temperature of coolers since the coolant flow rate on each exchanger was constant. Figure 5.29 illustrates the change in the flue gas outlet temperature in unit C-4 (stream 13's temperature).

128
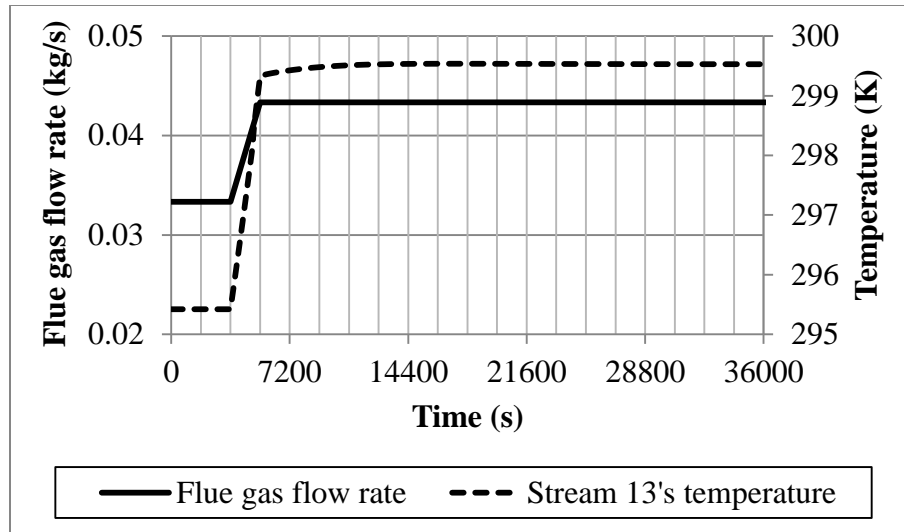
Figure 5.29 The increased flue gas flow rate and the stream 13's temperature response

As shown in Figure 5.29, increasing flue gas flow rate by 30% increased the temperature of stream 13 by 4 K and consequently caused an increase in stream 15's temperature by 3 K as shown in Figure 5.30. As shown in Figure 5.30, stream 15's temperature was linearly increased with increasing flue gas flow rate until it reached 252 K. Afterwards, the stream 15's temperature was increased rapidly and achieved 253.15 K at the end of the ramp change, i.e., around 5400 seconds. Because stream 15's temperature was continuously increased during the ramp change, the gas flow rate leaving from D-5 was increased and thus the flow rate of the recycle gas (stream 22) and stream 26 (hot gas feed of MHX-2) were correspondingly increased. When the ramp change reached its new steady-state, the temperature of stream 15 was yet steady and thus the recycle flow rate and stream 13's temperature were still increasing. Moreover, the temperatures of streams 29 and 36 (coolants in MHX-1) leaving from MHX-2 were also increased as a consequence of increasing stream 15's temperature. Therefore, stream 15's temperature was further increased and slowly reached to the new steady state at 254 K after 2 hours (7,200 seconds). Since the temperature of stream 15 significantly increased, the amount of liquid CO_2 recovered from D-5 decreased as shown in Figure 5.30. Note that within 1,800 seconds of the ramp change, the amount of liquid CO_2 obtained from D-5 was slightly increased due to the increase of flue gas flow rate.

129
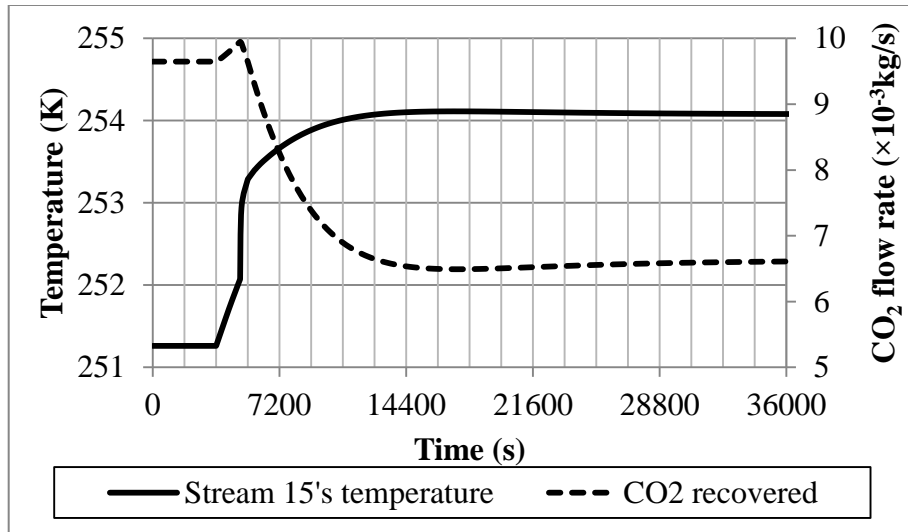
Figure 5.30 The stream 15's temperature and the CO_2 recovered from D-5 in response to the +30% ramp change in flue gas flow rate

Increasing stream 15's temperature increased the temperature and flow rate of stream 26, which is a hot gas feed of the MHX-2 unit. Similar to MHX-1, the effect of increasing the inlet temperature (stream 26's temperature) play a significant role in MHX-2 and thus the hot gas outlet temperature (stream 27's temperature) was increased as shown in Figure 5.31. Since D-6 operates at the temperature and pressure of stream 27, the change in stream 27's temperature affects the amount of liquid CO_2 recovered from D-6. Increasing temperature prevents the CO_2 condensation; therefore, the amount of CO_2 recovered from D-6 decreases. However, the results showed that more liquid CO_2 was obtained from D-6. Because the flue gas flow rate was increased, more CO_2 was fed to the process but the CO_2 recovered from D-5 decreased thereby increasing the CO_2 carried over from D-5 to D-6. Thus, the amount of liquid CO_2 recovered from D-6 was increased as shown in Figure 5.31.
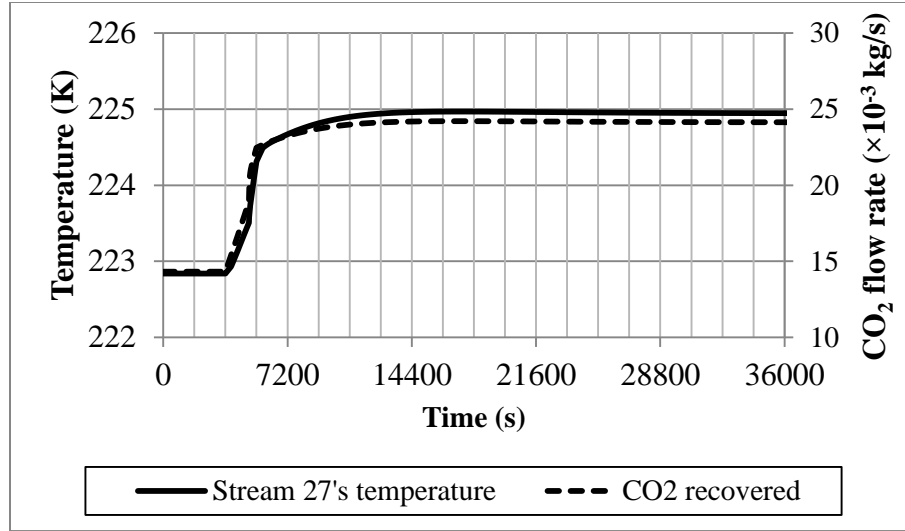
Figure 5.31 The stream 27's temperature and the CO_2 recovered from D-6 in response to the +30% ramp change in flue gas flow rate

The amount of liquid CO_2 obtained from D-5 and D-6 was added together and then divided by the amount of CO_2 in the flue gas feed in order to determine the CO_2 recovery of the process as shown in equation (5.1).

$$CO_2 \text{recovery (\%)} = \frac{\left(\text{mass } CO_2 \text{ in stream } 17\right) + \left(\text{mass } CO_2 \text{ in stream } 33\right)}{\text{mass } CO_2 \text{ in flue gas}} \times 100 \qquad (5.1)$$

Within 1,800 seconds, the amount of CO_2 in the flue gas was increased according to the ramp change of flue gas flow rate and the increase of CO_2 feed was more significantly than the increases in liquid CO_2 obtained from D-5 and D-6. Therefore, the CO_2 recovery was initially dropped as shown in Figure 5.32 (a).

131

(a)   (b)
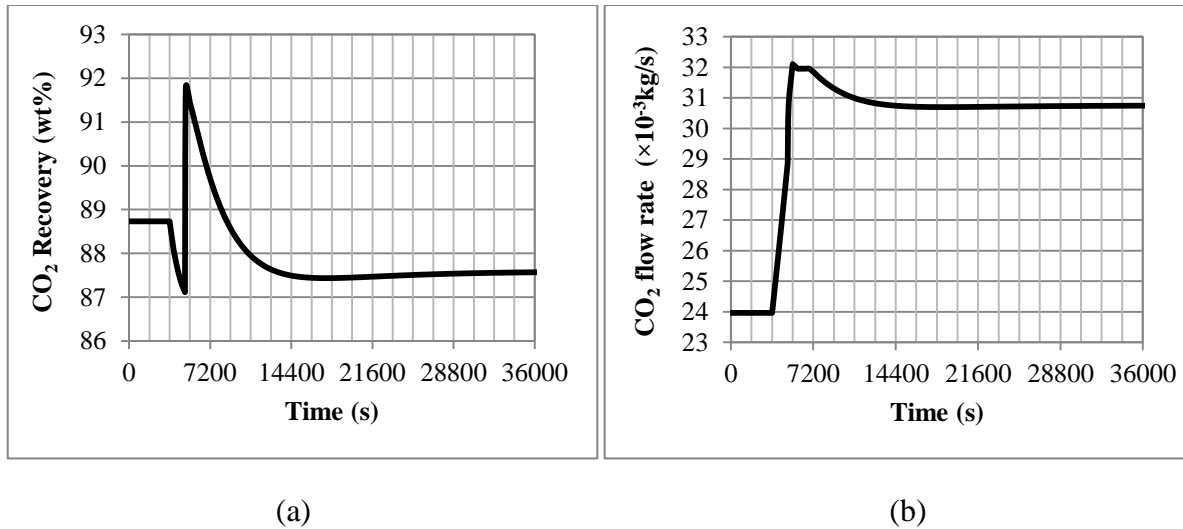
Figure 5.32 Responses to the +30% ramp change in flue gas flow rate (a) CO_2 recovery (b) sum of the CO_2 recovered from D-5 and D-6

Subsequently, the sum of liquid CO_2 obtained from D-5 and D-6 was significantly increased due to the rapid change in stream 15's temperature. Thus, the CO_2 recovery increased quickly and exceeded the initial steady state value to 92wt%. Afterwards, the liquid CO_2 obtained from D-6 was gradually increased along with decreasing liquid CO_2 from D-5. Hence, the total CO_2 recovered was slowly decreased resulting in decreasing CO_2 recovery as shown in Figure 5.32(b).

Figure 5.33 (a) presents the CO_2 product purity of the +30% ramp change in flue gas flow rate. The CO_2 purity is an averaged concentration between the CO_2 mole fraction obtained from D-5 and D-6, respectively. The CO_2 product purity depends on two factors; the CO_2 mole fractions and the total amount of liquid condensates obtained from D-5 and D-6. The total amount of liquid condensates changed in accordance with the total liquid CO_2 response shown in Figure 5.32 (b). The mole fractions of CO_2 obtained from D-5 and D-6 is shown in Figure 5.33 (b). The liquid mole fraction of the flash drum is determined by the equilibrium K-value which is a function of feed compositions; temperature and pressure of the drum. K-value is defined as the ratio of vapour mole fraction and liquid mole fraction. Increasing K-value decreases the liquid mole fraction. In D-5, the pressure was constant while the

132

temperature increased, which leads to an increase in the K-value of CO_2 in D-5. In addition, the inlet impurities were also increased due to the increase in recycle gas flow rate. Thus, the mole fraction of CO_2 the liquid condensate obtained from D-5 was decreased as shown in Figure 5.33 (b).

(a)   (b)
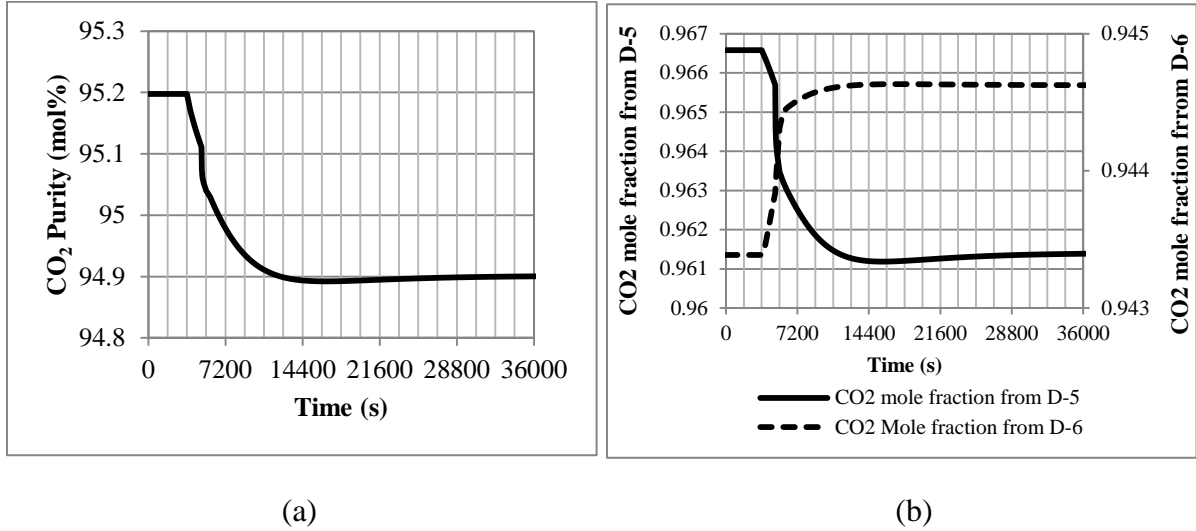
Figure 5.33 Responses to the +30% ramp change in flue gas flow rate (a) CO_2 purity (b) mole fraction of CO_2 obtained from D-5 and D-6

Consequently, the gas stream leaving from D-5 to D-6 contained high CO_2 content but less impurity. Thus, the mole fraction of CO_2 in the condensate obtained from D-6 increased. However, the increase was relatively small since the effect of having less impurity contents in the feed was balanced by the increase in the K-value of CO_2 in D-6. The K-value in D-6 was increased due to the increase in stream 27's temperature. The CO_2 product purity was decreased in accordance with the purity obtained from D-5 since the decrease of CO_2 mole fraction obtained from D-5 is greater than the increase in the CO_2 mole fraction obtained from D-6. The CO_2 product purity was reduced by 0.4 mol % when the flue gas flow rate was increased by 30% as shown in Figure 5.33 (a).

Five additional ramp changes were also implemented on the flue gas flow rate, i.e., ±10%, ±20% and -30%. The CO_2 recovery and the CO_2 product purity obtained from each test are presented in Figures 5.34 and 5.35, respectively.
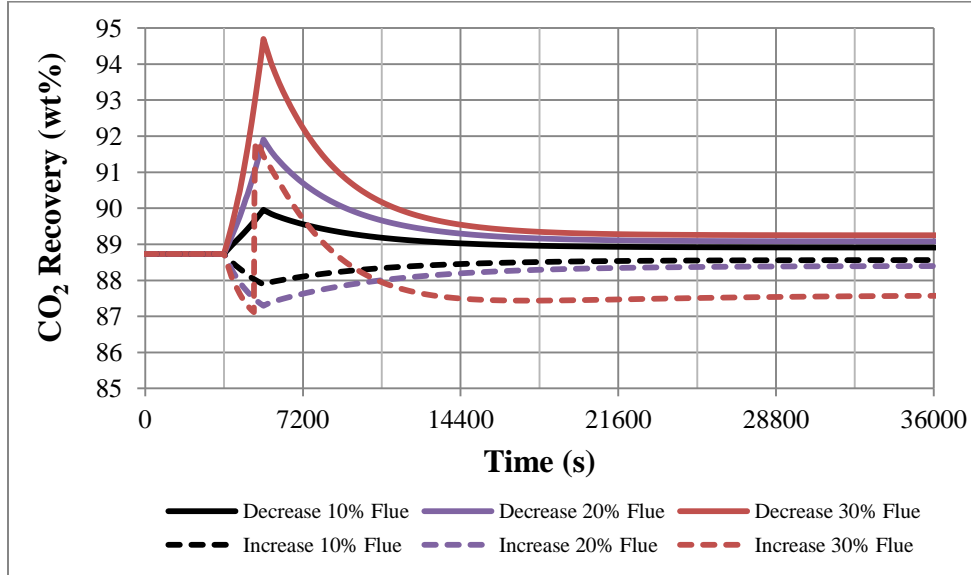
Figure 5.34 The CO_2 recovery in response to the ramp changes in flue gas flow rate
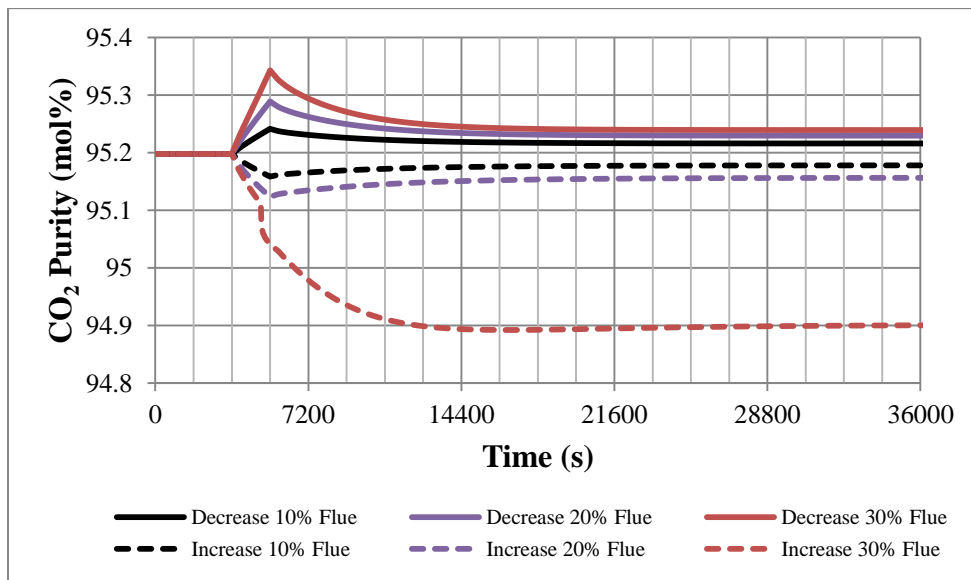
Figure 5.35 The CO_2 purity in response to the ramp changes in flue gas flow rate

These responses show that both the CO_2 recovery and the CO_2 product purity increase when the flue gas flow rate decreases at constant flue gas compositions. The CO_2 recovery is significantly affected by the temperature of stream 15 whereas the CO_2 purity response depends on the gas carried over from D-5 to D-6, the amount of gas recycled and the temperature of stream 27 in the similar way as for the +30% ramp change described above. However, those three variables that have a significant impact on the CO_2 purity are also determined by stream 15's temperature. Thus, the temperature of stream 15 plays a key role in this case. Figures 5.34 and 5.35 also show that the responses obtained from the +30% deviates from results obtained from other tests. This can be explained by considering the response of stream 15's temperature shown in Figure 5.36.
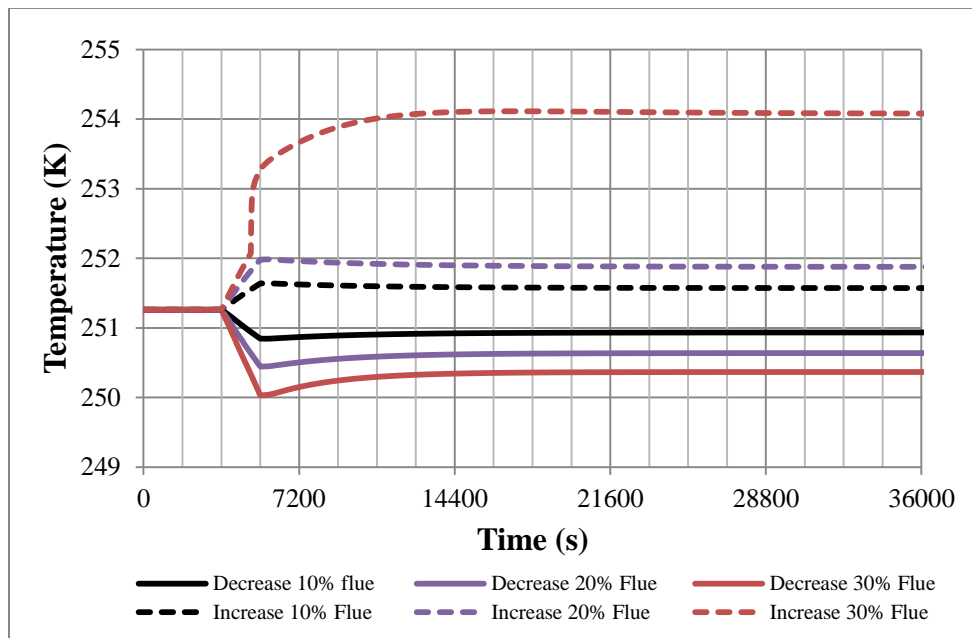
Figure 5.36 The stream 15's temperature in response to the ramp changes in flue gas flow rate

It was recognized that in the +30% flue gas change, stream 15's temperature reached 252 K prior to the end of the ramp change; then the temperature of that stream increased rapidly due to a continuous increase in flue gas flow rate, while the temperature of stream 15 obtained from the rest of ramp changes has never exceeded 252 K. It was found that at 252 K, the

vapour phase fraction of stream 15 shifts from 70% to 90% approaching the saturated vapour condition. Accordingly, the physical properties in the system varied significantly since the fluid changed from two-phase to vapour-like phase. The fluid viscosity was decreased by 20% when the vapour phase fraction was shifted to 90% whereas the thermal conductivity and the heat capacity decreased by 15% and 9%, respectively. The heat transfer ability of stream 15 was correspondingly dropped and thus a rapid increase in stream 15's temperature was obtained as shown in Figure 5.36. Hence, the CO_2 recovery and the CO_2 purity in the case of +30% ramp test dramatically changed in according to stream 15's temperature as explained above. The results obtained from this section indicate that the CO_2 recovery remained steadily within 88%-90% when the flue gas flow was varied between ±20% of the base case condition (120 kg/hr); however, an overshoot of CO_2 recovery was always obtained. The more flue gas flow rate change, the more aggressive the overshoot observed. The CO_2 product purity was relatively stable compared to the CO_2 recovery and no overshoots were observed. The maximum change of CO_2 purity was only 0.3mol% obtained from the +30% flue gas flow rate test. The results also indicated that the flue gas flow rate cannot be increased beyond 30% since stream 15 will be completely vaporized and the D-5 will dry-up.

5.7 Effect of flue gas composition

In this section, it was assumed that changes in the power plant operation will affect mainly the amount of CO_2 in the flue gas, similar to section 4.5 of the Air Products' CO_2CPU. Ramp changes were applied to the mass flow rate of CO_2 in the flue gas while the mass flow rates of other impurities contained in the flue gas, i.e. O_2, Ar, N_2, H_2O, SO_2 and NO, were held constant. In this section, six ramp changes were performed, ±10%, ±20% and ±30% on the CO_2 mass flow rate within 1,800 seconds. The final flue gas flow rate and compositions after each ramp change are shown in Table 5.2 including the base case value before applying the ramp change.

Increasing the mass flow rate of CO_2 in the flue gas increases the total flue gas flow rate and the mass fraction of CO_2. Since the coolants used in coolers C-1 to C-4 were constant while the amount of hot flue gas flowing through them was increased, the hot gas outlet temperatures of coolers were increased. Accordingly, the temperatures of streams 13 and 15 were increased. Figure 5.37 presents the changes of stream 15's temperature in response to the CO_2 flow rate ramp changes.

Table 5.2 Final flue gas conditions of ramp changes in CO_2 mass flow rate of the CanCO$_2$

Flue gas conditions		Percentage of the CO_2 flow rate change					
	Base case	-10%	-20%	-30%	10%	20%	30%
Total mass flow (kg/s)	0.033	0.031	0.028	0.025	0.036	0.039	0.041
Mass flow (kg/s)							
CO_2	0.027	0.024	0.022	0.019	0.030	0.032	0.035
O_2	0.002	0.002	0.002	0.002	0.002	0.002	0.002
Ar	0.001	0.001	0.001	0.001	0.001	0.001	0.001
N_2	0.003	0.003	0.003	0.003	0.003	0.003	0.003
H_2O	2.6E-04	2.6E-04	2.6E-04	2.6E-04	2.6E-04	2.6E-04	2.6E-04
SO_2	1.7E-04	1.7E-04	1.7E-04	1.7E-04	1.7E-04	1.7E-04	1.7E-04
NO	1.0E-05	1.0E-05	1.0E-05	1.0E-05	1.0E-05	1.0E-05	1.0E-05
Mole fraction							
CO_2	0.743	0.723	0.699	0.670	0.761	0.777	0.790
O_2	0.061	0.066	0.072	0.079	0.057	0.053	0.050
Ar	0.024	0.026	0.028	0.031	0.022	0.021	0.020
N_2	0.150	0.162	0.176	0.193	0.139	0.130	0.122
H_2O	0.018	0.019	0.021	0.023	0.016	0.015	0.014
SO_2	0.003	0.003	0.004	0.004	0.003	0.003	0.003
NO	0.000	0.000	0.000	0.001	0.000	0.000	0.000
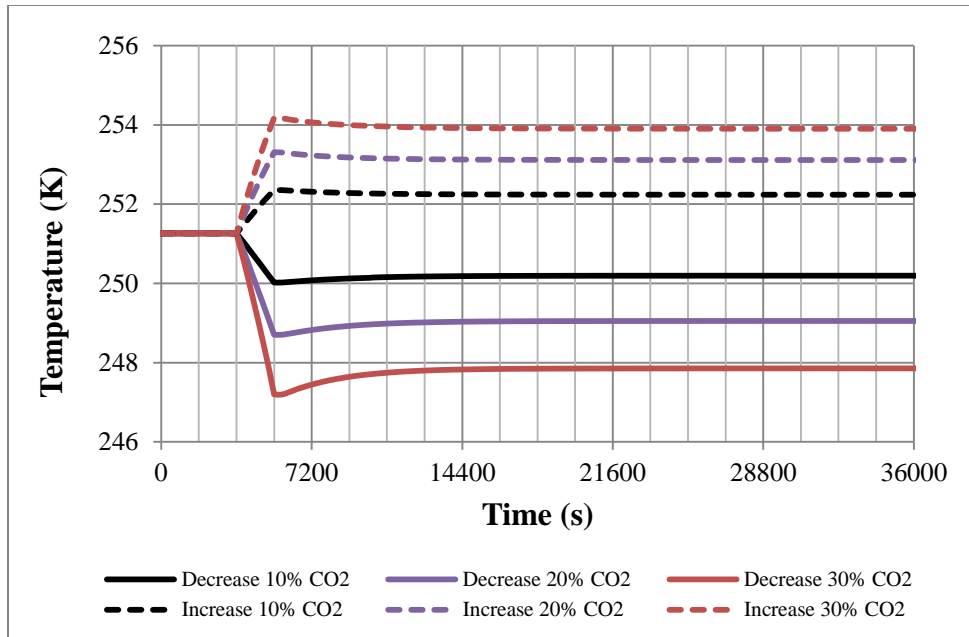
Figure 5.37 The stream 15's temperature in response to the ramp changes of CO_2 flow rate in the flue gas

The temperature of stream 15 significantly increased while the CO_2 flow rate in the flue gas continuously ramped within 1800 seconds and gradually achieved a new steady state afterwards. Because the flue gas compositions were changed, the saturation point was shifted away from 252 K and the vapour phase fraction of stream 15 did not exceed 90% in any case.

When the mass flow rate of CO_2 in the flue gas increased, the temperature also increased. Even though increasing stream 15's temperature prevents the CO_2 condensation in D-3, the amount of CO_2 recovered from D-3 was increased, as shown in Figure 5.38. Increasing stream 15's temperature increases the flow rates of streams 16 and 18 and also the flow rate of the recycle gas (stream 22). Thus, more CO_2 was recycled and the mass flow rate of CO_2 in stream 15 was increased. The effect of increasing CO_2 mass flow rate in stream 15 was more significant than the effect of increasing stream 15's temperature, therefore the liquid CO_2 recovered from D-5 was increased as shown in Figure 5.38. The opposite trends were obtained when decreasing CO_2 in the flue gas.
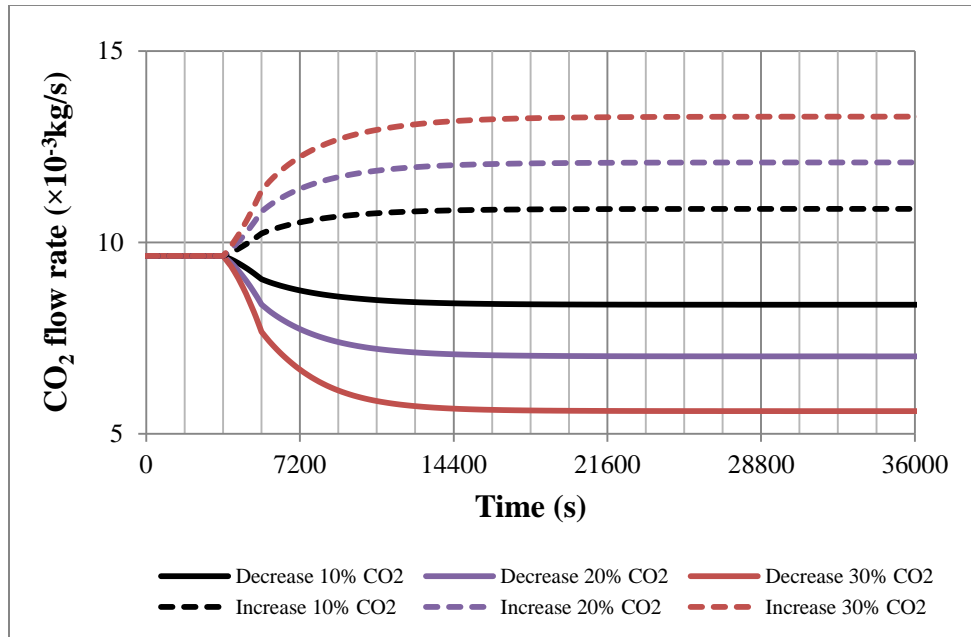
Figure 5.38 The amount of CO_2 recovered from D-5 in response to the ramp changes of CO_2 flow rate in the flue gas

The increments in the CO_2 recovered from D-5 were relatively small when compared to the increase of CO_2 in the flue gas. For example, in the +30% CO_2 ramp change, the amount of CO_2 in the flue gas was increased by 0.008 kg/s (28.8 kg/hr) while the CO_2 recovered from D-5 was increased by 0.004 kg/s (13 kg/hr). Thus, the amount of CO_2 carried over from D-5 to D-6 increased and the amount of CO_2 recovered from D-6 was increased accordingly. The decrease in CO_2 recovered from D-6 was obtained when the mass flow rate of CO_2 in the flue gas was ramped down. The total liquid CO_2 recovered from D-5 and D-6 obtained from each ramp change is shown in Figure 5.39. Overall, the amount of CO_2 recovered increased with increasing CO_2 in the flue gas flow rate and decreased with decreasing CO_2 in the flue gas flow rate. The total CO_2 recovered changed faster than the amount of CO_2 recovered from D-5 due to the effect of the recycle stream. The operation of D-5 is affected by the changes in the recycle stream, flue gas and also the coolants obtained from MHX-2. Thus, the liquid CO_2 obtained from D-5 slowly approached to the new steady state. Since in the MHX-2 the mass flow rate of hot gas inlet was determined by the splitter,and since the split fraction was fixed in this case, the recycle stream had less impact on the operation of D-6. Thus, the liquid

139

CO_2 obtained from D-6 moved to the new steady state faster than the liquid CO_2 obtained from D-5.
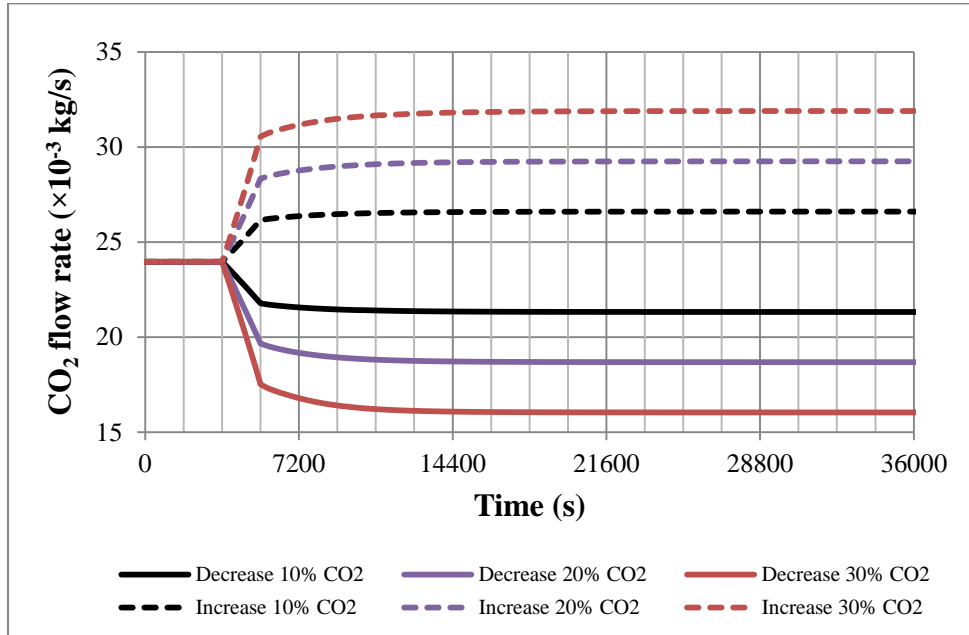
Figure 5.39 The sum of liquid CO_2 recovered from D-5 and D-6 in response to the ramp changes of CO_2 flow rate in the flue gas

The ratio between the total CO_2 recovered and the amount of CO_2 in the flue gas, i.e., the CO_2 recovery, was calculated and the response is shown in Figure 5.40. Inverse responses of the CO_2 recovery were observed when the flue gas composition was changed similar to the results obtained from the Air Products' CO_2CPU (see section 4.5 in chapter 4). Increasing the mass flow rate of CO_2 in the flue gas initially decreased the CO_2 recovery due to the dominant effect of increasing CO_2 feed. When the CO_2 flow rate remains constant, the effect of increasing CO_2 recovered from D-5 and D-6 starts to play a role and thus the CO_2 recovery increases. The maximum increase in the CO_2 recovery was about 2.1wt% achieved when the CO_2 flow rate was ramped up by 30%.
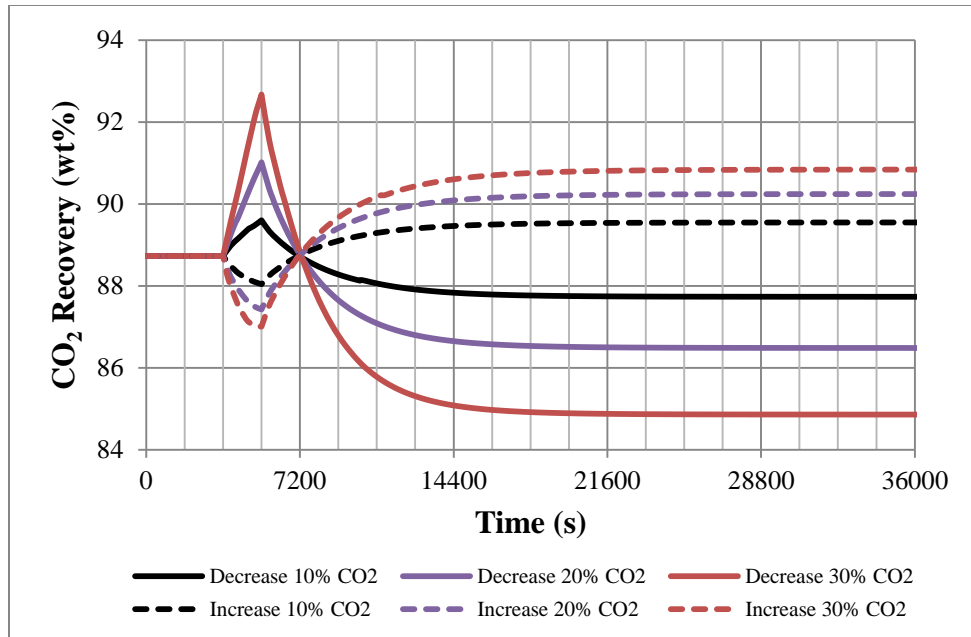
Figure 5.40 The CO_2 recovery in response to the ramp changes of CO_2 flow rate in the flue gas

Figure 5.41 presents the molar-averaged CO_2 purity obtained from each ramp change in the CO_2 mass flow rate. Increasing mass flow rate of CO_2 in the flue gas increases the total flue gas flow rate and the mass fraction of CO_2, but it also decreases the mass fraction of impurities (O_2, Ar, N_2, H_2O, SO_2 and NO). Thus, the CO_2 product purity increases when the CO_2 mass flow rate increases and vice versa. The maximum increase of the CO_2 product purity is approximately 0.4mol% and was achieved when the mass flow rate of CO_2 was increased by 30%. This is a largest change in CO_2 purity observed for the CanCO$_2$ process. This indicates that the CO_2 purity is sensitive to the flue gas compositions more than the flue gas flow rate and the operating conditions of the CanCO$_2$ process.
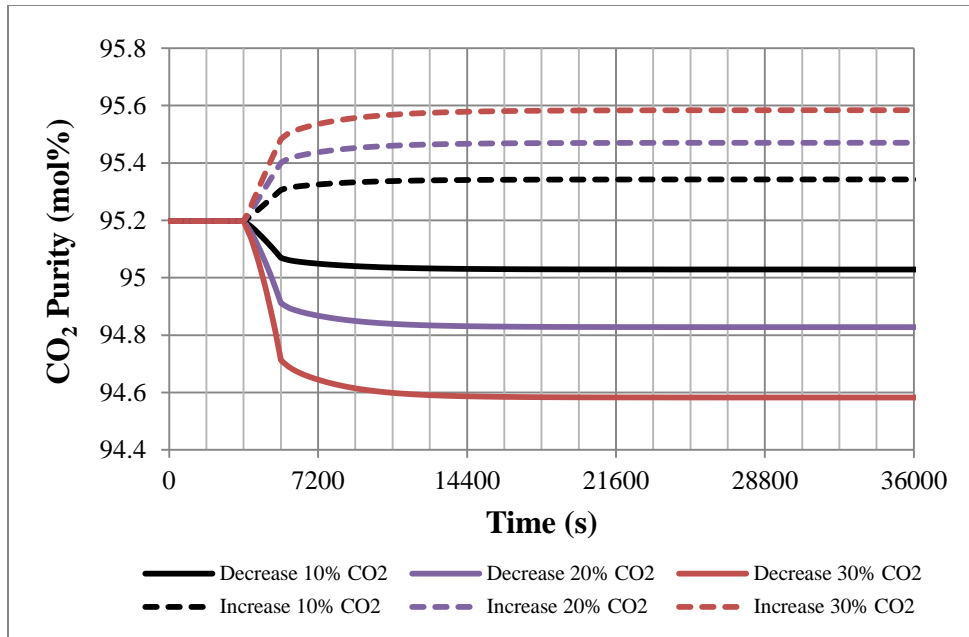
Figure 5.41 The CO_2 recovery in response to the ramp changes of CO_2 flow rate in the flue gas

5.8 Pilot plant flue gas composition

In this section, the variation in the flue gas composition of the Air Products Vattenfall Oxyfuel CO_2 Compression and Purification Pilot Plant (ACPP) pilot plant presented in Figure 4.35 was considered. The aim of this test is to examine dynamic behaviour and stability of the $CanCO_2$ in the presence of flue gas composition variation and noises. The simulation approach presented in section 4.5 for the Air Products' CO_2CPU model was also used here for the $CanCO_2$ model. The mass flow rate of CO_2 in the flue gas feed was changed in a rectangular impulse fashion starting from the base case value (75.5%) and then ramped up by 10% to reach the CO_2 concentration of 77.5% and then ramped down with the same pace as shown in Figure 5.42. This change is equivalent to the +10% ramp change in mass flow rate of CO_2 presented in section 5.7. The random noises from a normal distribution with mean 0 and standard deviation 1 were added to the CO_2 flow rate in order to make the change in CO_2 composition similar to the pilot plant trend presented in Figure 4.35.

142
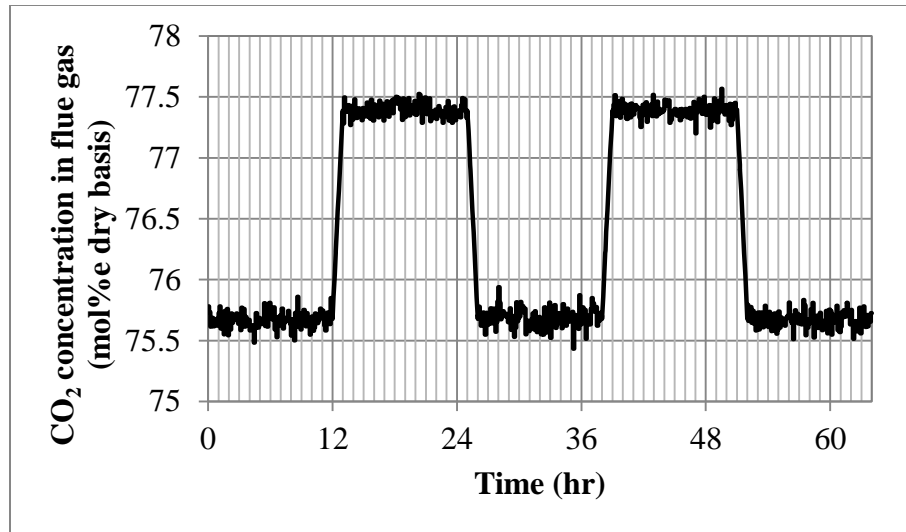
Figure 5.42 The rectangular impulse CO_2 concentration corrupted with noise (CanCO$_2$ process).

In section 5.7, it was observed that the $+10\%$ ramp change in CO_2 flow rate raised the CO_2 recovery from 88.7wt% to 89.6wt%. An inverse response of the CO_2 recovery was also obtained similar to section 5.7 but it was not obvious due to the presence of noises. It is expected that the CanCO$_2$ process will remain stable in this case and thus the CO_2 recovery should be alternated between 88.7% and 89.6% in accordance with results presented in section 5.7. The results obtained from the simulations support this assumption as illustrated in Figure 5.43.

The CO_2 recovery increased with increasing CO_2 concentration and then decreased back to the initial value when the CO_2 concentration was dropped. A small overshoot was observed in the CO_2 recovery response. Figure 5.43 also shows that the CO_2 recovery could not completely reach steady state within 12 hours in the presence of a corrupted signal with noise, unlike the Air Products' CO_2CPU (see Figure 4.37). Because the CanCO$_2$ has a recycle stream, the process usually takes more time to reach new steady states than the Air Products' CO_2CPU. Similar results were also observed in the previous tests. The results obtained from this section illustrated a significant impact of the developed noises on the CO_2

143

recovery of $CanCO_2$. Nevertheless, the CO_2 recovery can be alternated between 88.7 wt% to 89.6 wt% similar to the results obtained from section 5.7.
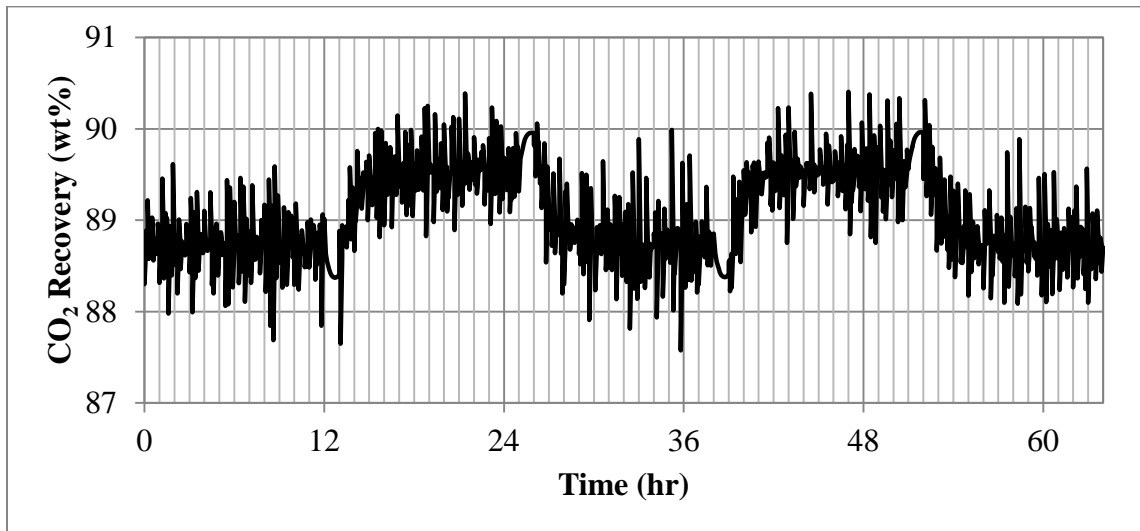
Figure 5.43 The CO_2 recovery in response to the noised rectangular impulse CO_2 concentration

The CO_2 purity obtained from the rectangular impulse of the CO_2 concentration corrupted with noise in flue gas feed is presented in Figure 5.44. Unlike the CO_2 recovery, the CO_2 purity of the $CanCO_2$ was considerably stable over the entire change in the CO_2 concentration. This result agrees well with the data presented by Kourosh and Shafeen (2010) and White et al. (2013). The CO_2 purity was alternated between 95.2mol% and 95.35mol% when the CO_2 concentration in the flue gas was changed between 75.5mol% and 77.5% mol. This change agrees well with the results obtained from section 5.7. Overall, the results obtained from this section indicate that the $CanCO_2$ remains stable in the presence of changes in CO_2 concentration that include noise. Further, the CO_2 purity is found to be less sensitive to the noisy signals and had a faster response to the input change when compared to the CO_2 recovery.
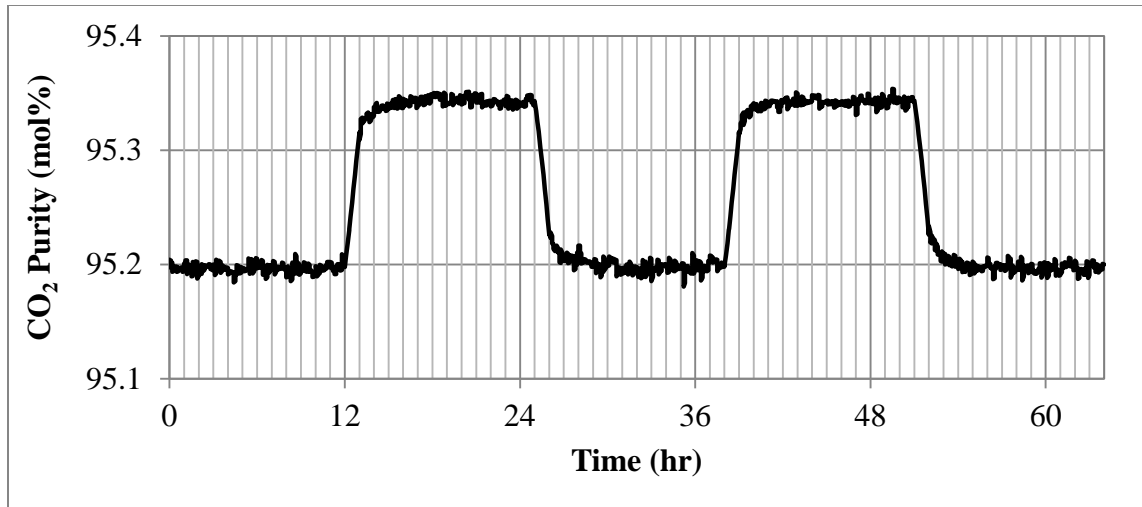
Figure 5.44 The CO_2 purity in response to the noised rectangular impulse CO_2 concentration

5.9 Summary

The $CanCO_2$ process model developed in this work was validated with design data at steady state that was available in the literature. A good agreement between the simulation results and design data was obtained. With 74 mol% CO_2 (wet basis) in the flue gas, the $CanCO_2$ achieved 88.7 wt% CO_2 recovery and 95.2 mol% CO_2 purity. The CO_2 recovery was slightly lower than that obtained from the Air Products' CO_2CPU because the first flash separator (D-5) in the $CanCO_2$ process was operated at a relatively high temperature. However, the CO_2 recovery obtained from the $CanCO_2$ is still comparable to the CO_2 recovery obtained from the Air Products' CO_2CPU due to the effect of the recycle stream. Increasing the amount of gas recycled to the process improved the CO_2 recovery of the CanCO2 plant but decreased the CO_2 product purity. Six case studies were performed to analyse the transient behaviour of the $CanCO_2$ process, i.e. ramp change in the K-4 discharge pressure, step change in the coolant flow rate of C-4, ramp change in the split fraction of gas splitter, ramp change in flue gas flow rate, ramp change in the mass flow rate of CO_2 in the flue gas and the pilot plant flue gas variation. Similar results between the Air Products' CO_2CPU process model and the $CanCO_2$ process model were obtained except for the CO_2 recovery response in the ramp change of K-4 discharge pressure. A large overshoot in the CO_2 recovery response was

145

observed from the CanCO$_2$ model while the Air Products' CO$_2$CPU model returned a first order response in CO$_2$ recovery when the operating pressure was increased by 3 bars. In addition, the time constants of all the process responses in the CanCO$_2$ are substantially larger than the time constants obtained from the Air Products' CO$_2$CPU model as a consequence of the gas recycle stream. The results obtained from all case studies indicate that the CO$_2$ recovery is more sensitive to the operating condition and feed disturbances than the CO$_2$ product purity. An overshoot in the CO$_2$ recovery response was observed, while typical first-order process responses were obtained from the CO$_2$ purity in most of the case studies performed. The inverse response of the CO$_2$ recovery occurred when the flue gas composition was changed; a similar response was obtained from the Air Products' CO$_2$CPU model. The CO$_2$ purity responded to all input changes faster than the CO$_2$ recovery while using both the CanCO2 and the Air Products' CO$_2$CPU models. The changes in CO$_2$ purity were essentially small and never exceeded 1mol%. Moreover, the CO$_2$ purity of both CO$_2$CPU configurations remained steady at 95% in all the case studies performed here. Similar results were reported by Zanganeh and Shafeen (2010) and White et al. (2013).

Chapter 6

Conclusions and recommendations

6.1 Conclusions

The main goal of this study was to understand and examine the dynamic behaviour of a CO_2 capture and purification unit (CO_2CPU). This study is part of a larger program aiming at scaling up and at developing efficient process control strategies. A critical component of this work was the development CO_2CPU dynamic models.

Two design configurations of the CO_2CPU were considered, i.e., the Air Products' CO_2CPU and the CanmetENERGY's proprietary CO_2CPU (CanCO$_2$). Both plants were designed based on a two-stage auto-refrigeration process. The CanCO$_2$ is an advanced design of the Air Products' CO_2CPU since the gas stream separated from the first flash drum is partially recycled to the compressor train instead of purging to the atmosphere as considered in the Air Products' design. The presence of the recycle stream is a major distinction between the two CO_2CPU configurations. Detailed mathematical models of each unit operation in the CO_2CPU plant were developed in this study.

The dynamic model describing the transient operation of a multi-stream heat exchanger was by far the most challenging process unit to model in the present analysis. This particular unit is challenging because it involves multiple streams entering and leaving this unit combined with two phase flows and phase changes due to heat transfer. The homogenous two phase flow model was implemented for the two phase region in multi-stream heat exchanger models in order to take the fluid properties variation during phase transition into account while calculating the heat transfer coefficients. In addition, the multi-stream heat exchanger model was developed based on a shell and tube configuration. The hot stream was assigned to flows inside the shell while cold streams passed through this unit counter-currently inside the tubes. The use of a shell and tube configuration allows for the assumption of one-dimensional flow, which is preferred at this stage of modelling since this work aims to develop a dynamic model of multi-stream heat exchanger that is not too complicated to slow

down the dynamic simulation of the entire CO_2CPU plant, but accurate enough to provide correct trends of temperature variation and time constants.

The use of product streams from flash drum as coolants in the auto-refrigeration process makes both CO_2CPU plant models highly integrated, and imposes difficulty in flowsheet convergence to both plant models, especially in the $CanCO_2$ plant model in which a gas recycle stream exists. The simulations required significant simulation times (i.e. 9 hours for the Air Products' CO_2CPU plant model and 21 hours for the $CanCO_2$ plant model) to converge based on limited steady state data obtained from Dillon et al. (2005) and CanmetENERGY. However, the steady state results obtained from the first trial were saved and used as initial conditions for the next run in order to reduce the convergence time for both plant models.

The flowsheet convergence of the $CanCO_2$ plant model is more challenging and time-consuming than the Air Products' CO_2CPU plant model due to the presence of a recycle stream. A traditional tear stream procedure, which is used to converge a recycle process simulation in commercial sequential modular simulation software, failed to achieve convergence for the $CanCO_2$ plant model in gPROMS. Thus, a new systematic procedure was developed in this study to overcome the difficulty of flowsheet convergence of the $CanCO_2$ plant model. A purge stream and valve were introduced into the $CanCO_2$ plant. The amount of gas recycled to the compressor train was adjusted by changing the recycle ratio; dynamic modelling of the $CanCO_2$ plant model started with a recycle ratio equal to 0, i.e. 0% gas recycled to the compressor train or 100% of the gas was purged. During the dynamic simulation, the recycle ratio was slowly ramped up until a recycle ratio of 1 was achieved, i.e. 100% gas recycled to the compressor train and no gas purged. Using this procedure, the $CanCO_2$ plant model converged without difficulty. The results obtained from the ramp change in recycle ratio indicate that the use of a recycle stream in the $CanCO_2$ can improve the CO_2 recovery while maintaining the CO_2 product purity at 95 mol%. This result gives the $CanCO_2$ an advantage over the Air Products' CO_2CPU.

The developed dynamic models of the Air Products' CO_2CPU and the $CanCO_2$ were validated at steady state using design data provided by the International Energy Agency Greenhouse Gas (IEAGHG) R&D programme (Dillon et al., 2005) and by CanmetENERGY, respectively. Good agreement between the developed model and design data were obtained for both models. Even though the developed models were validated only at steady state, this validation with limited data set is promising and was used to justify the pursuit of additional simulation results.

The developed models were used to characterize the transient behaviour of the CO_2CPU. Several dynamic tests were performed on both plant models and the main results are as follows:

- The operating temperature and pressure of the first flash drum, i.e. D-3 in the Air Products' CO_2CPU and D-5 in the $CanCO_2$, play a key role on the CO_2CPU performance. The operating conditions of these units determines the amount of liquid CO_2 recovered in the first drum, the amount of CO_2 carried over to MHX-2 and the mass flow rate of hot gas flowing to MHX-2, which directly affects the CO_2 recovery and CO_2 product purity.

- The CO_2 recovery is more sensitive to the operating conditions of the CO_2CPU than that observed for the CO_2 product purity.

- Overshoots were observed in the CO_2 recovery response to all changes performed in this study, thus strong interactions between the different process variables that determine the plant performance exist. A control system for this process may be challenging due to these strong interactions. The CO_2 purity is more sensitive to the flue gas composition and responds to all changes performed in this study faster than does the CO_2 recovery. However, the changes in CO_2 purity were small and never exceeded 1 mol%.

- The CO_2 purity of both CO_2CPU configurations remained essentially at its nominal operating condition (at 95%) in all case studies performed in this work.

- The temperatures of the process streams flowing through the second multi-stream heat exchanger and also the operating temperature of the second flash drum, i.e. D-4 in the Air Products' CO_2CPU and D-6 in the CanCO$_2$, were sensitive to changes in the flue gas conditions. An undershoot was observed in the second flash drum temperature response when the flue gas flow rate and the CO_2 content in the flue gas stream were decreased. This result demonstrates the possibility of CO_2 freezing in the MHX-2 in the presence of feed disturbances, especially in the Air Products' CO_2CPU where the nominal operating temperature of D-4 is close to the CO_2 freezing point. This finding, therefore, is the motivation for the implementation of a temperature controller in order to avoid CO_2 freezing in MHX-2.

- The developed model can therefore be used to design suitable control schemes for this process and study the dynamic operability of this process in closed-loop.

6.2 Recommendations

The following aspects are recommended for the future work:

1) Model validation using dynamic data

   Even though good agreement between the simulation results obtained from the developed model and the design data were obtained, it is necessary to validate the model using dynamic data in order to verify an accuracy of the developed model. However, dynamic data for this plant is not currently available in the open literature. Hence, the need to develop experimental studies that show the transient behaviour of this plant under various conditions. It is therefore recommended to validate the present plant model using dynamic data if it becomes available in the future.

2) Control structure design of the CO_2CPU

   The results obtained from this study can be used to design a control structure for the CO_2CPU. It is undoubtedly that the control objective of the CO_2CPU is to maintain the CO_2 product purity and the capture performance indicated by the CO_2 recovery. Thus, the

controlled variables of the CO_2CPU system may be the CO_2 recovery, the CO_2 product purity, and liquid levels of the first and second flash drums; the potential manipulated variables are the compressor train's outlet pressure, the compressor train's outlet temperature, valve V-1 and valve V-2. The presence of the recycle stream and gas splitter in the $CanCO_2$ provides an advantage over the Air Products' CO_2CPU in terms of control structure selection since the recycle stream and the gas splitter can be considered as additional manipulated variables. Thus, the $CanCO_2$ has more alternative control structures than the Air Products' CO_2CPU. However, the recycle loop included in the $CanCO_2$ process may add natural feedback into the system; which may impose challenges in the design of a suitable control scheme for this system. Moreover, the transient analyses obtained from this study show that the CO_2CPU is a highly nonlinear process, thus the method used for control structure selection may take into account the process nonlinearities. A simplified method may provide a poor measure of the control loop interactions and may lead to inappropriate control schemes. Furthermore, since overshoots were in the CO_2 recovery and the CO_2 purity responses, a conservative tuning design method is more preferable in the CO_2CPU to reduce the control loop interactions. An extension of the developed model to cover controllability analysis and control structure design for the CO_2CPU is recommended since the control system is necessary to maintain the CO_2CPU plant performance in the large-scale operation.

3) <u>Integration into a complete dynamic model of oxy-fired power plant</u>

The CO_2CPU model developed in this study can be integrated with an oxy-boiler, steam cycle and an air separation unit (ASU) models to specify a complete dynamic model of the oxy-fired power plant. An integrated model can provide insight regarding the dynamics of an oxy-coal-fired power plant with CO_2 capture. The combined power plant-CO_2 capture model can be used to analyze the dynamic operability and controllability of these systems in the presence of changes in the load or changes in the process operating conditions due to changes in the electricity demands. Further, this study will be very

useful for the transition towards commercial scale operation of oxy-fuel combustion technology.

4) Implementation of a more accurate two phase flow model

A more accurate two-phase flow model, e.g., separated flow model and two-fluid flow model, and the pressure drop correlations can be implemented in order to improve the accuracy of the multi-stream heat exchanger model and make the developed model more realistic. However, it will also make the dynamic model of the CO_2CPU plant computationally intensive and time-consuming while the dynamic responses of key variables, i.e. CO_2 recovery and CO_2 purity, are likely to be similar to the results presented in this study. A powerful computer may be required to simulate the CO_2CPU plant model with a complex two phase flow model. In addition, a complex two phase flow model will make the flowsheet convergence of the CO_2CPU plant model even more challenging. Initial conditions should be well defined in order to avoid the simulation failure. It should be noted that the pressure drop across each unit operation in the CO_2CPU is quite small according to the design data, so the impact of this variable on the dynamic behaviour of the CO_2CPU needs to be thoroughly studied.

References

Abdul-Razzak, A., Shoukri, M., Chang, J.S., 1995. Characteristics of refrigerant R134a liquid-vapour two-phase flow in horizontal pipe. ASHRAE Transaction Symposium. 101, 953-964.

Abraham, B.M., Asbury, J.G., Lynch, E.P., Toetia, A.S.P., 1982. Coal-oxygen process provides for enhance recovery. Oil Gas Journal, 80(11), 68-70.

Adams, D., Davison, J., 2007. Capturing CO_2. IEA Greenhouse Gas R&D Programme.

ALPEMA, 2000. The standards of the brazed aluminium plate-fin heat exchanger manufacturers' association.

AspenTech, 2004. Aspen Plus 2004.1 Getting Start Using Equation Oriented Modelling.

Averous, D., Hammadi, K., Pingaud, H., Joulia, X., Guittard, P., 1999. Dynamic Simulation of Brazed Plate-Fin Heat Exchangers. Comp. Chem. Eng. Sup. S447-S450.

Barton, P.I., 2000. The equation oriented strategy for process flowsheeting. Massachusetts Institute of Technology, Cambridge.

Barton, R., 1974. Sizing Liquid-Liquid Phase Separators. Chemical Engineering, July 8.

Besong, M.T., Maroto-Valer, M.M., Finn, A., 2013. Study of design parameters affecting the performance of CO2 purification units in oxy-fuel combustion. IJGGC. 12, 441-449.

Boehme, R., Parise, J.A.R., Marques, R.P., 2003. Simulation of multistream plate-fin heat exchangers of an air separation unit. Cryogenics. 43, 325-334.

BP, 2013. BP Energy Outlook 2030. [online] Available at:

    <http://www.bp.com/en/global/corporate/about-bp/statistical-review-of-world-energy-2013/energy-outlook-2030.html>.

BP, 2013. BP Energy Outlook 2030. [online] Available at:

    < http://www.bp.com/statisticalreview>.

Buhre, B.J.P., Elliott, L.K., Sheng, C.D., Gupta, R.P., Wall, T.F., 2005. Oxy-fuel combustion technology for coal-fired power generation. Prog. Energ. Combust. 31, 283-307.

Chalupa, P., Novak, J., Bobal, V., 2012. Comprehensive model of DTS200 Three Tank System in Simulink. Int. J. Mathematical Models and Methods in Applied Science. 6, 358-365.

Davidson, R., Santos, S., 2010. Oxyfuel Combustion of Pulverised Coal. Cheltenham: IEAGHG.

Dimian, A.C., 2003. Integrated design and simulation of chemical processes. Amsterdam: Elsevier.

Dillon, D.J., White V., Allam R.J., Wall R.A., Gibbins J., 2005. Oxy Combustion Processes for the CO_2 Capture from Power Plant. IEA Greenhouse Gas R&D Programme.

Energy Information Administration (EIA), 2012. Receipts, Average Cost, and Quality of Fossil Fuels for the Electric Power Industry, 2002 through 2011. [online] Available at: <http://www.eia.gov/electricity/annual/html/epa_07_01.html>.

Environment Canada, 2012. Canada Emission's Trend. [online] Available at: <http://www.ec.gc.ca/ges-ghg/default.asp?lang=En&n=985F05FB-1>.

Environment Canada, 2013. Canada Emission's Trend. [online] Available at: <http://www.ec.gc.ca/ges-ghg/default.asp?lang=En&n=985F05FB-1>.

ExxonMobil, 2013. The outlook for energy: A view to 2040. [online] Available at: <http://www.exxonmobil.com/energyoutlook>.

Faghri, A., Zhang, Y., 2006. Transport phenomena in multiphase system. Elsevier, USA.

Fu, C., Gundersen, T., 2011. Reducing the power penalty related to CO_2 conditioning in oxy-coal combustion plants by pinch analysis. Chemical Engineering Transactions. 25, 581-586.

Fu, C., Gundersen, T. 2012. Techno-economic analysis of CO_2 conditioning process in a coal based oxy-combustion power plant. IJGGC. 9, 419-427.

Global CCS Institute (GCCSI), 2012a. CO_2 Capture Technology Oxy Combustion with CO_2 Capture. California: GCCSI.

Global CCS Institute (GCCSI), 2012b. The Global CCS Status: 2012. Canberra: GCCSI.

Global CCS Institute (GCCSI), 2013. The Global CCS Status: 2013. Melbourne: GCCSI.

Gosh, I., Sarangi, S.K., Das, P.K., 2006. An alternate algorithm for the analysis of multistream plat fin heat exchangers. Int. J. Heat Mass Transfer. 49, 2889-2902.

Gosh, I., Sarangi, S.K., Das, P.K., 2007. Simulation Algorithm for Multistream Plate Fin Heat Exchangers Including Axial Conduction, Heat Leakage, and Variable Fluid Property. J. Heat Transfer. 129, 884-893.

Government of Canada, 2013. Canada's action on climate change. [online] Available at: <http://climatechange.gc.ca/default.asp?lang=En&n=4FE85A4C-1>.

Hadhipaschalis, I., Kourtis, G., Poullikkas, A., 2009. Assessment of oxyfuel power generation technologies. Renewable and Sustainable Energy, 13, 2637-2644.

Hall, S., 2012. Rules of Thumb for Chemical Engineers. 5th ed. USA: Elsevier.

Halman, J.P., 1997. Heat transfer. 8th ed. Ohio: McGraw-Hill College.

Horn, F.L., Steinber, M., 1982. Control of carbon dioxide emissions from power plant (and use in enhance oil recover). Fuel, 61(5), 415-422.

International Energy Agency (IEA), 2010. Energy technology perspective: Scenarios and strategies to 2050. Paris: IEA.

International Energy Agency (IEA), 2011. World Energy Outlook 2011. Paris: IEA.

International Energy Agency (IEA), 2012a. Technology Roadmap: High Efficiency, Low-Emissions Coal-Fired Power Generation. Paris: IEA.

International Energy Agency (IEA), 2012b. World Energy Outlook 2012: Executive Summary. Paris: IEA.

International Energy Agency (IEA), 2013. Redrawing the Energy Climate Map: World Energy Outlook Special Report. Paris: IEA.

Intergovernmental Panel on Climate Change (IPCC), 2005. Special report on carbon dioxide capture and strorage. New York: Cambridge University Press.

Jia, X., Tso, C.P., Chia, P. K., 1995. Distributed model for prediction of the transient response of an evaporator. Int. J. Refrig. 18, 336-342.

Jordal, K., Anheden, M., Yan, J., Stromberg, L., 2004. Oxyfuel combustion for coal-fired power generation with CO_2 capture capture-Opportunities and Challenges. 7th International Conference on Greenhouse Gas Technologies. Vancouver, Canada.

Kanniche, M., Gros-Bonnivard, R., Jaud, P., Valle-Marcos, J., Amann, J.M., Bouallou, C., 2010. Pre-combustion, post-combustion and oxy-combustion in thermal power plant for CO_2 capture. Applied Thermal Engineering. 30, 53-62.

Kern, D.Q., 1950. Process Heat Transfer. McGraw-Hill

Kohil, A.A., Farag, H., Ossman, M.E., 2010. Mathematical modelling of a multi-stream brazed aluminium plate fin heat exchanger. Thermal Science. 14, 103-114.

Ku, H.M., 2013. Flowsheet Convergence-Tear Streams. King Mongkut's Unviersity of Technology Thonburi, Bangkok.

Kuczynski, K.J., Fitzgeralda, F.D., Adamsa, D., Gloverb, F.H.M., White, V., Chalmersc, H., Erreyc, O., 2011. Dynamic Modelling of Oxyfuel Power Plant. Energy Procedia. Energy Procedia. 11, 2541-2547.

Levy, S., 1999. Two phase flow in complex systems. Jonh Wiley &Sons Inc., Canada.

Lockhart, R.W., Martinelli, R.C., 1949. Proposed correlations of data for isothermal two-phase, two-component flow in pipes. Chem. Eng. Prog. 45, 39-48.

Luo, X., Li, M., Roetzel, W., 2002. A general solution for one-dimensional multistream heat exchangers and their networks. Int. J. Heat Mass Transfer. 45, 2695-2705.

Madsen, S., Veje, C., Willatzen, M., 2012. Dynamic Modeling of Phase Crossing in Two-phase Flow. Commun. Comput. Phys. 12,1129-1147.

Mithraratne, P., Wijeysundera, N.E., Bong, T.Y., 2000. Dynamic simulation of a thermostatically controlled counter-flow evaporator. Int. J. Refrig. 23, 174-189.

Moran, M.J., Shapiro, H.N., 2010. *Fundamentals of engineering thermodynamics*. 6th ed. Delhi: Wiley.

National Resources Canada, 2011. CanmetEnergy. [online] Available at: <http://canmetenergy.nrcan.gc.ca/home>

NASA, 2013. NASA scientists react to 400 ppm carbon milestone. [online] Available at: <http://climate.nasa.gov/400ppmquotes/>.

Nyers, J., Stoyan, G., 1992. A dynamical model adequate for controlling the evaporator of a heat pump. Int. J. Refrig. 17,101-108.

Prasad, B.S.V., Gutukul, S.M.K.A., 1992. Differential Methods for the Performance Prediction of Multistream Plate-Fin Heat Exchangers. Journal of Heat Transfer. 114, 41-49.

Peng, D.Y., Robinson, D.B., 1976. A new two-constant equation of state. Ind. Eng. Chem. Fundamen, 15(1), 59-64.

Pingaud, H., Lann, J.M.L., Koehret, B., Bardin, M.C., 1989. Steady-state and dynamic simulation of plate fin heat exchanger. Comp. Chem. Eng. 13, 577-585.

Pipitone, G., Bolland, O., 2009, Power generation with CO_2 capture: Technology for CO_2 purification, IJGGC. 3, 528-534.

Pottmann, M., Engl, G., Stahl, R., Ritter, R., 2010. Dynamic simulation of oxyfuel CO_2 processing plants. Energy Procedia. 4, 951-957.

Posch S, Haider M. 2012. Optimization of CO_2 compressing and purification units (CO_2CPU) for CCS power plant. Fuel. 101, 254-263.

Process cooling, 2000. Brazed Aluminum Plate-Fin Heat Exchangers Reduce Costs. [online] Available at: <http://www.process-cooling.com/articles/84569-brazed-aluminum-plate-fin-heat-exchangers-reduce-costs?v=preview>.

Randalls, S., 2010. History of the 2°C climate target. Wiley Interdisciplinary Reviews: Climate Change, 1(4), 598-605.

Rubin, E.S., Mantripragada, H., Marks, A., Versteeg, P., Kitchin, J., 2012. The outlook for improved carbon capture technology. Prog. Energ. Combust. 38, 630-671.

Satish, R., 1999. Autorefrigeration separation of carbon dioxide. WO 99/35455.

Sawyer, D., Stiebert, S., 2012. Regulating Carbon in Canada: The impact of the federal government's proposed electricity coal performance standards. IISD.

Schultz, J.M., 1962. The polytropic analysis of centrifugal compressors. Journal of Engineering Power. 84, 69-81.

Shilling, R.L., Bernhagen, P.M., Goldschmidt, V.M., Hrnjak, P.S., Johnson, D., Timmerhaus, K.D., 2008. Heat transfer equipment. In: R.H. Perry, D.W. Green, 8th ed. Perry's Chemical Engineers' Handbook. New York: MaGraw-Hill Professional. Ch.11.

Sinnott, R.K., 2005. Chemical Engineering Design, sixth ed. Elsevier Butterworth-Heinemann, Oxford.

Sioshansi, F., 2010. Generating Electricity in a Carbon-Constrained World. USA: Elsevier.

Toftegaard, M.B., Brix, J., Jensen, P.A., Glarborg, P., Jensen, A.D., 2010. Oxy-fuel combustion of solid fuels. Prog. Energ. Combust. 36, 581-625.

UNFCCC, 2009. Copen Climate Change Conference-December 2009. [online] Available at: <http://unfccc.int/meetings/copenhagen_dec_2009/meeting/6295.php>.

Wall, T.F., 2007. Combustion processes for carbon capture. Proceeding of the Combustion Institute, 31, 31-47.

Wall, T.F., Stanger, R., Santos, S., 2011. Demonstration of coal-fired oxy-fuel technology for carbon capture and storage and issues commercial deployment. IJGGC. 5S, S5-S15.

White, V., Wright, A., Tappe, S., Yan, J., 2013. The Air Products Vattenfall Oxyfuel CO2 Compression and Purification Pilot Plant at Schwarze Pumpe. Energy Procedia. 37, 1490-1499.

World Coal Association, 2013a. Coal Matter: Coal and Electricity Generation. [online] Available at: <http://www.worldcoal.org/resources/coal-statistics/coal-matters/>.

World Coal Association, 2013b. Coal Matter: Global availability of coal. [online] Available at: <http://www.worldcoal.org/resources/coal-statistics/coal-matters/>.

Zanganeh, K.E., Shafeen A., Gupta, M., Salvador, C., 2006. Comparative Performance Evaluation of CO_2 Capture and Compression Processes for Advanced Oxy-fuel Power

Plants, 31st International Technical Conference on coal utilization and fuel systems, Clearwater, FL, May 21-25, 2006.

Zanganeh, K.E., Shafeen, A., Salvador, C., 2009. CO_2 capture and development of an advanced pilot-scale cryogenic separation and compression unit. Energy Procedia. 1,247-252.
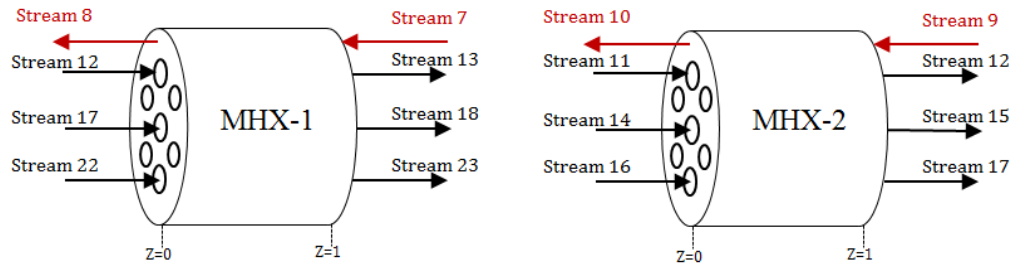
Zanganeh, K.E., Shafeen, A., 2010. Auto-refrigerated gas separation system for carbón dioxide capture and compression. US 2012/0137728 A1.

Zero Emission Platform (ZEP), 2013. CCS needs rapid and widespread deployment. [online] Available at: <http://www.zeroemissionsplatform.eu/carbon-capture-and-storage.html>.

Appendix A

Equipment sizing of the Air Products' CO₂CPU model

Table A.1 Multi-stream heat exchangers

Design variables	MHX-1	MHX-1
Shell diameter (m)	2	2.15
Number of shell pass	1	2
Tube diameter (m)	0.01905	0.01905
Tube length (m)	8.2	5.1
Number of tubes per inlet 1, 2 and 3	2000, 2200, 2000	1200,1800,1200
Flow through the shell	Stream 7-8*	Stream 8-9*
Flow through the tube inlet 1	Stream 12-13*	Stream 11-12*
Flow through the tube inlet 2	Stream 17-18*	Stream 14-15*
Flow through the tube inlet 3	Stream 22-23*	Stream 16-17*
Tube pitch (m)	0.0238	0.0238
Baffle cut	20%	20%
Baffle spacing (m)	0.4	0.43

*Stream numbers refers to Figure 3.1

Table A.2 Heater and coolers

Design variables	C-1	C-2	C-3	C-4
Shell diameter (m)	1.13	1.13	0.78	1.07
Number of shell pass	1	1	1	1
Tube diameter (m)	0.01905	0.01905	0.01905	0.01905
Tube length (m)	9	13	4.25	5.25
Number of tubes	2000	2000	900	1800
Tube pitch (m)	0.0238	0.0238	0.0238	0.0238
Baffle cut	20%	20%	20%	20%
Baffle spacing (m)	0.2258	0.2258	0.1555	0.215

Table A.3 Flash drums

Design variables	D-1	D-3	D-4
Vertical drum design factor (K_v)	0.028	0.37	0.27
Maximum vapour velocity (m/s)	0.05	0.42	0.34
Drum diameter (m)	12	7	5
Total height (m)	24	14	10
Maximum flow area (cm^2)	8	5.1	5.1

Appendix B

Equipment sizing of the CanCO₂ model

Table B.1 Multi-stream heat exchangers
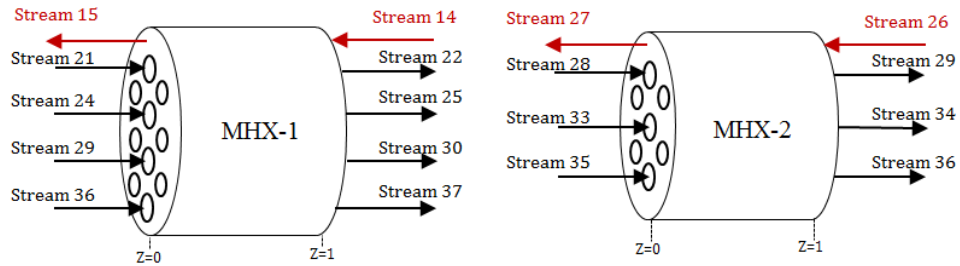
Design variables	MHX-1	MHX-1
Shell diameter (m)	0.1016	0.1524
Number of shell pass	1	2
Tube diameter (m)	0.0127	0.0127
Tube length (m)	10	5.5
Number of tubes per inlet 1, 2 and 3	4, 1, 4, 2	1, 1, 1
Flow through the shell	Stream 14-15[*]	Stream 26-27[*]
Flow through the tube inlet 1	Stream 21-22[*]	Stream 28-29[*]
Flow through the tube inlet 2	Stream 24-25[*]	Stream 33-34[*]
Flow through the tube inlet 3	Stream 29-30[*]	Stream 35-36[*]
Flow through the tube inlet 4	Stream 36-37[*]	-
Tube pitch (m)	0.016	0.016
Baffle cut	20%	20%
Baffle spacing (m)	0.02	0.03

*Stream numbers refers to Figure 3.1

Table B.2 Heater and coolers

Design variables	C-1	C-2	C-3	C-4	H-1	H-2
Shell diameter (m)	0.3048	0.3048	0.3048	0.3048	0.1016	0.1016
Number of shell pass	1	1	1	1	1	1
Tube diameter (m)	0.0127	0.0127	0.0127	0.0127	0.0127	0.0127
Tube length (m)	4.5	5.4	5.1	5.1	3	3
Number of tubes	6	6	6	8	0.86	0.65
Tube pitch (m)	0.016	0.016	0.016	0.016	0.016	0.016
Baffle cut	20%	20%	20%	20%	20%	20%
Baffle spacing (m)	0.06	0.06	0.06	0.06	0.02	0.02

Table B.3 Flash drums

Design variables	D-1	D-2	D-3	D-4	D-5	D-6	D-7
Vertical drum design factor (K_v)	0.17	0.21	0.32	0.32	0.44	0.24	0.38
Maximum vapour velocity (m/s)	1.28	1.25	0.97	0.97	0.5	0.3	0.6
Drum diameter (m)	0.1016	0.1016	0.1016	0.1016	0.1524	0.1524	0.1016
Total height (m)	1	1	1	1	1	1	1
Maximum flow area (cm^2)	0.97	0.97	0.97	0.97	1.27	1.27	0.97